Flow Induced Polymer Degradation During Ink-Jet Printing

A thesis submitted to the University of Manchester for the degree of Doctor of

Philosophy in the Faculty of Engineering and Physical Sciences

2010

Khalid A. Alamry

School of Chemistry

Table of Contents

List of Figures

List of Tables

Abbreviations

PMMA	Polymethyel methacrylate
PMAA	Polymethyacrylaic acid
PS	Polystyrene
DOD	Drop-on-demand
CIJ	Continuous inkjet printing
TIJ	Thermal inkjet printing
SOHO	Small office home office
CE	Cellulous ester
CAB2	Cellulose Acetate Butyrate
PEDOT-PSS	Poly(4-ethylenedioxythiophene)-Poly(styrenesulfonate
OLED	Organic light emitting displays
OTFT	Organic thin film transistors
ITO	Indium Tin Oxide
DBSA	Dodecylbenzenesulfonic acid
GOx	Glucose oxidase
GPC	Gel Permeation Chromatography
SEC	Size Exclusion Chromatography
DSC	Differential Scanning Calorimetry
TGA	Thermal Gravimetric Analysis
^{1}HNMR	Nuclear Magnetic Resonance Spectroscopy

DMP	Dimatix Materials Printer
Vazo 67	2,2'-azobis(2-methylbutyronitrile
HSP	Hansen Solubility Parameters
RED	The Relative Energy Difference number
CMC	Carboxymethyl Cellulose
FM9	t-Bbutylstyrene and Mmethacrylic acid
PDMA	PolydiMethylAcrylamide
TABS	Thermally Activated Barried to Scission
GG	Guar Gum
XG	Xanthan Gum
DR	DragReduction
DM	Dimorphandra Ggardneriana
Ara	Arabinose
PJ	Prosopis Juliflora

Symbols

c	Polymer concentration
c*	Overlap concentration
η	Dynamic viscosity
[η]	Intrinsic viscosity
Mw	Weight average molecular weight
Mn	Number average molecular weight
PDi	Polydispersity index
γ	Gamma
Hz	Hertz
k	Boltzmann's constant
v	Velocity of droplets
γ	Surface tension
ε	Critical elongational rate
τ_1	The longest relaxation time of polymer chain
t_d	The delay between the initial voltage rise and the appearance of an outwardly moving meniscus
t_{rup}	The time from the first initial movement of the external meniscus and ligament break-off and rupture
We_{crit}	Critical The Weissenberg number
We	Weber number
Oh	Ohnesorge number
μs	Micro second
V	Voltage

t	The flow time for the polymer solution
t_O	The flow time for pure solvent
R_o	The interaction radios
δ_d	Dispersion parameter
δ_h	Hydrogen bonding parameter
δ_p	Polar parameter
D	Nozzle diameter
De	Deborah number
T_P	The rotating speed for the polymer solution.
T_0	The torque that is required for rotating in the solvent
ϕ	Volume fraction of particles

Abstract

The effect of hydrogen bonding interactions on the drop generation of both acid and hydroxyl-containing polymer solutions is reported showing that polymer chain relaxation can be influenced through the use of appropriate polymer co-solvent interactions for polymers having weight average molecular weight (M_w) < 100 kDa.

Reported for the first time is evidence of flow-induced polymer degradation during inkjet printing for both poly(methylmethacrylate) and polystyrene in good solvent. Polymers having M_w either less than 100 kDa or greater than approximately 1,000 kDa show no evidence of molecular weight degradation. The lower boundary condition is a consequence of low Deborah number imposed by the printhead geometry and the upper boundary condition due to visco-elastic damping. For intermediate molecular weights the effect is greatest at high elongational strain rate and low solution concentration with higher polydispersity polymers being most sensitive to molecular weight degradation. For low polydispersity samples, PDi ≤ 1.3 chain breakage is essentially centro-symmetric induced either by overstretching when the strain rate increases well beyond a critical value, that is the stretching rate is high enough to exceed the rate of relaxation or by turbulence. For higher polydispersity samples, PDi chain breakage is consistent with almost random scission along the chain inferring that the forces required to break the chain are additionally transmitted either by valence bonds, i.e. network chains and junctions or discrete entanglements rather than solely by hydrodynamic interaction.

Preliminary results are presented on the degradation of molecular structure in water of two galactomannan's in water after inkjet printing. Galactommann's are known to form complex H-bonded structures in water and the results are consistent with breaking of the H-bonding structure at low reduced concentration with evidence of main chain breakage at higher reduced concentration , c/c* = 0.25.

Declaration

That no portion of the work referred to in the thesis has been submitted in support of an application for another degree or qualification of this or any other university or other institute of learning.

COPYRIGHT AND OWNERSHIP OF INTECTUAL PROPRTIES RIGHTS

i. The author of this thesis (including any appendices and/or schedules to this thesis) owns certain copyright or related rights in it (the "Copyright") and s/he has given The University of Manchester certain rights to use such Copyright, including for administrative purposes.

ii. Copies of this thesis, either in full or in extracts and whether in hard or electronic copy, may be made **only** in accordance with the Copyright, Designs and Patents Act 1988 (as amended) and regulations issued under it or, where appropriate, in accordance with licensing agreements which the University has from time to time. This page must form part of any such copies made.

iii. The ownership of certain Copyright, patents, designs, trade marks and other intellectual property (the "Intellectual Property") and any reproductions of copyright works in the thesis, for example graphs and tables ("Reproductions"), which may be described in this thesis, may not be owned by the author and may be owned by third parties. Such Intellectual Property and Reproductions cannot and must not be made available for use without the prior written permission of the owner(s) of the relevant Intellectual Property and/or Reproductions.

iv. Further information on the conditions under which disclosure, publication and commercialisation of this thesis, the Copyright and any Intellectual Property and/or Reproductions described in it may take place is available in the University IP Policy (see http://www.campus.manchester.ac.uk/medialibrary/policies/intellectual-property.pdf), in any relevant Thesis restriction declarations deposited in the University Library, The University Library's regulations (see http://www.manchester.ac.uk/library/aboutus/regulations) and in The University's policy on presentation of Theses

ACKNOWLEDGMENT

I would like to give a big thank to my supervisor Prof.S.G. Yeates for his super patience, and his knowledge that was really useful for my PhD thesis. I cannot find any more word tha really more than thank you.

Dr. G. Henry. And Dr.D.Crouch for their real help and good advice in the laboratory, beside that unforgettable fun time

M. Alsohibani. for giving a useful idea and help for Endnote

I would also, thank my parents as family who always support me.

Finally, I have to admit that I will miss a lot OMIC and everybody in the office and hope we will meet one day all the best lovely people.

Chapter One

Introduction

In this chapter the subject of inkjet printing is introduced. The use of and role of polymers in inkjet printing is discussed and the effect of process on polymer chain conformation is highlighted with respect to rheological and polymer chain mechanical stability.

1.1 Introduction

In inkjet printing there are two mechanisms through which drops are generated and positioned, *continuous ink-jet printing* (CIJ) and *drop-on-demand ink-jet printing* (DOD). For CIJ and DOD the individual drop generation process and ink management systems present different challenges and constraints on ink design, making them more or less suitable for the specific application in mind.

1.2 Continuous Inkjet

In continuous inkjet printing, a high-pressure pump directs liquid ink from a reservoir through a gun body where a piezoelectric crystal creates an acoustic wave vibrating at a frequency of between 64 and 160 KHz, causing the stream of liquid to break into droplets via the Rayleigh instability, as in Figure 1.1[1].
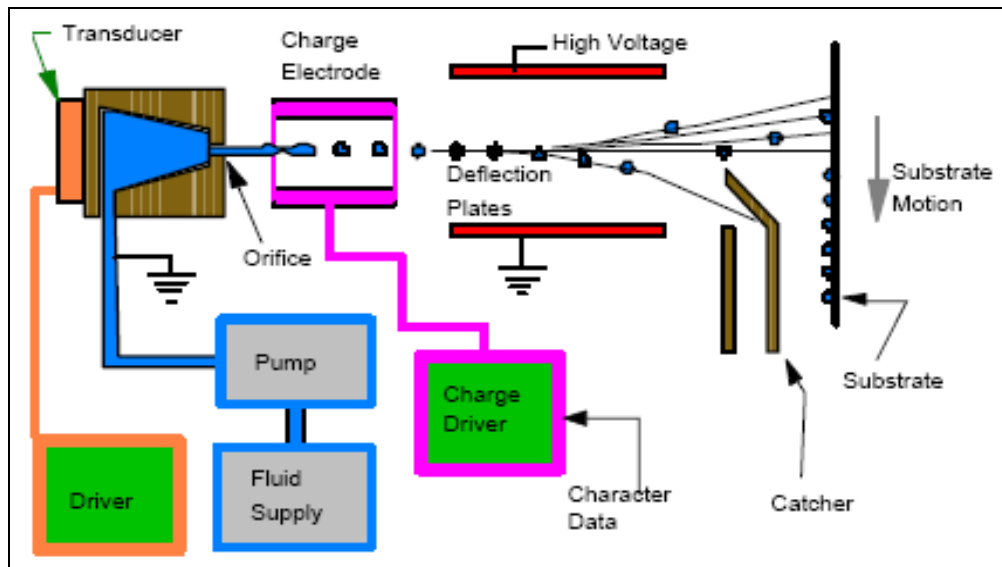
Figure 1.1 Schematic of a continuous type inkjet printing system[2].

The ink droplets, which have conductivity typically in the range CIJ 50–2000 Ω.cm, are then subjected to an electrostatic field created by a charging electrode as they form, the field being varied according to the degree of drop deflection desired. This results in a controlled, variable electrostatic charge on each droplet. Charged droplets are separated by one or more uncharged "guard droplets" to minimize electrostatic repulsion between neighbouring droplets. The charged droplets pass through an electrostatic field and are directed (deflected) by electrostatic deflection plates to print on the receptor material (substrate), or allowed to continue on undeflected to a collection gutter for re-use, whilst the more highly charged droplets are deflected to a greater degree. Only a small fraction of the generated droplets are used for printing, the majority being recycled. Since the non-printed ink is recycled, the ink system requires active solvent regulation to counter solvent evaporation during the time of flight (time between nozzle ejection and gutter recycling), and from the venting process whereby air that is drawn into the gutter along with the unused drops is vented from the reservoir. Viscosity is monitored and a solvent (or solvent blend) is added in order to counteract the solvent loss. The continuous inkjet method is used primarily for commercial marking and coding of products and packages.

Specific ink formulation challenges include:

- Ink stability at high drop generation frequency with elongation shear rates of up to 1,000,000 s^{-1}.

- The ability to recycle ink without loss of jetting performance or final product performance.

- The generation of stable charge through the use of additives such as potassium thiocyanate (0.5 – 2.0 wt-%) which may have a negative effect on final device performance, especially in electronic and biological print applications.

1.3 Thermal Drop on Demand

The majority of thermal drop on demand inkjet (TIJ) printers use print cartridges with a series of tiny electrically-heated chambers constructed by photolithography behind each nozzle[1, 3].

TIJ requires the fluid to have a high vapour pressure and low boiling point, and consequently water-based inks using dyes or pigments are used exclusively, as in Figure 1.2. To produce an image, an electrical current is passed through the heating elements causing a vapour bubble to form in the chamber. When the ink droplet is ejected the heat pulse is removed, causing the bubble to collapse which pulls a further charge of ink into the chamber through a narrow channel attached to an ink reservoir.
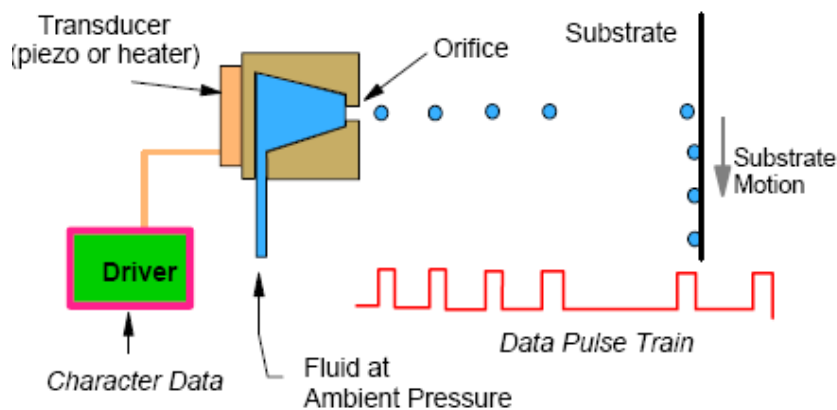
Figure 1.2 Schematic of DOD inkjet printing system[4].

TIJ has found wide utility in both Small Office Home Office (SOHO) and industrial graphics applications, but the effective limitation to water-based inks has limited its use in digital fabrication applications. Specific formulation challenges include formulation of stable inks with respect to kogation[5]- the phenomenon by which ink ingredients are thermally decomposed and deposited on the surface of the heating element – and avoidance of ink dryout at the nozzle plate. More recent designs have been proposed where direct contact between the heater and the ink is

eliminated, thus minimizing kogation issues and extending the range of potential fluids that can be used[6].

1.4   Piezoelectric Drop on Demand

Piezo drop on demand inkjet printers use a piezoelectric material adjacent to the ink chamber behind each nozzle. When a voltage is applied, the piezoelectric material changes shape or size, which generates a pressure pulse in the fluid, forcing from the nozzle a droplet of ink with volumes typically in the range 10–100 pl[7-9]. This is essentially the same mechanism as thermal inkjet but it generates the pressure pulse using a different physical principle[10, 11].

Because the drop generation process imposes fewer design constraints on the ink than does either CIJ or thermal DOD, piezo-DOD has found wide utility in both SOHO and commercial and industrial applications. This ability to print using a wide range of different fluid formulations is the reason why the majority of new digital fabrication applications utilize piezoelectric DOD inkjet head technology[10, 12-17]. In this thesis we are concerned only with piezo-DOD and hence all further discussion will be related to this method.

1.5   Physical Considerations of DOD Droplet Formation

The printing process consists of three distinct stages: drop generation, drop flight, and drop impact. Each of these operations imposes physical limitations both on the ink formulation and the printing process.

In a DOD print head, the pressure pulse that drives drop formation can be generated, as we have seen, either by a piezoelectric actuator or a thermal pulse that creates a vapour bubble. Liquid is contained at the orifice by surface tension and, if the pressure pulse exceeds some critical value, a liquid column protrudes from the orifice with surface tension leading to an unstable neck forming and a drop separating. The timescale for the whole process is of the order of 5–250 µs and is shown schematically in Figure 1.3.

The important physical properties of a droplet-forming fluid are its density, ρ, surface tension, γ, and viscosity, η, commonly grouped in dimensionless form using the Weber number,

$We = v^2 d\rho/\gamma$, and Reynolds number, $Re = vd\gamma/\eta$, where v and d are the fluid velocity and a characteristic length. The Weber number is important in the early stage of drop generation where the interplay of forward inertia and surface tension is important (I) and the Reynolds number in the middle to later stages where the interplay with the viscoelasticity of the ligament is critical (II).
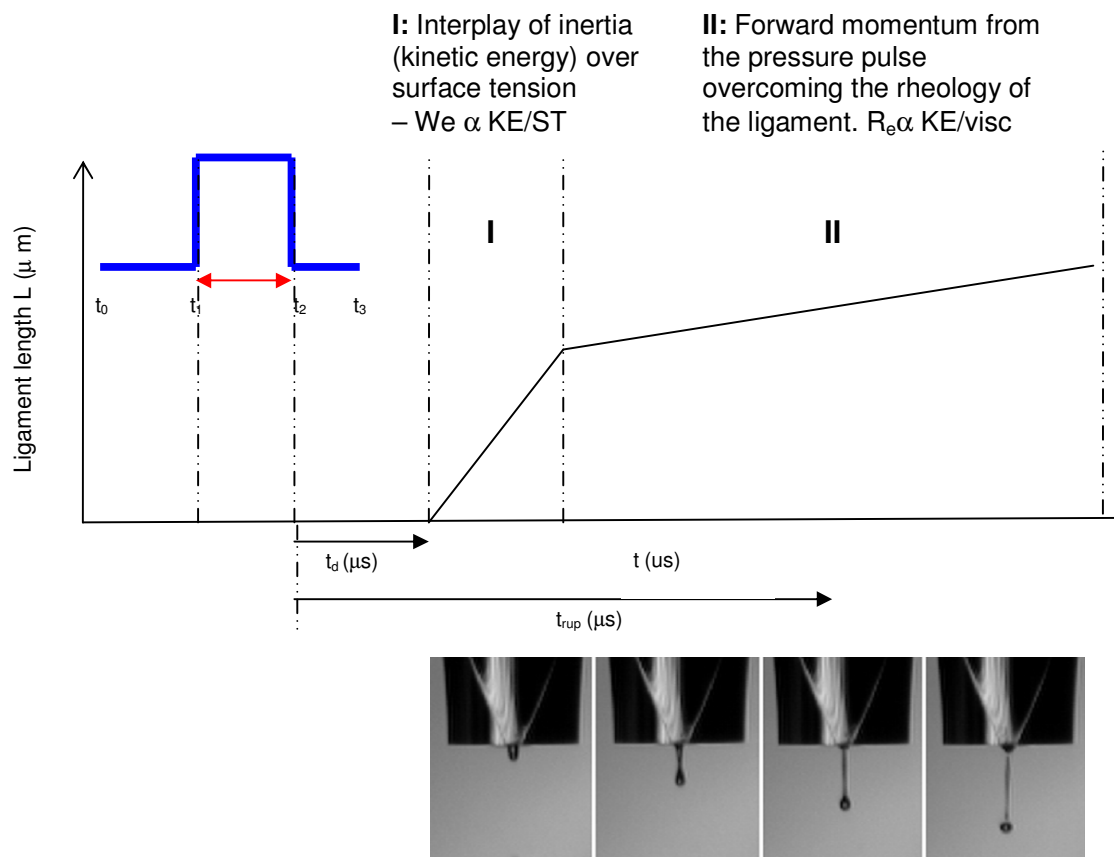
Figure 1.3 Schematic representation of pressure pulse generation and stroboscopically visualized droplet ejection for DOD inkjet

Fromm[8] used the dimensionless Ohnesorge number, $Oh = We^{1/2}/Re$, to remove the velocity dependence of the kinetic energy and calculated that DOD printing should be possible if $Oh < 0.5$ with the drop volume increasing as Oh decreases. Derby and Reis[11] investigated the inkjet printing conditions for a range of different fluids and further explored the influence of Oh through fluid dynamics simulations to define a range $0.1 < Oh < 1$, within which DOD printing is possible. When $Oh > 1$ viscous dissipation within the liquid prevents drop formation, and if $Oh <$

0.1 the balance between surface tension and viscosity results in the liquid breaking into a series of satellite drops rather than a single drop as desired. They found that, for a range of fluids of different physical properties, printing was possible within these limits[18] and that, for a number of different fluids ejected through the same print head, the droplet volume was controlled by the Ohnesorge number[11], consistent with the prediction by Fromm[8]. In practice, systems where *Oh* is much less than 0.1 can be printed although satellites are generated.

A further consideration for inkjet printing is aerodynamic drag on the droplet in flight. This can slow the drop's velocity significantly before impact and also allow random fluctuations in the surrounding atmosphere to deflect a drop away from its desired trajectory, which is especially important where absolute drop placement is critical. Derby showed [19] that the critical value of *Re* will vary from 19.5 for a liquid of viscosity 1 mPa.s to 0.48 for a liquid of viscosity 40 mPa.s.

During the impact process, the drop loses kinetic energy through viscous dissipation and by surface extension. A balance of surface forces defines the final equilibrium of drop shape and substantial oscillations may occur before this is achieved. However, if the impact velocity is too high the drop may splash, thus defining the limiting drop velocity for printing which is strongly dependent on the roughness and porosity of the surface[20-23].

The above considerations define the limits of drop generation, drop flight and drop impact define a parameter space, in terms of the Reynolds and Weber numbers, within which DOD inkjet printing is feasible under normal atmospheric conditions at standard temperature and pressure, as in Figure 1.4[19] . Taking these considerations into account, the optimal range of static values for DOD inkjet printing are typically viscosity (η) lying in the range 2-20 mPa.s and surface tension (γ) in the range 20-50 mN.m^{-1}. It is according to these parameters that inks are initially formulated and specified, being print head specific.
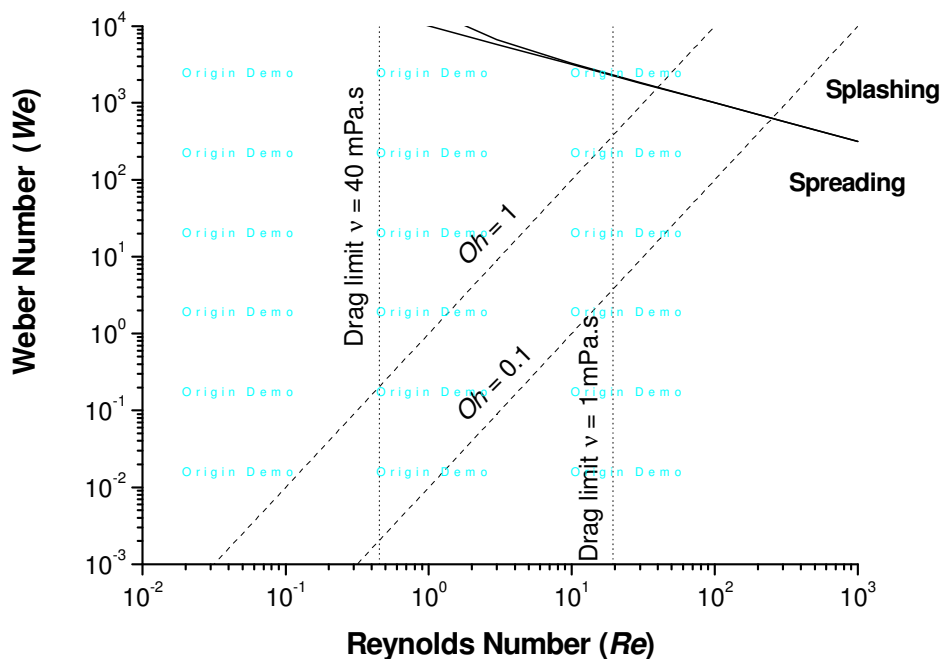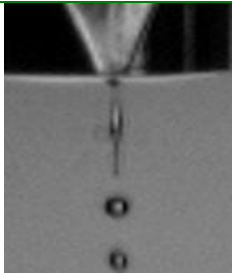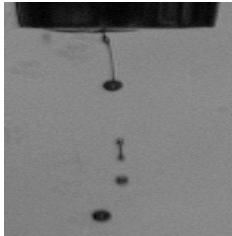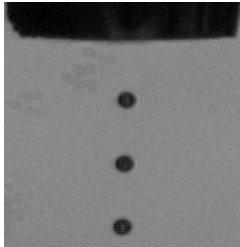
Figure 1.4 Diagram illustrating the region bounded by the Ohnesorge number that defines the limiting region for drop generation in a DOD inkjet print head. Further limits determined by the splashing transition (upper right) and atmospheric drag (vertical lines) for liquids of viscosity 1 mPa.s and 40 mPa.s are indicated[19].

However, given the high elongational shear rates experienced by the ink upon drop generation[22], typically greater than 10^5 s^{-1}, it is the dynamic properties that are most important. It is either difficult or impossible to measure these directly in the laboratory, and consequently direct visualisation of the drop generation process becomes a key aspect in successful ink design[23]. For many digital fabrication opportunities, it is necessary to inkjet print with high molecular weight polymer at a high concentration in order to maximise material throughput and/or functionality. However, the addition of polymer to an ink has a strong impact on the nature of the drop generation and ejection process[24-31].

The influence of added polymer on drop formation and filament break-up has been studied as a function of both concentration, typically in the dilute regime for polyacrylamide[24] [(23)] polyethyleneoxide[25-28,30], polystyrene[3], poly[2-methoxy-5-(2'-ethylhexyloxy)-1,4-phenylenevinylene] (MEH-PPV)[32] and cellulose ester [33].

25

Four different regimes have been observed in inkjet drop generation behaviour as a combined function of concentration and molecular weight, as illustrated in Table 1.1 [23, 24, 29] with regime 3 offering the desired result.

Table 1.1 Details of the four different regimes observed in polymer solution inkjet drop generation behaviour [34]

Regime	Characteristic behaviour	Typical picture
1	The first regime occurs at very low concentrations and/or molecular weight, where a long tail is formed that simultaneously disintegrates along its axis to form several satellite droplets. This regime can often be highly chaotic and irreproducible in nature. Characteristic of the dilute polymer regime.	
2	The second regime occurs upon increasing concentration or molecular weight when only a few satellites appear at the tail's end.	
3	Raising concentration or molecular weight further yields a single droplet without a tail. Characteristic behaviour of dilute to semi-dilute solutions.	
4	At high concentration or molecular weight the polymer solution becomes highly visco-elastic and the droplet does not detach, returning instead into the nozzle. Characteristic of the concentrated regime.	

Rather than consider the polymer concentration within an ink in terms of g/dl it is better to define the reduced concentration as [η].c or c/c*, where c* is the coil overlap concentration, the point at which individual polymer chains in solution are just in contact[33], [η] is the polymer intrinsic viscosity in dl/g, and $c* = 1/[\eta]$ [35]. Regime 3, Table 1.1, is typically observed for reduced concentrations between 0.2 and 1.0 in which relative viscosity scales approximately as c^1, and above which as $c^{15/4}$, as shown in Figure 1.5 for cellulose ester in a good solvent γ-butyrolactone over the range M_w = 6 KDa – 155 KDa[35].

(a)   (b)
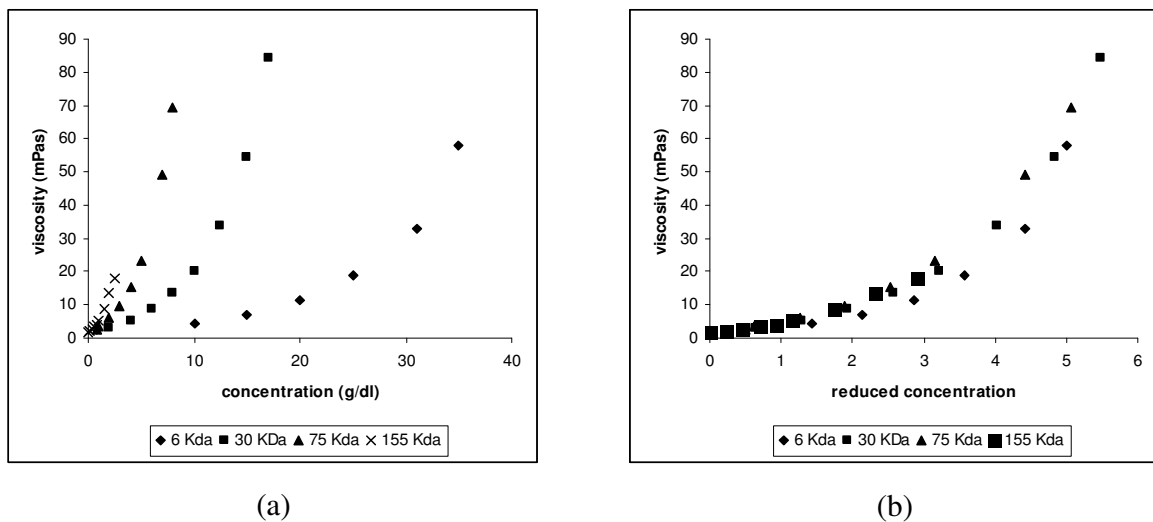
Figure 1.5 Effect of polymer molecular weight and concentration on solution viscosity expressed as (a) g/dl and (b) reduced concentration c/c* for cellulose ester in γ-butyrolactone[35].

Drop break-up behaviour of polymer-containing inks is not simply a function of the effect of polymer concentration on the low shear, static, solution viscosity typically measured by standard laboratory techniques. It has been found that drop break-up behaviour is strongly related to the strain hardening resulting from the presence of polymer at a high strain rate [23, 24, 36-40]. The micro rheological explanation for strain hardening is the sudden transition of the polymer chain from a coiled to a stretched state, which is accompanied by a strong increase of the hydrodynamic drag which must relax over the timescale of the drop formation process as shown schematically in Figure 1.6.
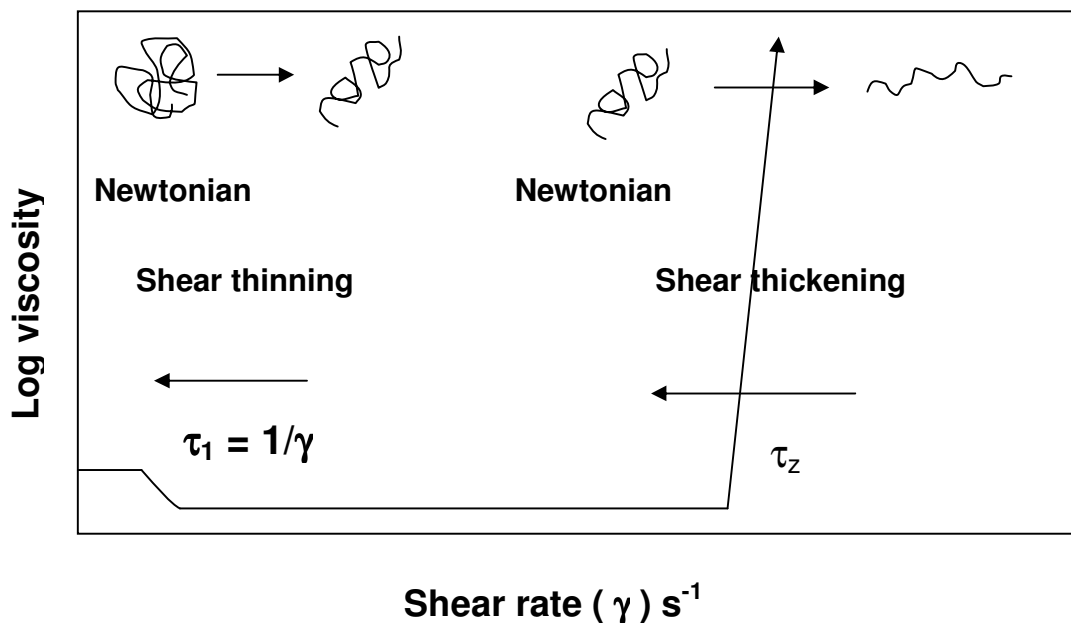
Shear rate (γ) s^{-1}

Figure 1.6 Schematic representation of the effect of extensional shear rate on polymer chain conformation and solution viscosity.

The coil-stretch transition occurs for linear polymers at a critical strain rate (ε_{crit}) where the rate of deformation of the chain exceeds its rate of relaxation so that it passes from a slightly distorted random coil to an extended state. This critical condition is achieved when the critical Weissenberg-number ($W_{ecrit} = \varepsilon_{crit}.\tau_z$) > 0.5, where τ_z denotes the longest relaxation time[29, 36]. The longest polymer chain relaxation time is typically described by the Zimm non-free-draining relaxation time, λz[13, 40] $\tau_1 = \eta_s[\eta]M_w/RT$, where η_s is the viscosity of the solvent, $[\eta]$ is the intrinsic viscosity of the polymer solution, and M_w is the average molecular weight. The apparent universality of Zimm behaviour is believed to arise either from the fact that elongational flow experiments only probe the dynamics of the partially stretched coil[38] or that the coil-stretch transition is essentially non-equilibrium, since molecules only experience a finite residence time in the flow field [39]. For the inkjet process, the strain rate at the nozzle tip is > 50,000 s^{-1}, this critical condition being typically exceeded for all polymers having Mw > 20,000 Da at the pinch region, which is the point at which the ligament is attached to the nozzle tip meniscus [26] as in Figure 1.7.
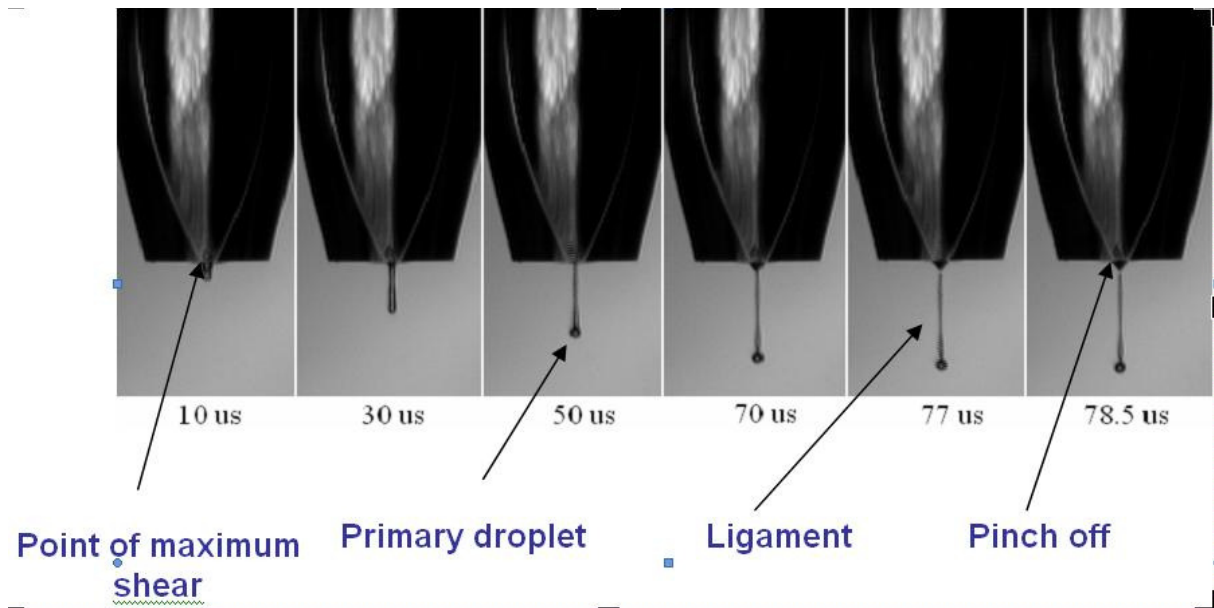
Figure 1.7 Change in polymer coil conformation during inkjet drop generation for cellulose ester in γ-butyrolactone at c/c* = 0.6 using a MicroFab print head[31, 35].

1.6 Role of polymers in inkjet printing

The use of polymeric additives in aqueous ink formulations is widely reported. Examples include:

- Use of low concentrations, 100 ppm, of high molecular weight water-soluble polymers such as polyethylene oxide and polyacrylamide, both as drag reduction agents and to control droplet generation.

- Use of low molar mass water-soluble dispersible polymers such as styrene acrylates[41], aqueous polyurethanes[42], cellulose esters[43] and polyesters[44] at 0.1 – 5 wt-% as binders to improve image permanence on the substrate, especially with respect to water and humidity. An example of the use of reactive polymer binders is in the inkjet fabrication of liquid crystal display colour filters[45, 46].

- As pigment dispersants and stabilizers[47, 48].

More recently, solvent based inks have come to the fore for a number of applications. These inks, based upon MEK, short chain glycols, lactates and alcohols, are widely used in, for example, industrial marking using CIJ[1, 3]. However, the increasing realisation and utilisation of inkjet printing as a fabrication tool, primarily driven by the electronics industry, has necessitated the use of increasingly aggressive solvents such as toluene, anisole, tetralin and other substituted aromatics[49]. This has been driven by the need to form low viscosity solutions of high molecular weight polymers such as polyphenylene-vinylenes, polyflourenes[50,51] and poly 3-hexylthiophene[52] structured carbons including carbon nanotubes[53], as well as low molar mass conjugated molecules such as PCBM[54] and substituted polyacenes[55]. The move to more aggressive solvents has not been without its challenges, as these can interact in a negative manner with the materials used in construction of the print head. Coupled with the additional challenges of exceptional drop uniformity and directionality, this has brought about the development of new families of print heads. The formulations are generally 'simple', comprising solute (functional material) and a mixture of solvents. Solvent selection is critical and must fulfil a number of primary functions:

- Must be a good solvent for the solute and stable to precipitation or gelation over extended periods.

- Must not have any unfavourable interactions with the materials used in construction of the print head.

- Must be stable to drying out of the ink at the nozzle to avoid print failure. For this reason, solvents having boiling points greater than 130°C tend to be preferred, with anisole (154°C), mesitylene (164°C), ortho-dichlorobenzene (180°C) and tetralin (207°C) frequently being cited.

- Must dry in such a way that no solvent is retained within the printed feature, which could result in downgraded performance, and avoid undesired print phenomena such as pinholing and/or coffee staining[56]. For these reasons, there tends to be a upper boiling point limit of around 210°C, with the use of binary mixtures of low and high boiling point solvents to eliminate the coffee staining effect[57, 58].

The use of thermo-cleavable solvents for printing conjugated polymers in solar cell applications has recently being reported; these combine the benefits of low volatility at room temperature and thermal decomposition at 130°C to 180°C to low boiling point highly volatile products[59].

1.7 Applications in Electronic Devices

Patterning is a vital part of the development and future production of organic electronic devices, and as such inkjet printing is ideally suited for a number of process steps on account of being additive and maskless in nature. Here we discuss a number of the material sets used, with specific reference to the relationship between material properties and inkjet performance.

1.7.1 Organic Conducting Polymers

The use of conductive poly(4-ethylenedioxythiophene)-poly(styrenesulfonate) (PEDOT-PSS) blends is widely used and reported in the fabrication of organic thin film transistors (OTFT), organic solar cells, organic light emitting displays (OLED) and sensors. The sulfonyl groups on PSS are deprotonated and carry a negative charge, whilst PEDOT carries a positive charge together with the charged polymers forming a polymeric salt which is dispersible in water[60].

Dependent upon the specific formulation, typically through the use of high boiling point solvents like methylpyrrolidone, dimethylsulfoxide, sorbitol and glycerol, the conductivity of the resultant transparent polymer film can vary over several orders of magnitude from 10^{-4} to 10^{3} S/cm, making it suitable both as a replacement for indium tin oxide (ITO) and for printing conducting features such as interconnects[61, 62]. In order to spatially modify the conductivity still further, the inkjet printing of hydrogen peroxide ink on to a PEDOT:PSS anode, in order to alter its oxidation state, has been reported[63]. This ability to spatially modify the local conductivity of the PEDOT:PSS layer opens up the possibility of electrical greyscale imaging capability [64]. PEDOT:PSS layers have been deposited by inkjet for a number of sensor applications, exploiting the change in conductivity as a function of external stimuli including humidity[65] and strain[66].

The use of PEDOT:PSS as printed source, drain and gate electrodes in OTFTs has been reported[67-69] , although direct inkjet printing leads to large scale features where the critical

dimensions are typically > 10 µm. An innovative way of increasing both resolution and drop placement is the sequential printing of a hydrophobically modified PEDOT:PSS line, either by surfactant or carbon tetrafuoride plasma, followed by a hydrophilic PEDOT:PSS ink which dewets from the first feature to give a channel down to 250nm[70] PEDOT:PSS as the conductive anode in OLED displays. This has been extensively reported, both to modify the ITO work function and to planarise the anode surface to avoid shorts and black spots[71].

Recent reports have demonstrated the use of inkjet in the fabrication of organic solar cells [72, 73] and highlighted the importance obtaining the correct PEDOT:PSS layer morphology for enhanced performance. PEDOT:PSS inks with additives of glycerol and surfactant show improved surface morphology and high conductivity, resulting in enhanced photovoltaic performance. Using optimized ink formulation and print patterns, solar cell efficiencies greater than 3.5% have been reported[72].

Whilst there is a large volume of literature on the inkjet printing of PEDOT:PSS, proportionately less has been reported on the use of water-dispersible polyaniline (PANI), which may be due either to the lack of easy and reliable procedures for preparing the high quality nanometer-size particles required for robust inkjet printing or the need for highly corrosive and acidic dopants such as dodecylbenzenesulfonic acid (DBSA)[74] which, with the advent of more robust print heads, are only now becoming feasible. The use of PANI-PSS has been reported as a chemical sensor for ammonia, showing enhanced response when compared with conventional PANI-based chemical sensors[75, 76].

More recently, the inkjet printing of carbon nanotubes, both as conductors[77,78] and as the semiconductor in an OTFT, has been reported. These inks consist of a dispersion of carbon nanotubes in solvents such as N-methyl--2-pyrrolidone and dimethylformamide, which have been shown to partially break up the strong van der Waals forces of attraction between individual carbon nanotubes under ultrasonic treatment, enabling the formulation of stable inks. The use of additional agents such as single strand DNA has been reported to aid further dispersion[79].

1.7.2 Conjugated organic semiconductors

Many early developments in high resolution inkjet printing using solvent based inks were driven by the desire to fabricate organic light emitting displays. The desire to print using highpolymers molecular weight conjugated polymers such as polyphenylene-vinylenes and polyflourenes required print heads to be developed which not only had tolerance to aggressive solvents but, at the same time, also had exceptional drop to drop uniformity coupled with high absolute print accuracy[53]. These approaches have now been extended to the printing of both polymeric[80] and small molecule organic semiconductors[81]. In all cases, once robust droplet generation is obtained and high accuracy drop placement is achieved, the need for uniform pinhole free film formation is required, which can be achieved both through formulation with solvent mixtures[56, 57] and by considering droplet substrate interaction.

When printing conjugated materials, and in particular polymers, inter-chain interactions in solution are important as these can lead to aggregation in solution and an increase in solution viscosity at low concentration coupled with undesirable viscoelastic behaviour when printing as reported for MEH-PPV[58]. This can be overcome using mild ultrasonic treatment which can partially break down the physical aggregates, but care needs to be observed if main chain degradation is to be avoided. Recently, the inkjet printing of water-based dispersions of MEH-PPV with high molecular weight polyethylene oxide has been reported in order to overcome some of the issues with printing solutions[82].

High performance small molecule semiconductors are currently being developed for OTFT applications. These materials are generally soluble in strong aromatic solvents such as dichlorobenzene, up to a few weight percent[81]. These materials form high ly crystalline thin films and control of the evaporation rate of the solvent(s) is critical in ensuring uniformity across a given device[83]. Blends of 1,2,4-trichlorobenzene and cyclohexanol have been shown to be particularly effective at controlling viscosity. Low viscosity is often an issue, as is device uniformity[84]. Similarly, when printing the active p-n hetero junction layer in a organic solar cell by use of a mixture of ortho-dichlorobenzene and mesitylene, it is possible to print PCBM, P3HT having the correct morphology giving device efficiency of around 3.5%[73].

1.7.3 Printing of Natural Polymers

The requirements of a large number of research groups and commercial concerns are the reason for the adoption that was made of inkjet printing of biomaterials. Printing is a very straightforward process that is reasonably priced and its best strength is that it dispenses small amounts of liquid, usually in picolitres. The low volumes allowed researchers to use valuable proteins such as purified enzymes and it also allowed them to be placed in the desired locations. Inkjet, being a non- impact printing technique, helps to reduce contamination when dealing with purified materials. Another strong characteristic of the printing is markless patterning technology. The material can be accurately positioned without recourse to a number of patterning steps. The reduction of the number of process steps makes the technique cheaper and it reduces waste. The first biosensors were prepared by screen printing, which meant that the sensitive materials were wasted due to them being coated on the screen. Screen printing requires one physical swap between the screens. In inkjet printing, the user is able to switch between computer programmers whereas in screen printing it needs to be cleaned and stored.

Inkjet printing has proven to be a very effective tool for patterning and manufacture of biosensor structures, with direct printing on enzymes and living cells. Glucose biosensors are used to monitor the blood sugar levels in patients who suffer from diabetes. Glucose oxidase (GOx) is immobilized on the electrode in order to measure the glucose levels in the blood. Early methods used to manufacture these sensors included pipetting and biodotting, but they are limited methods in that they both offer fluid volumes in the region of microlitres or nanolitres[85]. In 1987 the first patent for an enzyme-based biosensor by inkjet printing[86-88] was granted.

1.7.4 Printing living cells

Strategies have been reported that immobilize proteins under cell culture conditions for sufficient time to carry out cell biology experiments. For example, Boland has used thermal DOD inkjet for cell deposition[89] , reporting that less than 3% of the cell population was lysed during printing and that less than 15% was lysed during the preparation of the fluid prior to the printing process. Nakamura et al have printed bovine vascular endothelial cells by using DOD[90]. Survival and viability of the human fibroblast cell membrane under print conditions remains, however, an

ongoing concern[4, 11]. Cell death rates at drive frequencies and voltages just sufficient for printing with a low elongational shear rate nozzle were found to be statistically indistinguishable from the unprinted control cell population at less than 2%, with increasing drive voltage resulting in increased kills up to 5%[91].
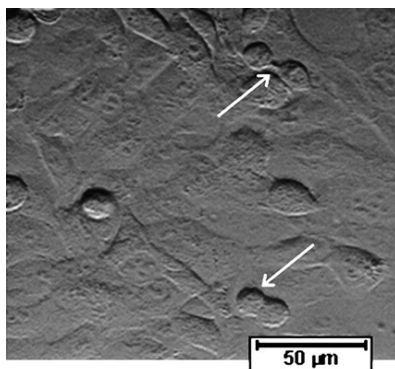
Figure 1.8 Human fibrosarcoma showing viability and division after inkjet printing[91]

1.8 Polymer degradation in elongational flow

Flow induced deformations can also lead to irreversible change in the structure of a complex fluid. The mechanical degradation of polymers in elongational flow fields has long been recognised and can lead to a reduction in average polymer molecular weight[92-94]. The passage through an elongational flow field exerts strong hydrodynamic forces upon a coiled polymer molecule in solution as it stretches orients and extends in the direction of flow. If the elongational forces on the molecule are sufficiently strong, and the rate of chain stretching far exceeds the rate of chain relaxation, the polymer backbone can be broken[95]. The precise mechanism of chain scission is not fully understood, but scientists suggest that the forces acting upon the molecule will be greatest at its centre, leading to chain scission near the centre [95]. As previously discussed, it has been known for some time that polymers can undergo extension in an elongational flow under certain critical conditions[92]. For instance, Keller and Rabin used a planar elongational flow field to study the degradation of stretched polymer molecules in a strong extensional flow field. In their study, two different high molecular weight polymers (atactic polystyrene and polyethylene oxide) were degraded, showing that the polymer chain scission was close to the centre of the molecules.

35

Such experiments have been performed in geometries that exert either a long residence time in the elongational flow or where the sample is exposed to a number of short residence time exposures. We can consider the inkjet printhead as a short residence time contraction in that the fluid is forced from the large diameter ink chamber through the nozzle constriction. Typically a Microfab glass capillary represents a constriction ratio on the order of 10:1, whist for the Dimatix head the constriction ratio is unknown but believed to be of the same order of magnitude. Based upon average measured drop velocities the residence time of the fluid in the constriction is short, on the order of 10 μs, after which the fluid begins to relax as the ligament and droplet form. To date there have been no reported observations of molecular weight degradation during inkjet printing.

1.9 Aims of the Project

In this thesis, two aspects of inkjet printing with polymer-containing fluids are considered.

1. The effect of hydrogen bonding interactions on the drop generation of both acid and hydroxyl-containing polymer solutions. To understand whether polymer chain relaxation can be influenced through the use of appropriate hydrogen bonding co-solvent interactions.

2. Investigation into whether molecular weight degradation of synthetic and natural polymer can occur as a consequence of inkjet printing.

1.10 References

1. Cameron, N. L., *Coatings Technology Handbook*. 3rd ed.; **2006**; Vol. 25/1-24/4.
2. MicroFab technote. http://www.microfab.com/equipment/technotes/technote99-01.pdf. (22/8/2008),
3. Dawson, T., *Colourage* **2004,** 51, (10), 75.
4. Saunders, R. E.; Gough, J. E.; Derby, B., *Biomaterials* **2008,** 29, (2), 193-203.
5. Shirota, K. S., M. ; Suga, Y. ; Eida, T. , *Recent Progress in Inkjet Technologies*. **1996**; Vol. 218.
6. Sen, A., *Journal of Micromechanics and Microengineering* **2007,** 17, (8), 1420.
7. Dijksman, J. F., *Journal of Fluid Mechanics* **1984,** 139, (1), 173-191.
8. Fromm, J. E., *IBM Journal of Research and Development* **1984,** 28, (3), 322-333.
9. Tekin, E.; Smith, P. J.; Schubert, U. S., *Soft Matter* **2008,** 4, (4), 703-713.
10. Shin, D. Y.; Grassia, P.; Derby, B., *Journal of the Acoustical Society of America* **2003,** 114, (3), 1314-1321.
11. Reis, N.; Ainsley, C.; Derby, B., *Journal of Applied Physics* **2005,** 97, (9), 1-6.
12. Calvert, P., *Chemistry of Materials* **2001,** 13, (10), 3299-3305.
13. de Gans, B. J.; Duineveld, P. C.; Schubert, U. S., *Advanced Materials* **2004,** 16, (3), 203-213.
14. Böhmer, M. R.; Schroeders, R.; Steenbakkers, J. A. M.; de Winter, S. H. P. M.; Duineveld, P. A.; Lub, J.; Nijssen, W. P. M.; Pikkemaat, J. A.; Stapert, H. R., *Colloids and Surfaces A: Physicochemical and Engineering Aspects* **2006,** 289, (1-3), 96-104.
15. Chang, C.-J.; Tzeng, H.-Y., *Polymer* **2006,** 47, (26), 8536-8547.
16. Xue, C.-H.; Shi, M.-M.; Chen, H.-Z.; Wu, G.; Wang, M., *Colloids and Surfaces A: Physicochemical and Engineering Aspects* **2006,** 287, (1-3), 147-152.
17. Dijksman, J. F.; Duineveld, P. C.; Hack, M. J. J.; Pierik, A.; Rensen, J.; Rubingh, J. E.; Schram, I.; Vernhout, M. M., *J. Mater. Chem. FIELD Full Journal Title:Journal of Materials Chemistry* **2007,** 17, (6), 511-522.
18. Derby, B.; Reis, N., *MRS Bulletin* **2003,** 28, (11), 815-818.
19. Stringer, J.; Derby, B., *Journal of the European Ceramic Society* **2009,** 29, (5), 913-918.
20. Mundo, C.; Sommerfeld, M.; Tropea, C., *International Journal of Multiphase Flow* **1995,** 21, (2), 151-173.
21. Wu, Z.-N., *Probabilistic Engineering Mechanics* **2003,** 18, (3), 241-249.
22. Xu, L.; Zhang, W. W.; Nagel, S. R., *Physical Review Letters* **2005,** 94, (18).
23. Hoath, S. D.; Hutchings, I. M.; Martin, G. D.; Tuladhar, T. R.; Mackley, M. R.; Vadillo, D., *Journal of Imaging Science and Technology* **2009,** 53, (4), 041208.
24. Meyer, J. D. B., A. A. ;Rozkhov, A. N. ;, In *Int. Conf. on Digital Printing Technologies*, 1997; Vol. 13, p 675.
25. Mun, R. P., *Journal of Non-Newtonian Fluid Mechanics* **1998,** 74, (1-3), 285-297.
26. Christanti, Y.; Walker, L. M., *Journal of Non-Newtonian Fluid Mechanics* **2001,** 100, (1-3), 9-26.
27. Christanti, Y.; Walker, L. M., *Journal of Rheology* **2002,** 46, (3), 733-748.
28. Cooper-White, J. J.; Fagan, J. E.; Tirtaatmadja, V.; Lester, D. R.; Boger, D. V., *Journal of Non-Newtonian Fluid Mechanics* **2002,** 106, (1), 29-59.

29.   De Gans, B. J.; Kazancioglu, E.; Meyer, W.; Schubert, U. S., *Macromolecular Rapid Communications* **2004,** 25, (1), 292-296.

30.   Shore, H. J.; Harrison, G. M., *Physics of Fluids* **2005,** 17, (3).

31.   Xu, D., *Journal of materials chemistry* **2007,** 17, (46), 4902-4907.

32.   Tekin, E., *Advanced Functional Materials* **2007,** 17, (2), 277-284.

33.   Hamley, I. W., *Introduction to Soft Matter: Synthetic and Biological Self-Assembling Materials*. First Edition ed.; 2007.

34.   Xu, D. Inkjet deposited conductive Tracks via Electroless Deposition. PhD, University of Manchester, 2009.

35.   Burke, J., AIC Book and Paper Group Annual. **1984,** 3, 13-58.

36.   De Gennes, P. G., *The Journal of Chemical Physics* **1974**, 5030-5042.

37.   Peng, S. T. J., *Japanese journal of applied physics* **1981,** 52, (10), 5988-5993.

38.   Rabin, Y., *J. Polym. Sci., Polym. Lett. Ed. FIELD Full Journal Title:Journal of Polymer Science, Polymer Letters Edition* **1985,** 23, (1), 11-13.

39.   Rabin, Y., *In Polymer-Flow Interaction*. AIP: New York, 1985.

40.   Doi, M. R., S.F,, *The Theory of Polymer Dynamics,*. First ed.; Oxford University Press: 1986.

41.   Merrington, J.; Yeates, S. G.; Hodge, P.; Christian, P., *Journal of materials chemistry* **2008,** 18, (2), 182-189.

42.   Sarkisian, G. M. US 2007/0225401, 2007.

43.   Xu, D.; Sanchex-Romaguera, X.; Barbosa, S.; Travis, W.; de Wit, J.; Swan, P.; Yeates, S. G. Cellulose Esters and Solus 2100 Performance Additive in Ink Jet Application. AN 2008:777525, 2008.

44.   Pears, D. A. GB 2351292 A1, 2000.

45.   Koo, H. S.; Pan, P. C.; Kawai, T.; Chen, M.; Wu, F. M.; Liu, Y. T.; Chang, S. J., *Applied Physics Letters* **2006,** 88, (11).

46.   Shin, D. Y.; Smith, P. J., *Journal of Applied Physics* **2008,** 103, (11).

47.   Merrington, J.; Hodge, P.; Yeates, S., *Macromolecular Rapid Communications* **2006,** 27, (11), 835-840.

48.   Pedrosa, J. M. L.; Bradley, M., *Pigm. Resin Technol. FIELD Full Journal Title:Pigment & Resin Technology* **2008,** 37, (3), 131-139.

49.   Gregory, P., *High-Technology Applications of Organic Colorants* First Edition ed.; Springer: 1991.

50.   Kobayashi, H.; Kanbe, S.; Seki, S.; Kigchi, H.; Kimura, M.; Yudasaka, I.; Miyashita, S.; Shimoda, T.; Towns, C. R.; Burroughes, J. H.; Friend, R. H., *Synthetic Metals* **2000,** 111, 125-128.

51.   Steiger, J.; Heun, S.; Tallant, N., *J. Imaging Sci. Technol. FIELD Full Journal Title:Journal of Imaging Science and Technology* **2003,** 47, (6), 473-478.

52.   Speakman, S. P.; Rozenberg, G. G.; Clay, K. J.; Milne, W. I.; Ille, A.; Gardner, I. A.; Bresler, E.; Steinke, J. H. G., *Organic Electronics: physics, materials, applications* **2001,** 2, (2), 65-73.

53.   Hopkins, A. R.; Kruk, N. A.; Lipeles, R. A., *Surface and Coatings Technology* **2007,** 202, (4-7), 1282-1286.

54.   Hoth, C. N.; Choulis, S. A.; Schilinsky, P.; Brabec, C. J., *Journal of materials chemistry* **2009,** 19, (30), 5398-5404.

55.   Anthony, J. E.; Eaton, D. L.; Parkin, S. R., *Organic Letters* **2002,** 4, (1), 15-18.

56.   Deegan, R. D.; Bakajin, O.; Dupont, T. F.; Huber, G.; Nagel, S. R.; Witten, T. A., *Nature* **1997,** 389, (6653), 827-829.

57.   De Gans, B. J.; Schubert, U. S., *Langmuir* **2004,** 20, (18), 7789-7793.

58.   Tekin, E.; De Gans, B. J.; Schubert, U. S., *Journal of materials chemistry* **2004,** 14, (17), 2627-2632.

59.   JÃ¸rgensen, M.; Hagemann, O.; Alstrup, J.; Krebs, F. C., *Solar Energy Materials and Solar Cells* **2009,** 93, (4), 413-421.

60.   Yuka, Y. J., G.E. , Handbook of Conducting Polymers. In 3rd Edition ed.; 2007; Vol. 2.

61.   LÃ³pez, M. A.; SÃ¡nchez, J. C.; Estrada, M. In Proceedings of the 7th International Caribbean Conference on Devices, Circuits and Systems, ICCDCS, 2008; 2008.

62.   Ouyang, J.; Chu, C. W.; Chen, F. C.; Xu, Q.; Yang, Y., *Advanced Functional Materials* **2005,** 15, (2), 203-208.

63.   Ouyang, J.; Xu, Q.; Chu, C. W.; Yang, Y.; Li, G.; Shinar, J., *Polymer* **2004,** 45, (25), 8443-8450.

64.   Yoshioka, Y.; Jabbour, G. E., *Advanced Materials* **2006,** 18, (10), 1307-1312.

65.   Yoshioka, Y.; Calvert, P. D.; Jabbour, G. E., *Macromolecular Rapid Communications* **2005,** 26, (4), 238-246.

66.   Mabrook, M. F.; Pearson, C.; Petty, M. C., *IEEE Sensors Journal* **2006,** 6, (6), 1435-1443.

67.   Zhang, X. H.; Lee, S. M.; Domercq, B.; Kippelen, B., *Applied Physics Letters* **2008,** 92, (24).

68.   Sawhney, A.; Agrawal, A.; Lo, T. C.; Patra, P. K.; Chen, C. H.; Calvert, P., *AATCC Review* **2007,** 7, (6), 42-46.

69.   Gohda, T.; Kobayashi, Y.; Okano, K.; Inoue, S.; Okamoto, K.; Hashimoto, S.; Yamamoto, E.; Morita, H.; Mitsui, S.; Koden, M. In Digest of Technical Papers - SID International Symposium, 2006; 2006; pp 1742-1745.

70.   Burns, S. E.; Cain, P.; Mills, J.; Wang, J.; Sirringhaus, H., *MRS Bulletin* **2003,** 28, (11), 829-834.

71.   Shimoda, T.; Morii, K.; Seki, S.; Kiguchi, H., *MRS Bulletin* **2003,** 28, (11), 821-827.

72.   Aernouts, T.; Aleksandrov, T.; Girotto, C.; Genoe, J.; Poortmans, J., *Applied Physics Letters* **2008,** 92, (3).

73.   Hoth, C. N.; Choulis, S. A.; Schilinsky, P.; Brabec, C. J., *Advanced Materials* **2007,** 19, (22), 3973-3978.

74.   Steirer, K. X.; Berry, J. J.; Reese, M. O.; van Hest, M. F. A. M.; Miedaner, A.; Liberatore, M. W.; Collins, R. T.; Ginley, D. S., *Thin Solid Films* **2009,** 517, (8), 2781-2786.

75.   Ngamna, O.; Morrin, A.; Killard, A. J.; Moulton, S. E.; Smyth, M. R.; Wallace, G. G., *Langmuir* **2007,** 23, (16), 8569-8574.

76.   Jang, J.; Ha, J.; Cho, J., *Advanced Materials* **2007,** 19, (13), 1772-1775.

77.   Cho, J. J., J. , *PMSE Preprints* **2008,** 98, 432.

78.   KordÃ¡s, K.; Mustonen, T.; TÃ³th, G.; Jantunen, H.; Lajunen, M.; Soldano, C.; Talapatra, S.; Kar, S.; Vajtai, R.; Ajayan, P. M., *Small* **2006,** 2, (8-9), 1021-1025.

79.   Beecher, P.; Servati, P.; Rozhin, A.; Colli, A.; Scardaci, V.; Pisana, S.; Hasan, T.; Flewitt, A. J.; Robertson, J.; Hsieh, G. W.; Li, F. M.; Nathan, A.; Ferrari, A. C.; Milne, W. I., *Journal of Applied Physics* **2007,** 102, (4).

80.   Vulto, S. I. E.; Buechel, M.; Duineveld, P. C.; Dijksman, F.; Hack, M.; Kilitziraki, M.; de Kok, M. M.; Meulenkamp, E. A.; Rubingh, J.-E. J. M.; van de Weijer, P.; de Winter, S. H., *Proc.*

SPIE-Int. Soc. Opt. Eng. FIELD Full Journal Title:Proceedings of SPIE-The International Society for Optical Engineering **2004,** 5214, (Organic Light-Emitting Materials and Devices VII), 40-49.

81.   Barret, M.; Sanaur, S.; Collot, P., *Organic Electronics: physics, materials, applications* **2008,** 9, (6), 1093-1100.

82.   Llorente, G. R.; Dufourg-Madec, M. B.; Crouch, D. J.; Pritchard, R. G.; Ogier, S.; Yeates, S. G., *Chemical Communications* **2009**, (21), 3059-3061.

83.   Lim, J. A.; Lee, W. H.; Kwak, D.; Cho, K., *Langmuir* **2009,** 25, (9), 5404-5410.

84.   Choi, M. H.; Lee, S. H.; Han, S. H.; Kim, Y. H.; Choo, D. J.; Jang, J.; Kwon, S. K. In Digest of Technical Papers - SID International Symposium, 2008; 2008; pp 440-443.

85.   Tianming Wang, C. C., and Brian Derby,; . *the Electrochemical Society* **2008,** 16, (11), 15-20.

86.   Miyahara, Y.; Moriizumi, T.; Ichimura, K., *Sensors and Actuators* **1985,** 7, (1), 1-10.

87.   Kuriyama, T. 1988.

88.   Delaney, J. T.; Smith, P. J.; Schubert, U. S., *Soft Matter* **2009,** 5, (24), 4866-4877.

89.   Xu, T.; Jin, J.; Gregory, C.; Hickman, J. J.; Boland, T., *Biomaterials* **2005,** 26, (1), 93-99.

90.   Nakamura, M.; Kobayashi, A.; Takagi, F.; Watanabe, A.; Hiruma, Y.; Ohuchi, K.; Iwasaki, Y.; Horie, M.; Morita, I.; Takatani, S., *Tissue Engineering* **2005,** 11, (11-12), 1658-1666.

91.   Derby, B., *Journal of materials chemistry* **2008,** 18, (47), 5717-5721.

92.   Carrington, S. P.; Tatham, J. P.; Odell, J. A.; SÃ¡ez, A. E., *Polymer* **1997,** 38, (16), 4151-4164.

93.   Teng, W. D.; Huneiti, Z. A.; Machowski, W.; Evans, J. R. G.; Edirisinghe, M. J.; Balachandran, W., *Journal of Materials Science Letters* **1997,** 16, (12), 1017-1019.

94.   Buchholz, B. A.; Zahn, J. M.; Kenward, M.; Slater, G. W.; Barron, A. E., *Polymer* **2004,** 45, (4), 1223-1234.

95.   Odell, J. A.; Keller, A.; Rabin, Y., *The Journal of Chemical Physics* **1988,** 88, (6), 4022-4028.

Chapter Two

Experimental Methods

2.1 Determination of Polymer Solvent Solubility

The solubility characteristic of the polymers used were determined by preparing 1 wt.-% solutions in a range of common solvents at 25°C and visually assessing solubility after 1 hour and after 24 hours, Table 2.1. These where then classified as either soluble, partially soluble, gel or insoluble. Utilizing standard Teas notation[1] ernary plots for each polymer were generated to identify parameter space where the polymers were most soluble. It is acknowledged that the construction of the Teas graph is based on the hypothetical assumption that all materials have the same Hildebrand value[1-4]. Whilst this is not the case the approach it is an accurate and useful tool by which solubility data can be obtained. After that, they were classified as either soluble, partially soluble, gel or insoluble. Data was recorded as: ++ Soluble immediately, + Soluble after 24 hours, G Gel after 24 hours, - Insoluble after 24 hours.

Table 2.1 Percentage solubility parameters of solvents used in this project

	Boiling Point (C)	Flash Point (C)	Solubility parameter	Percentage Hansen dispersion	Percentage Hansen polarity	Percentage Hansen hydrogen bonding
Cyclohexane	80.7	-18	16.6	98.6	0	1.4
Mesitylene	163	44	17.7	86.7	4.8	8.5
Xylene	138	27	17.9	86.6	4.4	9
Toluene	111	-93	18.1	86.8	3.6	9.6
Ethyl acetate	77	-3	18.1	25.4	18.9	25.4
2 Butanone	80	-3	19.0	52.9	30	17.1
Anisole	154	51	19.5	61.9	14.4	23.7
Acetone	56	-17	20.0	47.1	31.5	21.4
Dichloromethane	40		20.2	59.5	20.6	19.9
Cyclopentanone	130.5	30	20.4	57.7	24.4	17.8
Ethylene glycol butyl ether	169		20.7	47.7	15.4	36.9
2-Dichloroethane	83	15	21.0	61.6	25.1	13.3
Hexyl alcohol	156.5	60	21.1	49	11.78	39.2
Acetophenone	202	82	21.7	61.5	26.9	11.6
Methyl methacrylate	100	10	21.7	48.8	37.3	13.9
N-methyl-2-pyrollidone			23.0	48	32.8	19.2
Propan-2-ol	82.4	22	23.5	41.2	16	42.8
Benzyl alcohol	206	100	23.8	47.87	16.37	35.76
Methanol	64.5	11	29.6	30.4	24.7	44.9
Glycerol	290	160	36.5	29.5	20.7	49.8

2.2   Intrinsic Viscosity

2.2.1   Dilute Solution Viscometry

Because it is a relatively simple technique, dilute solution viscometry is widely used for the molecular characterization of polymers. A capillary viscometer, such as a Ubelohde or Anton Parr viscometer, is used to study dilute polymer solutions. An intrinsic viscosity (or limiting viscosity number), [η], is determined, which is a measure of the viscosifying power of the polymer and may be related to its molar mass. This gives information on the size of the polymer chain in solution.

In a capillary viscometer, the time, t, is measured for a certain volume of a polymer solution to flow through a length of capillary. The measurement is normally repeated for solutions at various polymer concentrations, c (mass of polymer per unit volume of solution).   The corresponding flow time for pure solvent, t_o, is also measured.

The relative viscosity (viscosity ratio) is given by equation 2.1:

$$\eta_r = \frac{\eta}{\eta_o} \approx \frac{t}{t_o} \qquad\qquad 2.1$$

Where η is the viscosity of the solution, η_O is the viscosity of pure solvent, t is the flow time for the solution and t_O is the flow time for pure solvent.

The specific viscosity is:

$$\eta_{sp} = \eta_r - 1 = \frac{\eta - \eta_o}{\eta_o} = \frac{t - t_o}{t_o} \qquad\qquad 2.2$$

Both η_{sp} and η_r depend on polymer concentration, c. A plot of η_{sp}/c against c is a straight line, provided that the concentration is not too high, and the intercept at zero concentration (infinite dilution) is the intrinsic viscosity, $[\eta]$. A plot of $(\ln\eta_r)/c$ against c is also approximately a straight line, with the same intercept.

The intrinsic viscosity (limiting viscosity number) is thus determined as

$$[\eta] = \left(\frac{\eta_{sp}}{c}\right)_{c \to 0} = \left(\frac{\ln \eta_r}{c}\right)_{c \to 0}$$

2.3

$[\eta]$ has units of reciprocal concentration (e.g., $cm^3\ g^{-1}$, $dl\ g^{-1}$).

$[\eta]$ is empirically related to molar mass, M_v, by the Mark-Houwink relationship:

$$[\eta] = KM_v^a, \quad \text{i.e. } \log [\eta] = \log K + a\log M_v$$

2.4

Where K and a are constants for a particular polymer in a given solvent at a given temperature. The constants a and K are constants for specific polymer, solvent, temperature combinations. The constant K depends on primary molecular features such as the persistence length, so for a Gaussian coil it can be calculated from first principles. (Persistence length is the distance which we should travel from one end of the chain to bend it by 90 degrees). For a linear, flexible polymer, the value of a is 0.5 in a theta (θ) solvent and up to 0.8 in a good solvent [5-7].

2.2.2 The Anton Parr AMVn automated micro- viscometer

Intrinsic viscosities for all PMMA and PS solutions where determined using an Anton Parr AMVn automated micro-viscometer. The Anton Parr AMVn automated micro- viscometer is based on the rolling/falling ball principle. Using a 1.8mm diameter capillary at 25 ± 0.5 ℃ at an angle of 70 ° times were determined as the average of four determinations ± 0.05 s. First, the time for the pure solvent was measured and then the times for the polymer solutions were determined. Values up to 4 times the value of the pure solvent were considered, beyond which the polymer solution was thought to be too concentrated as polymer chain interaction could occur. The process started with a low concentration and moved towards higher concentrations (1 % to 10 %) [8]. Also, the second method was Unbelhoder viscometer which describe below

2.2.3 Ubbelohde Capillary Viscometer

Intrinsic viscosities for all CAB2 and polysaccharide solutions were determined using three arms Ubbelohde capillary viscometer at 25 +/- 0.1 ℃ .

This instrument was invented by a German chemist Leo Ubbelohde in the early 1900s who aimed to obtain the measurements of a viscosity independently of the concentration.

The Ubbelohde type viscometer also known as the suspended level viscometer. The Ubbelohde viscometer is a type of an instrument which is used to measure viscosity of Newtonian liquids which are transparent enough to allow the meniscus of the liquid to be measured. The main advantage of the Ubbelohde viscometer from other viscometer is that the values which are obtained are independent of the concentration.

2.3 Surface Tension

Surface tension measurement is based on monitoring a drop of solvent using a sensitive camera connected to a PC. The device used in this method is called a Kruss 100 Tensiometer which is equipped with a syringe. The syringe was filled with solvent and fixed in the holder of the tensiometer. The camera was turned on and focused at the nozzle of the syringe to monitor a drop of the solvent. The syringe was then squeezed gently until a meniscus started to appear at the nozzle of the syringe. After that, software was used to surround and select the zoomed picture of the meniscus. Finally, the extraction button was pressed to focus only on the meniscus and then the feed button was pressed to find the surface tension. The surface tension for any solution was made the same as that of the pure solvent.

2.4 Gel Permeation Chromatography (GPC)

Molecular weights were measured using size exclusion chromatography (SEC), on an instrument equipped with two ViscoGel $GMH_{H\ R}$-M columns and a differential refractive index (RI) detector. The eluent was tetrahydrofuran (THF) at a flow rate of 1 mL /min^{-1}. The system was calibrated with polystyrene standards and was calibrated with a series of narrow range standards of PMMA.

2.4.1 Aqueous GPC

In order to obtain the molecular weight of water soluble polymer, an aqueous Gpc with equipped with two columns TSKgel 5000 and 6000 in different high and low column system. The solvents used was mix with water and azide, with flow rate of 0.5ml per 1 min, also, and using the Ethylene Glycol as a marker .The aqueous GPC is used for all the experimental and calibrated with PEO .

2.5 Differential Scanning Calorimetry (DSC)

This is a thermo-analytical technique that can be used to obtain the glass transition temperature of a material by changing the temperature over time in order to heat the sample up to a certain temperature then cool it down. The device used in this technique is called a Perkin Elmer Differential Scanning Calorimeter. The device was operated at a heating rate of 20 ^{o}C /min.

2.6 Thermal gravimetric analysis (TGA)

The material's behaviour can be determined using thermal analysis when it is influenced by thermal loads. TGA can be used to find the thermal stability of a material where the material weight changes with temperature. A TGA-Q5000 was used and operated at a heating rate starting from 20 ^{o}C /min to 800 ^{o}C /min.

2.7 Nuclear Magnetic Resonance Spectroscopy (NMR)

^{1}H NMR was performed and recorded using a Varian Inova 300 (300 MHz) Spectrometer. The solvents used were either deuterated DMSO or chloroform as stated.

2.8 InkJet Printing

2.8.1 Microfab[TM] DOD Dispenser.

Inkjet printing was carried out using a MicroJet [TM] drop-on-demand dispensing device for room-temperature operation (Microfab, MJ-AB-01).

Using a glass microfibre filter of specifications diameter 47 mm, 0.26 mm thick, 1.2 µm retention and filtration speed 100/100 ml, each polymer solution (100 ml) was filtered at the specified dilution. The solvent γ-butyrolactone was used to wash the print head before and after inkjet printing each dilution. Trial inkjet printing of each dilution was subsequently observed at a temperature of 25 ℃ over a period of 5 minutes. The resulting waveform was adjusted to give optimal performance.

The drop generator, developed for fluids with low shear viscosities in the range 0.5 – 20 cP and surface tensions in the range 20 – 70 mN/m, consists of a 50 µm inside diameter glass nozzle with a piezoelectric actuator sleeve driven by an external power supply. In all our experiments a bipolar waveform, with a 10 µs rise time, 25 µs duration and 5 µs decay followed by a 5 µs echo and 5µs rise, was employed with an external drive frequency of 4000 Hz (Figure 1.1). Pulses ranging from 30 to 60 V were employed. To prevent nozzle tip wetting and to create reproducible printing conditions, the glass capillary was regularly cleaned with a 20 wt.-% solution of potassium hydroxide in demineralized water and rigorously flushed with γ-butyrolactone.
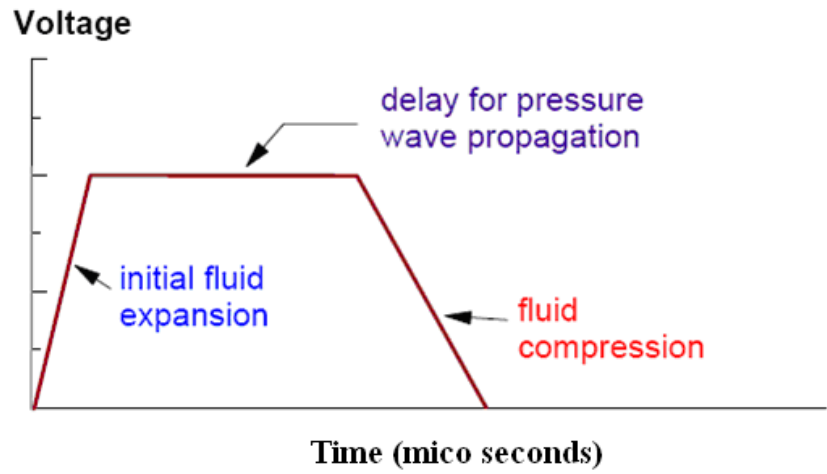
Figure 2.1 Drive waveform effects on inkjet device performance.

The waveform used in this project is listed in Tables 2.2 and 2.3.

Table 2.2 Typical pulse shape parameters.

	Time (μs)	Voltage (V)
Idle		0
Rise	10	
Dwell	25	30
Fall	5	
Echo	5	0
Final Rise	5	

Table 2.3 Parameters of trigger settings.

Source	PC Trig.
Mode	Continuous
Drops/Trigger	1
Frequency	4000 Hz
Strobe Driver	1
Strobe Enable	on
Strobe Delay	0 μs

2.8.2 Dimatix Materials Printer (DMP)

The Dimatix Materials Printer (DMP) is a laboratory scale tool that allows the evaluation of inkjet use for new technologies. It has multiplexing capabilities to enhance experimental capacity and optimise process parameters for various applications. The main constraints for material requirements are the viscosity and surface tension, which have to be between 10 - 12 cP and 28 - 33 mN/m respectively. It has a cartridge which fills with ink to a maximum 1.5 ml. The cartridge has the advantage of being compatible with most organic solvents, and has 16 nozzles at 254 μm spacing. Each nozzle has a 21.5 μm diameter[9]. In all the experimental work done, a drop watcher was used to view the jetting nozzles, faceplates and the jetting of the fluids. The waveform used had a voltage range between 17 and 30 V and duration of 7.424 μs; also, with different pulse widths between 65 and 100 μs, and frequency of 5 KHz. After each run, the polymer solution was collected and precipitated with methanol and then evaporated to dryness before being characterised by GPC.

2.9 References

1.   Macosko, C. W., *Rheology: Principles, Measurements, and Applications*. 1st Edition ed.; Wiley-VCH: **1994**.
2.   Atkins, P.; de Paula, J., *Physical Chemistry*. 8th Edition ed.; Oxford University Press: **2006**.
3.   Burke, J., *AIC Book and Paper Group Annual*. **1984**; Vol. 3, p 13-58.
4.   Raunvis, I. http://www.raunvis.hi.is/~agust/ee3maetti.htm
5.   Cowie, J. M. G., *Polymers: Chemistry and Physics of Modern Materials*. 2nd Edition ed.; Blackie Acedemic & Professional,: **1993**.
6.   Stevens, M. P., *Polymer Chemistry: An Introduction*. 3rd Edition ed.; Oxford University Press: **1999**.
7.   Young, R. J.; Lovell, P. A., *Introduction to Polymers*. Chapman & Hall: **1991**.
8.   Xu, D.; Sanchez-Romaguera, V.; Barbosa, S.; Travis, W.; Wit, J. d.; Swan, P.; Yeates, S. G., *Journal of Materials Chemistry* **2007,** 17, (46), 4902-4907.
9.   www.dimatix.com. .

Chapter Three

Synthesis and characterisation of methacrylic acid methyl methacrylate statistical copolymers

In this chapter the free radical solution polymerization of a series of methacrylic acid (MAA)containing statistical copolymers is described and discussed. Methyl methacrylate (MMA) was chosen as comonomer because the reactivity ratios of MMA (r1) and MAA (r2) are r1 =0.87, 1.81, 1.28, 0.77 and r2 = 0.48, 1.63, 1.84, 2.16) respectively such that a non blocky copolymer will result [1-5] .The design of the copolymers was focused on a range of low to medium molar mass polymers in a range typically used as polymer additives in SOHO inkjet printing. Monomer ratios are expressed as wt-% in all cases.

3.1 Polymerization of methacrylic acid-co-methylmethacrylate via continuous free radical polymerization
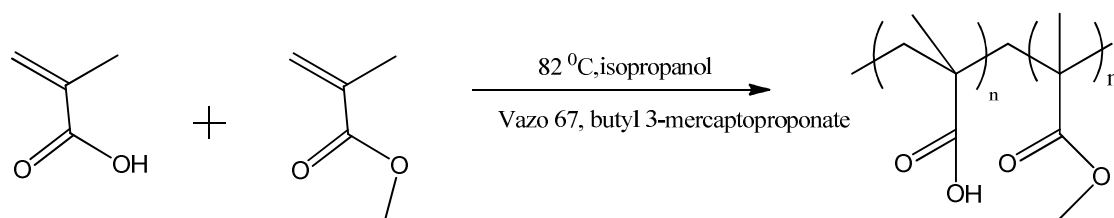
The reaction illustrated above shows the free radical synthesis of statistical copolymers which contain methylmethacrylate (MMA) and methacrylic acid (MAA) as monomers. Vazo 67 [6] (2,2'-azobis(2-methylbutyronitrile) was used as free radical initiator, $\log(t_{1/2}) = 7492$ (1/T) - 19.215 (t in minutes, T in Kelvin). For Vazo 67 in 1,3,5-trimethylbenzene $t_{1/2}$ is 10 hours at 67 ^{o}C. Butyl 3-mercaptoproponate was used as a chain transfer agent.

The method used involved feeding both monomers, initiator and chain transfer agent into solvent at reaction temperature over time so as to give instantaneous conversion of monomer.

3.1.1   Materials

All materials except Vazo 67 (DuPont) were obtained from Sigma Aldrich UK and were used as received.

3.2   Experimental Method Ka1/24 MMA/MAA (80/20)

All polymers were prepared using the following method exemplified for Ka1/24 MMA/MAA (80/20). The 250 ml round bottom flask containing the solvent (35 g of isopropanol) was placed in an oil bath and thermostatically heated, under reflux with stirring at 300rpm, up to the boiling point which is 82 ℃. Separately, 0.35 g of Vazo 67 dissolved in isopropanol with 0.35 g of chain transfer agent (butyl 3-mercaptoproponate). and the monomers – 28 g of methylmethacrylate and 7 g of methacrylic acid -- were fed in over 2 hours and left for a further 4 hours to ensure complete conversion. The polymer was then analysed by ^{1}H NMR, GPC, TGA, and DSC.

3.3   Characterisation Ka1/24 MMA/MAA (80/20)

1HNMR (500 MHz, DMSO): 1.8 ppm (1H, CH3) and 3.6 ppm (1H, OCH3), 2 ppm (2H,CH2), 1.2 ppm (1H,CH3).
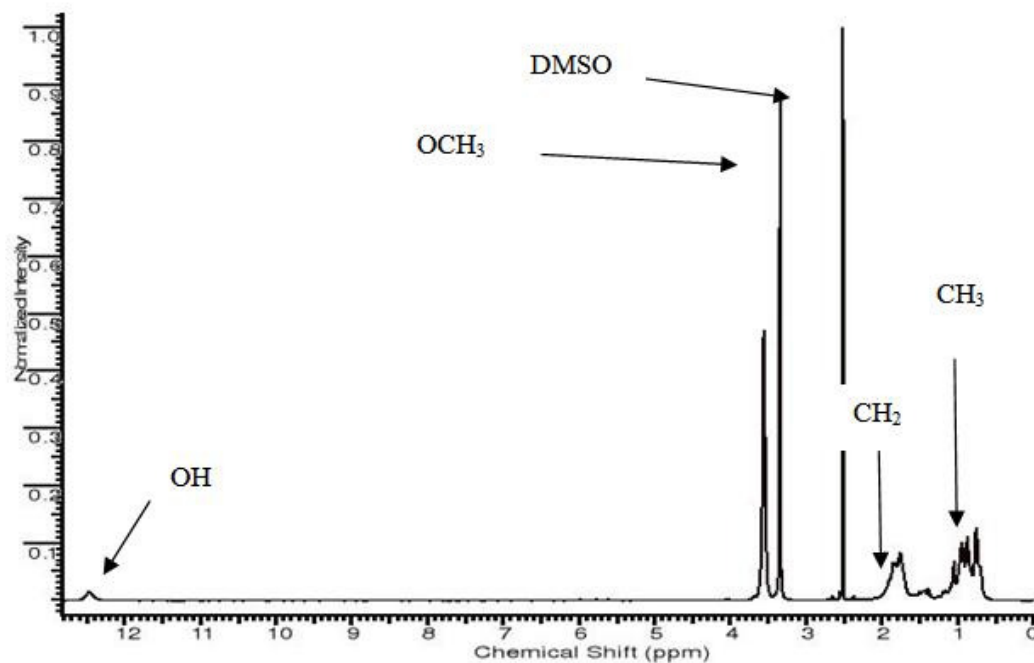
Figure 3.1 HNMR Spectrum of MMA/MAA 80/20 (Ka1/024).
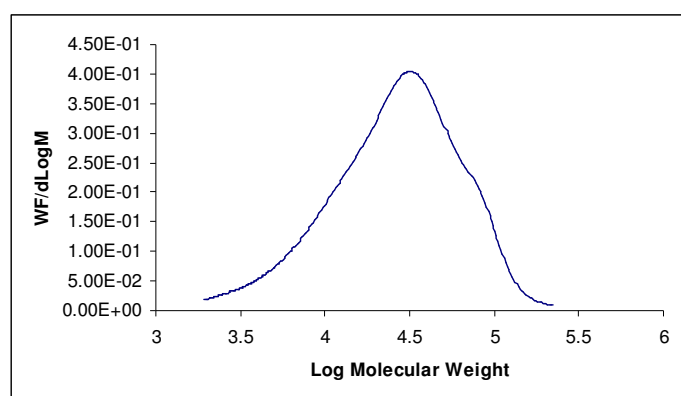
Figure 3.2 GPC of MMA/MAA 80/20 (Ka1/024): Mn = 15491, Mw = 34101, PDi = 2.2.

TGA: 4.411 mg was heated at the rate of 5 ^{o}C / minute to 600 ^{o}C. The onset of weight loss was around 313 ^{o}C with peak weight loss at around 363 ^{o}C. The polymer was fully decomposed at around 420 ^{o}C.
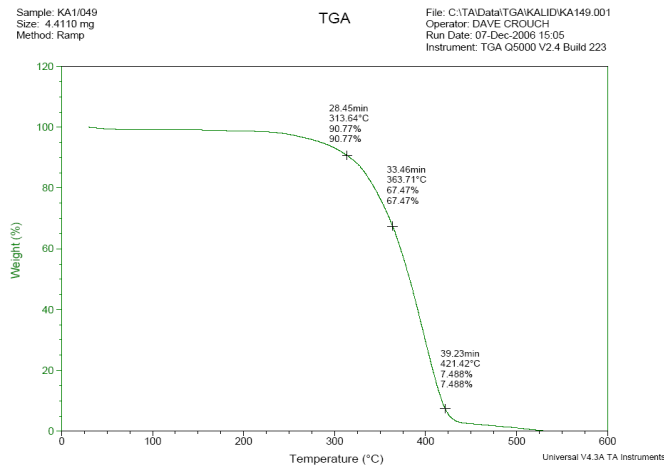
Figure 3.3 TGA of MMA/MAA 80/20 (Ka1/024).

DSC: ca 10 mg was heated up from 20 ^{o}C to 250 ^{o}C at the rate of 20 ^{o}C /min and then cooled down using the same scale. The glass transition was at 143 ^{o}C.
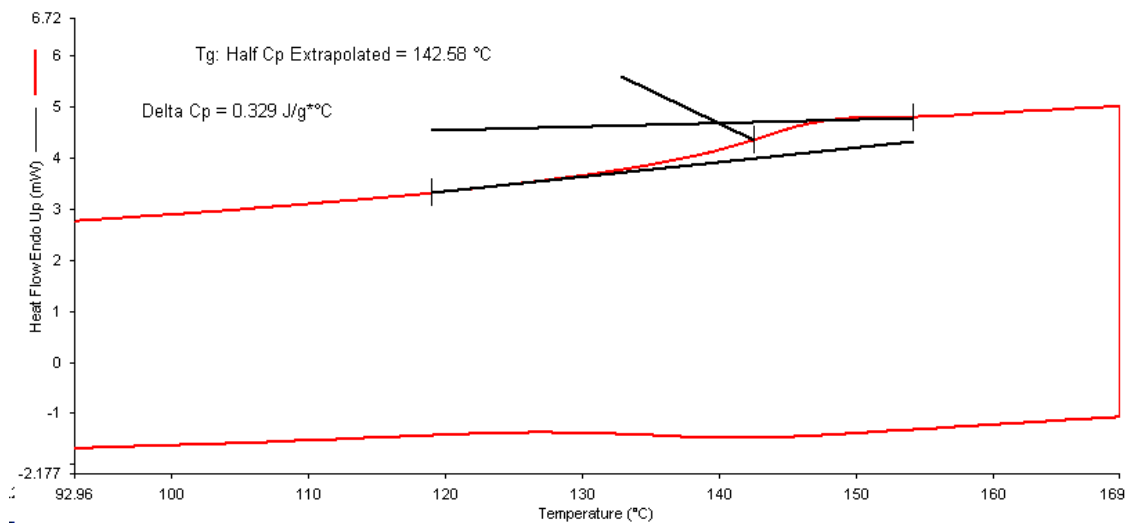
Figure 3.4 DSC of MMA/MAA 80/20 (Ka1/024).

The glass transition (Tg) of the PMMA and PMAA can be calculated using Flory-Fox equation[7]:

$$\frac{1}{Tg\,(copolymer)} = \frac{\Phi_1}{Tg_1} + \frac{\Phi_2}{Tg_2} \qquad\qquad 3.1$$

Where Φ_1 = wt fraction of monomer 1 (MMA); Φ_2 = wt fraction of monomer 2 (MAA); Tg_1 is the Tg of homopolymer 1(MMA = 273K), Tg_2 is the Tg of homopolymer 2 (MAA = 505 K) [8-13]. For KLa1/024 the calculated Flory-Fox Tg is 142.5 which is in good agreement with DSC and supportive of the statistical nature of the polymer.

Table 3.1 Summary of the MMA/MAA polymers made, with different chain transfer agents.

Polymer Code	MMA (wt-%)	MAA (wt-%)	% CTA	Mn (kDa)	Mw (kDa)	PD
Ka1/004	70	30	0	20442	43422	2.12
Ka1/005	70	30	0	20906	36537	1.75
Ka1/006	70	30	0.1	17460	34336	1.97
Ka1/007	70	30	0.2	18345	33582	1.83
Ka1/008	70	30	0.4	27418	46212	1.69
Ka1/009	80	20	0	43113	85782	1.99
Ka1/010	80	20	0.1	40187	81007	2.02
Ka1/017	80	20	0.4	29725	61460	2.07
Ka1/012	90	10	0	29572	57698	1.95
Ka1/013	90	10	0.1	28169	57954	2.06
Ka1/014	90	10	0.2	27284	55207	2.02
Ka1/016	90	10	0.4	25355	54327	2.14
Ka1/24	80	20	0.99	15491	34102	2.02
Ka1/25	80	20	1.96	12120	28499	2.35
Ka1/26	80	20	2.91	8175	17110	2.09

Table 3.2 Series of MMA/MAA with 3 wt-% of chain transfer agent.

Polymer Code	MMA (wt-%)	MAA (wt-%)	Mn (kDa)	Mw (kDa)	PD
Ka1/59	100	0	7.5	11.4	1.5
Ka1/60	98	2	6.8	11.7	1.7
Ka1/61	96	4	6.8	11.6	1.7
Ka1/62	94	6	6.4	10.5	1.6
Ka1/63	92	8	9.5	14.5	1.5
Ka1/64	90	10	7.1	11.5	1.6
Ka1/65	80	20	8.2	12.4	1.5
Ka1/66	70	30	8.3	11.1	1.3
Ka1/67	60	40	7.5	13.3	1.7
Ka1/68	50	50	7.5	12.4	1.6
Ka1/69	40	60	6.4	9.8	1.5

Table 3.3 Series of MMA/MAA with 1 wt-% of chain transfer agent.

Polymer Code	MMA (wt-%)	MAA (wt-%)	Mn (kDa)	Mw (kDa)	PD
Ka1/79	100	0	9.9	19.3	1.9
Ka1/80	98	2	12.7	24.4	1.9
Ka1/81	96	4	13.5	24.9	1.8
Ka1/82	94	6	13.4	25.9	1.9
Ka1/83	92	8	13.6	25.5	1.8
Ka1/84	90	10	13.6	26.6	1.9
Ka1/85	80	20	15.9	30.8	1.9
Ka1/86	70	30	17.8	34.2	1.9
Ka1/87	60	40	13.8	27.7	2
Ka1/88	50	50	14.5	28.4	1.9
Ka1/89	40	60	12.2	21.9	1.8

3.4 References

1.   Ryabov, A. V. D. S.; S.-s, Y. D. S. a. N. N., Dokl. AN SSSR **1962**, 145, 822.

2.   Sengupta, P. K.; MukherJee, A. R.; Ghosh, P., J. Macrom. Chem **1966**, 1, 481.

3.   Ryabov, A. V.; Semchikov, Y. D.; Slavnitskaya, N. N., Vysokomol. soyed **1970**, (A12), 553.

4.   Bezugly, V. D.; Voskresenskaya, I. B.; Alekseeva, T. A.; Germer, M. M., Vysokomol. Soedin **1972**, 14, (Ser A), 540.

5.   Brandrup , J.; Immergut, E. H., Polymer Handbook. 3rd Edition ed.; John Wiley & Sons: **1989**.

6.   http://www2.dupont.com/Vazo/en_US/products/grades/grade_selector.html.

7.   Cowie, J. M. G., Polymers: Chemistry and Physics of Modern Materials. 2nd Edition ed.; Blackie Acedemic & Professional: **1993**.

8.   Fox, T. G.; Garrett, B. S.; Goode, W. E.; Gratch, S.; Kincaid, J. F.; Spell, A.; Stroupe, J. D., Journal of the American Chemical Society **1958**, 80, (7), 1768-1769.

9.   Biswas, M.; Roy, A., Journal of Applied Polymer Science **1993**, 49, (12), 2189-2196.

10.   Milton, A. J.; Monkman, A. P., Journal of Physics D: Applied Physics **1993**, 26, (9), 1468-1474.

11.   Champagne, M. F.; Prud'Homme, Journal of Polymer Science, Part B: Polymer Physics **1994**, 32, (4), 615-624.

12.   Weldon, L. M.; Pomeroy, M. J.; Hampshire, S., Key Engineering Materials **1996**, 241-248.

13.   Srinivas, S.; Caputo, F. E.; Graham, M.; Gardner, S.; Davis, R. M.; McGrath, J. E.; Wilkes, G. L., Macromolecules **1997**, 30, (4), 1012-1022.

Chapter Four

Solution Properties of Inkjet Fluids

This chapter details the solution properties of the fluids used in the inkjet studies reported in Chapters 5, 6 and 7. The optimal range of static values for DOD inkjet printing are typically viscosity (η) lying in the range 2-20 cP (mPa.s) and surface tension (γ) in the range 20-50 mN.m^{-1} and all inks were formulated where possible to reside within these limits. However, given the high elongational shear rates experienced by the ink upon drop generation[1], typically greater than 10^5 s^{-1}, it is the dynamic properties that are most important however it is either difficult or impossible to measure these directly in the laboratory and hence low shear data are presented here.

4.1 Solution Properties of Methacrylic Acid Containing Methacrylate Copolymers in γ-butyrolactone.

4.1.1 Solvent solubility and selection

Details of the synthesis of a series of carboxylic acid - containing methylmethacrylate (MMA) / methacrylic acid (MAA, unionised) statistical copolymers (MMA/MAA) are given in Chapter 3. An extended range was synthesised in advance of the inkjet studies, but as there evaluation progress it became apparent that as a class they were not appropriate for the study and hence only a limited number had there solution properties characterised, Table 3.1 - 3.

The solubility characteristic of the carboxylic acid-containing polymers up to an acid content of 70 wt-% was determined by preparing 1 wt.-% solutions in a range of common solvents at 25 $^{\circ}$C and visually assessing solubility after 1 hour and after 24 hours, Chapter 2.1. These were then classified as either soluble, partially soluble, gel or insoluble. Using standard Teas notation[2],

ternary plots for each polymer were generated to identify the parameter space where the polymers were most soluble. γ-butyrolactone, Dihydrofuran-2(3H)-one, was identified as a good solvent having suitable physical properties for inkjet printing (boiling point = 204 $^{\circ}$C; surface tension = 40.4 mN/m; viscosity = 1.7 cP at 25 $^{\circ}$C) and was used in all further work. Figure 4.1 shows the Teas ternary graph for copolymer Ka1/24 (MMA/MAA = 80/20).
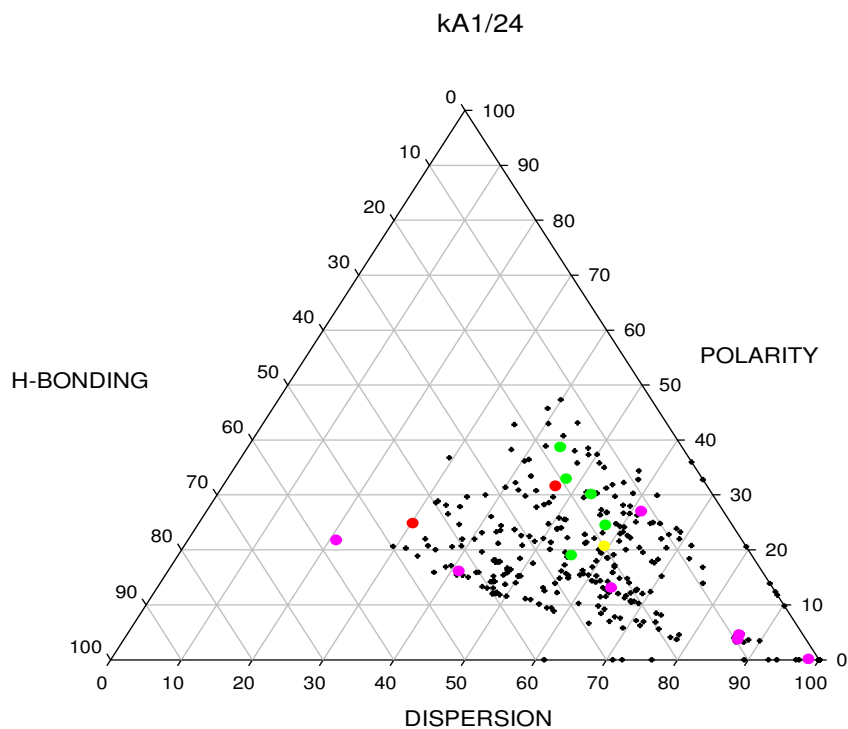
Figure 4.1 Teas Ternary solubility graph for Ka 1/24 MMA/MAA = 80/20 w/w at 25 $^{\circ}$C. Red spots soluble, green gel, yellow partially soluble purple insoluble.

As is shown in Table 4.1, PMMA is soluble in γ-butyrolactone with copolymers having ≤ 30 wt-% MAA also giving clear solutions. Beyond this increasing the wt-% of MMA makes the copolymers less soluble γ-butyrolactone becoming insoluble at MAA contents ≥ 70 wt-%. As the concentration of MAA increases in the polymer, its solubility characteristics become more dominated by the H-bonding and polar contributions (Hildebrand parameters). Beyond 30 wt-% only MMA segments of the polymer chain are fully solvated, with segments rich in MAA

starting to self-associate in solution leading to more dispersion-like behaviour. Beyond ca. 70 wt-%, there is insufficient MMA in the polymer chain to be solvated, leading to insolubility.

Table 4.1 Solubility of MMA/MAA copolymer in γ-butyrolactone.

Wt-% MAA in copolymer	Observation
≤ 30	Soluble solutions clear
> 30 - ≤ 50	Partially soluble at lower acid levels leading to clear gel at higher acid levels
> 50 - ≤ 70	'Solutions' milky white
> 70	Insoluble

4.1.2   Determination of Overlap Concentration (c*) for copolymers having MAA ≤ 30 wt-%

The overlap concentration is the point at which each individual coil begins to overlap with other polymer chains. Flory[3] showed that, for flexible polymer chains, the overlap concentration is given by:

$$c^* = 1/ [\eta] \qquad\qquad 4.1$$

where $[\eta]$ is the intrinsic viscosity. The overlap concentrations determined for polymers with MAA % ≤ 30 wt-%; Mn = 7 – 16 kDa are given in Table 4.2 as it is only valid for true polymer solutions.

Table 4.2 Overlap concentration of selected MMA/MAA copolymers, Mn = 7- 18 kDa. Mw = 11 – 31 kDa.

Code	%MAA	Mn / Da	c* g/dl
Ka1/79	0	9890	15.4 +/- 0.8
Ka1/80	2	12750	21.3 +/- 1.1
Ka1/81	4	13500	23.5 +/- 1.2
Ka1/82	6	13380	18.2 +/- 0.9
Ka1/83	8	13590	13.5 +/- 0.7
Ka1/84	10	13560	14.2 +/- 0.7
Ka 1/24	20	15880	15.3 +/- 0.8
Ka1/85		15490	
Ka1/86	30	17830	12.5 +/- 0.6
Ka1/59	0	7500	15.1 +/- 1.0
Ka1/60	2	6800	17.1 +/- 0.8
Ka1/61	4	6800	19.6 +/- 1.0
Ka1/62	6	6400	16.3 +/-0.8
Ka1/63	8	9500	22.7 +/- 1.1
Ka1/64	10	7100	28.6 +/- 1.4
Ka1/65	20	8200	8.8 +/-0.4
Ka1/66	30	8300	12.9 +/- 0.6

Figures 4.2 and 4.3 show the effect of polymer molecular weight on overlap concentration. Within the limits of the determination c* shows a rise up to 10 wt-% MAA for polymers having Mn < 10 kDa beyond which it falls. For higher molecular weight polymers, Mn = 10 – 18 kDa a similar observation is made with a peak at around 5 wt-% MAA. This suggests that the polymer chains are becoming more swollen at low MAA suggesting that the overall polymer composition is more closely matched to the solubility parameters of γ-butyrolactone.
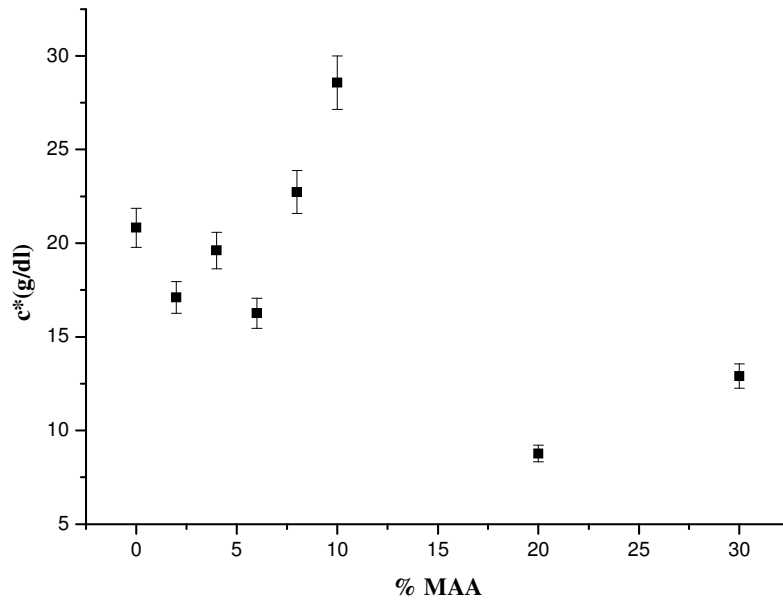
Figure 4.2 Effect of MAA concentration on c* in γ-butyrolactone for low molecular weight Mn = 7.5 – 9.5. kDa at at 25 $^{\circ}$C.
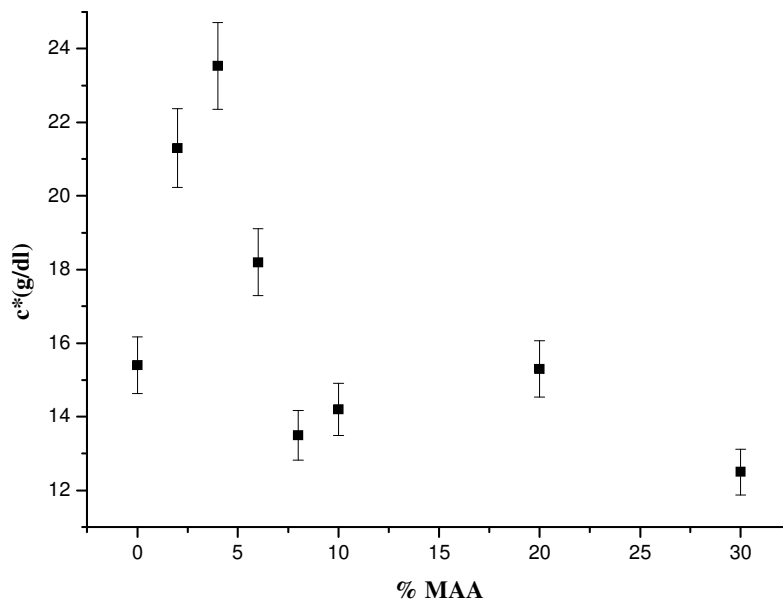
Figure 4.3 Effect of MAA concentration on c* in γ-butyrolactone for higher molecular weight Mn = 10 -18. kDa at 25°C.

4.1.3   Viscosity of MAA containing copolymer γ-butyrolactone solutions.

The MMA/MAA = 80/20 the effect of polymer concentration and molecular weight on solution viscosity in γ-butyrolactone is shown in Figure4.4
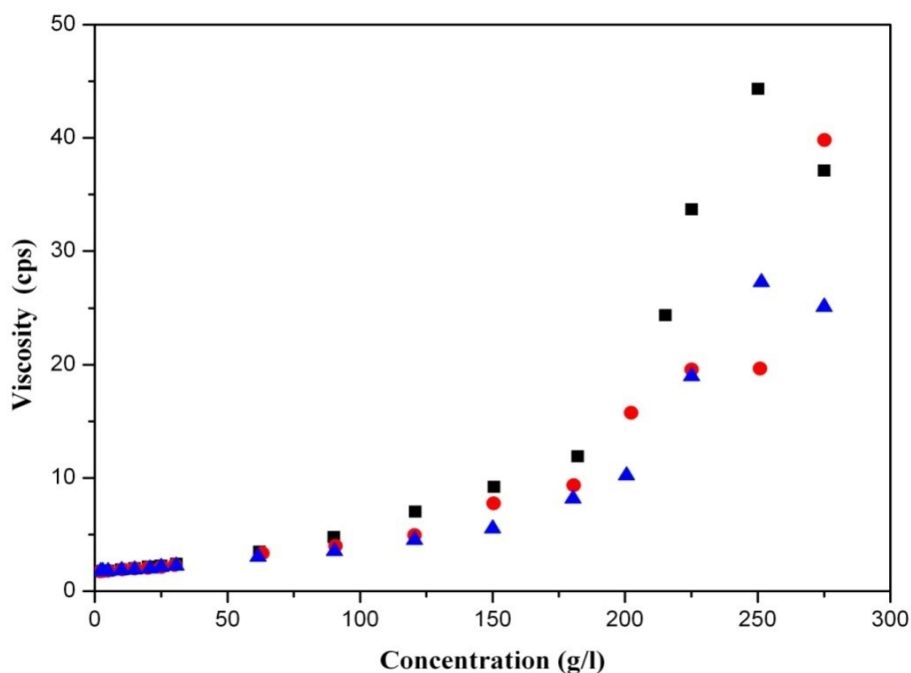
Figure 4.4 Effect of polymer concentration and molecular weight on solution viscosity for MMA/MAA = 80/20 in γ-butyrolactone at 25 $^{\circ}$C: (■) Ka 1/24 Mn 15490; (●) Ka 1/25 Mn 12120; (▲) Ka 1/26 Mn 8175.

 All three polymers show an increase in viscosity at c*. Below c* all three have the same slope, where the polymer chains are essentially isolated (dilute regime), where polymer chains are isolated and the viscosity is controlled by the solvent and intermolecular interaction.; above c* (semidiulte regime, c ~ c*) the polymer chains become partially entangled, overlap, resulting in a sharp increase in viscosity due to the effect of chain entanglement as well as intermolecular H-bonding between carboxylic acid groups. Beyond the semi-dilute regime the concentrated regime is observed, c > c*, wher polymer chain entanglement increases while c increases[4].

4.1.4 Surface tension of MAA containing copolymer γ-butyrolactone solutions.

The surface tensions for dilute solutions in γ-butyrolactone of Kal/24 (MMA/MAA = 80/20 w/w, Mn = 15.5 kDa were measured, Table 4.3, Figure 4.5.

Table 4.3 Surface tension values in γ-butyrolactone for the (MMA/MAA) Ka1/24.

Concentration (g/dl)	Surface tension (mN/m) at 25 ^{o}C
0.5	36.5
1	36.5
2.0	33.3
3.5	35.4
5.0	34.7
7.0	35.3
8.0	34.8
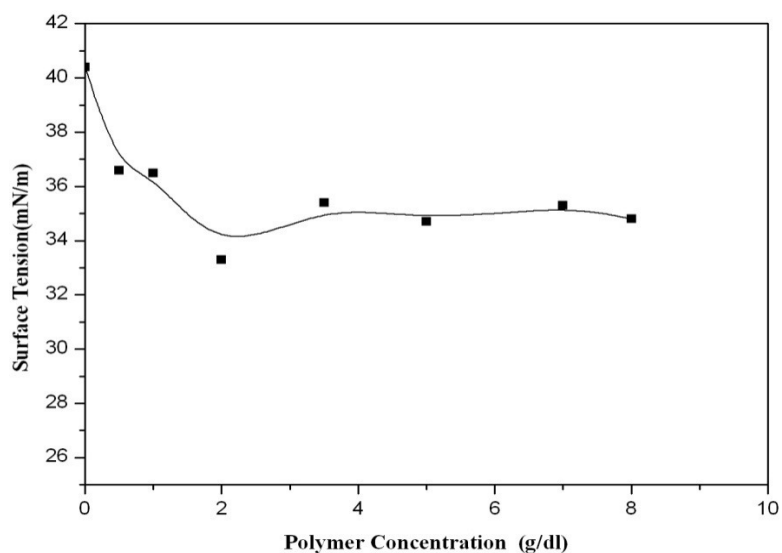
Figure 4.5 Surface tension as a function of concentration for (MMA/MAA) 80/20 Ka1/24 in γ-butyrolactone at 25 ^{o}C.

The surface tension of all polymer containing solutions are lower than that for pure solvent (40.4 mN/m) due to the fact that the polymer preferentially adsorbs at the air/solvent interface[5]. However in all case the surface tension is within the generally accepted limits for inkjet printing.

4.2 Characterisation of Poly(methyl methacrylate) and Polystyrene Inkjet Solutions

The preparation and characterisation of model solutions comprising polymethyl-methacrylate (PMMA) and polystyrene (PS) separately in good solvent(s) for use in inkjet molecular weight degradation studies are reported here.

4.2.1 Materials

All solvents, linear poly(methyl methacrylate) (PMMA) and polystyrene (PS) standards (see Table 4.4), were obtained from Sigma Aldrich UK and were used as received. Samples are denoted by their average molecular weight (kDa) as determined by GPC using PMMA and PS standards respectively. All polymers have typical polydispersities in the range of 1.15 – 1.45, except those denoted B, where the polydispersity is broad and between 1.6 and 1.8.

Table 4.4 PMMA and PS samples used in this study, denoted by their determined average molecular weight (kDa). B denotes broad molar mass distribution samples.

Sample	Mw (kDa)	Mn (kDa)	PDi
PMMA 145	145	110	1.31
PMMA 395	395	232	1.7
PMMA 590	590	540	1.09
PMMA 909 B	909	506	1.80
PMMA 1390	1390	1170	1.19
PMMA 1630	1630	1124	1.45
PS 170			
PS 290	324	306	1.1
PS 320 B	320	197	1.6
PS 575	616	573	1.1
PS 650	595	549	1.2
PS 770	772	659	1.17
PS 996	1019	947	1.1
PS 1630	1632	1124	1.45

4.2.2 Solvent Selection

Solvent selection was made considering the respective Hansen Solubility Parameters (HSP) of PMMA and PS and the respective solvents, Table 4.5[6]. The HSP takes into account the relative strengths of the dispersion forces (δ_d), polar forces (δ_p) and hydrogen bonding forces (δ_h).

Table 4.5 Hansen Partial Solubility Parameters of PMMA, PS and Solvents considered for use in the inkjet degradation studies described in Chapter 6.

Solvent	Bpt (^{o}C)	Solubility Parameter (MPa$^{1/2}$)		
		δ_d	δ_p	δ_h
PMMA	-	18.6	10.5	7.5
PS	-	21.3	5.8	4.3
Tetrahydrofuran	50	16.8	5.7	8
Toluene	111	18	0.7	2
p-xylene	140	17.8	0.9	1.8
Anisole	152	17.8	4.1	6.8
Dimethyl acetamide	164	16.8	11.5	10.2
Butylcarbitol		16.0	6.3	6.3
Acetophenone	202	19.6	8.7	3.7
Tetralin	207	17.5	1.5	6.2
γ-butyrolactone	204	19	16.6	7.4
Butanone	80	15.9	9.0	5.1

These can be used to define the centre of a solubility sphere for a solute, and the interaction radius R_o determined experimentally as described by Hansen the model. Using the 3D model of Crowly, Hansen was able to plot polymer solubility's. A spherical volume of solubility of interaction radius is formed by doubling the dispersion parameter axis as shown in figure 4.6. The model indicates that the closer a solvents solubility parameters are elative to the polymer then the greater the miscibility and solubility. R_o is the interaction radius determined experimentally and if a solvent lies within this then it is deemed a good solvent.
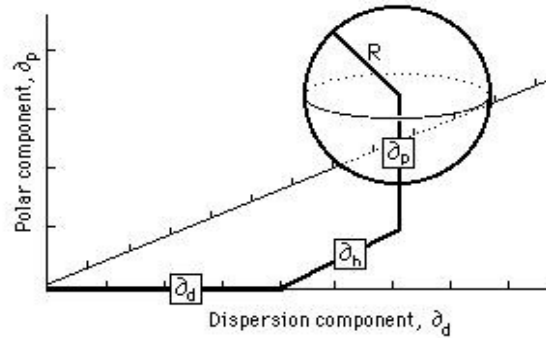
Figure 4.6 Hansen model of polymer solubility using a 3-D, three component parameter repesentation with the polymer at the centre of a sphere radius of interaction Ro[7].

For PMMA, R_o is 10.6 MPa$^{1/2}$ and for PS R_o is 12.7 MPa$^{1/2}$ [8]. If R$_o$ is known along with the respective solubility parameters for solute and solvent then the distance of the solvent from the solute in solubility space can be calculated, Ra, Equation 4.2 where the subscripts here are 1 for solute (PMMA or PS) and 2 for the respective solvent:

$$(R_a)^2 = 4(\delta_{d1} - \delta_{d2})^2 + (\delta_{p1} - \delta_{p2})^2 + (\delta_{h1} - \delta_{h2})^2 \qquad 4.2$$

Consequently a simple composite affinity parameter, the Relative Energy Difference number (RED), is then defined according to Equation 4.3:

$$RED = R_a/R_o \qquad 4.3$$

For a potentially miscible blend RED < 1.0 with progressively immiscible blends having higher RED.

Table 4.6 shows the calculated Relative Energy Difference number for a range of selected solvents. The solvents used in this study, anisole, acetophenone, butanone, tetralin (1,2,3,4 tetrahydronapthalene) and γ-butyrolactone, were chosen because they all have boiling points in the range of 152 – 204 $^{\circ}$C, suitable for sustained inkjet printing at room temperature without significant nozzle blockage (see Table 4.5).

70

Table 4.6 Relative Energy Difference number (RED) for different PMMA solvent blends.

Solvent	R_a (MPa$^{1/2}$)	RED
PMMA		
Anisole	7.3	0.69
Acetophenone	4.7	0.44
γ-butyrolactone	6.2	0.58
Butanone	6.3	0.59
PS		
Acetophenone	4.5	0.35
Tetralin	8.9	0.7
Anisole	8.9	0.7
γ-butyrolactone	11.8	0.9
Butanone	13.8	1.1

4.2.3 Determination of polymer solution overlap concentration c*.

Polymer solutions were prepared by gentle agitation and allowed to stand for 24 hours before use. The solutions had low shear viscosities in the range of 1 – 10 cP and surface tensions in the range of 29 – 40 mN/m at 25 ^{o}C, suitable for inkjet printing. Intrinsic viscosities [η] for each were determined using both an Anton Parr AMVn automated micro-viscometer, which is based on the rolling/falling ball principle (DIN 53015) and ISO 12058; 1.8mm diameter capillary at 25 +/- 0.5 ^{o}C at an angle of 70° times were determined as the average of 4 determinations (+/- 0.05 s). Intrinsic viscosity plots are shown in Figures 4.7 to 4.11 for PMMA. Lowest concentration values from which intrinsic viscosity was determined ,in all cases where $\geq$ 1.5 g/l and maximum run value having t $\leq$ 4 t_0.
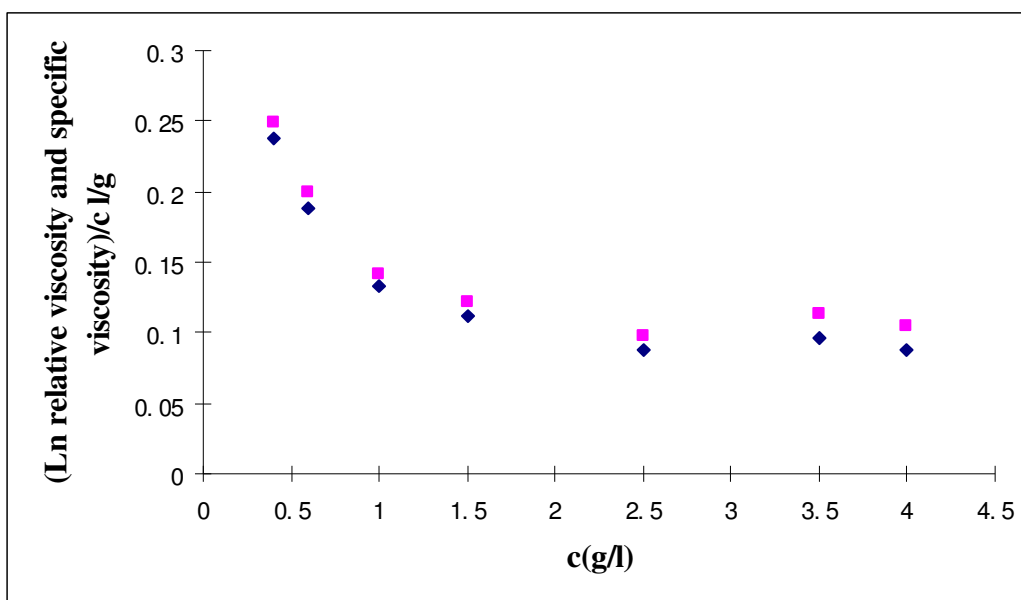
Figure 4.7 Intrinsic viscosity plot of PMMA 909B in anisole at 25 ^{o}C. (♦) ln relative viscosity/c and (■) specific viscosity/c. [η] = 0.14 l/g.

72
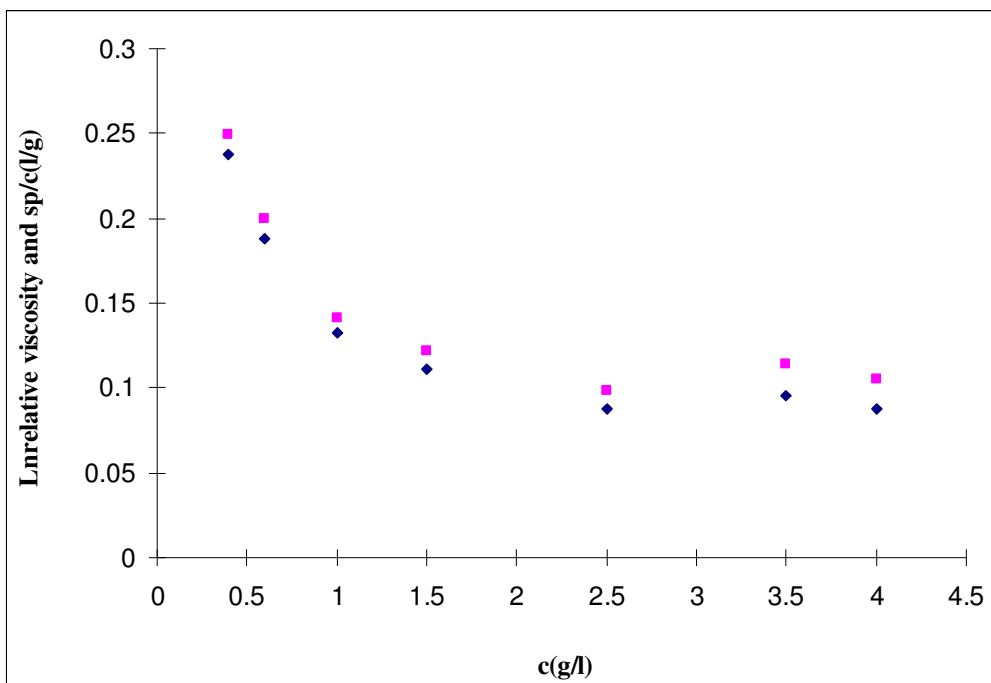
Figure 4.8 Intrinsic viscosity plot of PMMA 395 in anisole at 25 $^\circ$C. (♦) ln relative viscosity/c and (■) specific viscosity/c. $[\eta] = 0.12$ l/g.
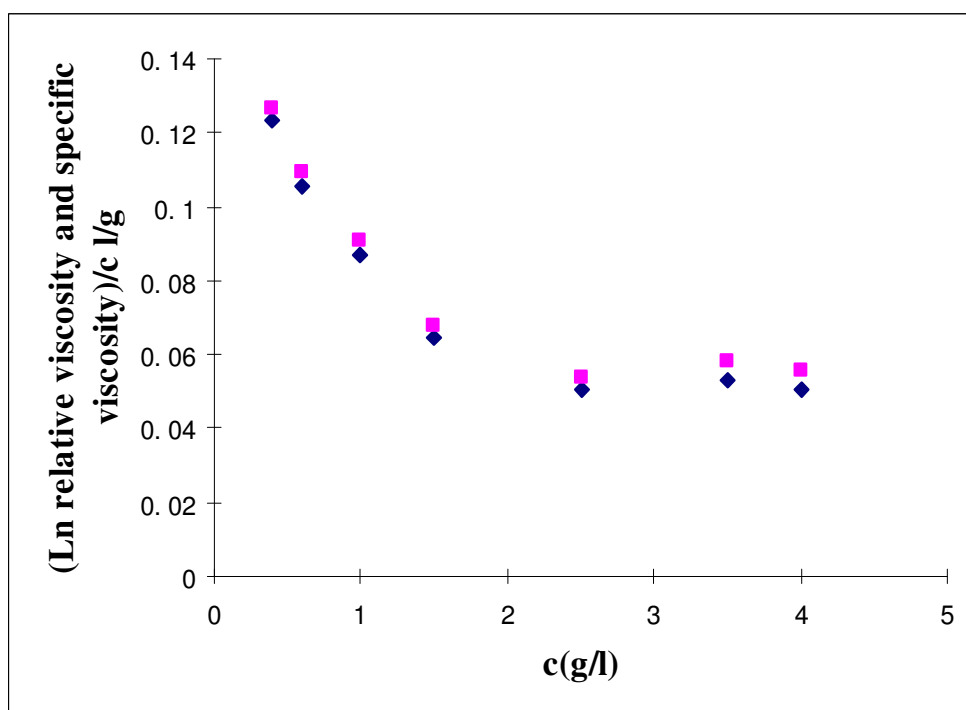
Figure 4.9 Intrinsic viscosity plot of PMMA 145 in anisole at 25 $^\circ$C. (♦) ln relative viscosity/c and (■) specific viscosity/c. $[\eta] = 0.05$ l/g.
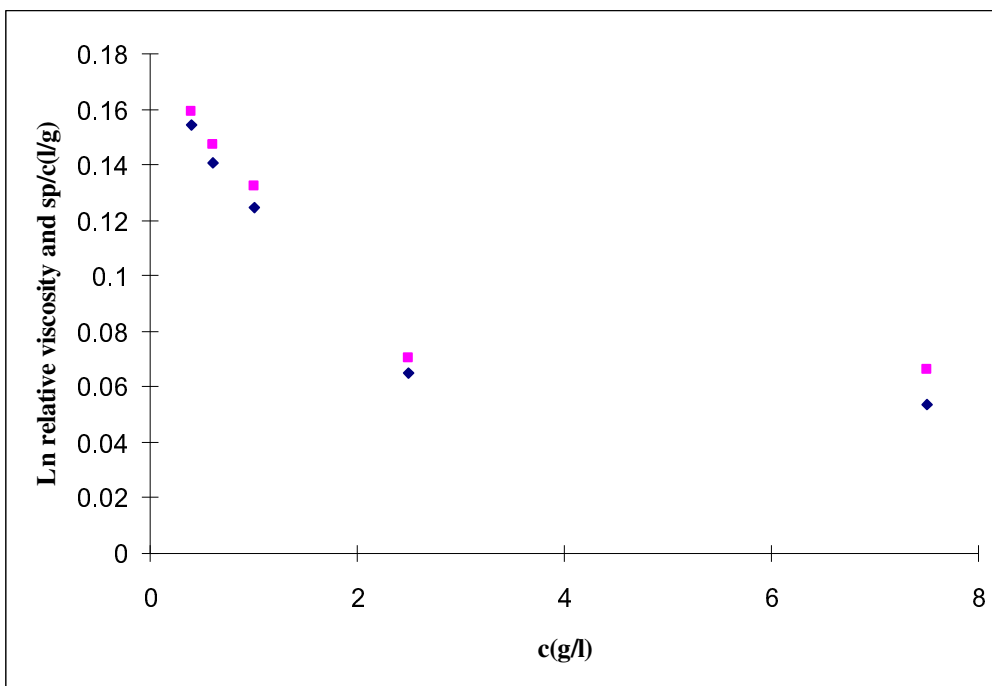
Figure 4.10 Intrinsic viscosity plot of PMMA 909 in γ-butyrolactone at 25 $^{\circ}$C. (♦) ln relative viscosity/c and (■) specific viscosity/c. [η] = 0.07 g/l
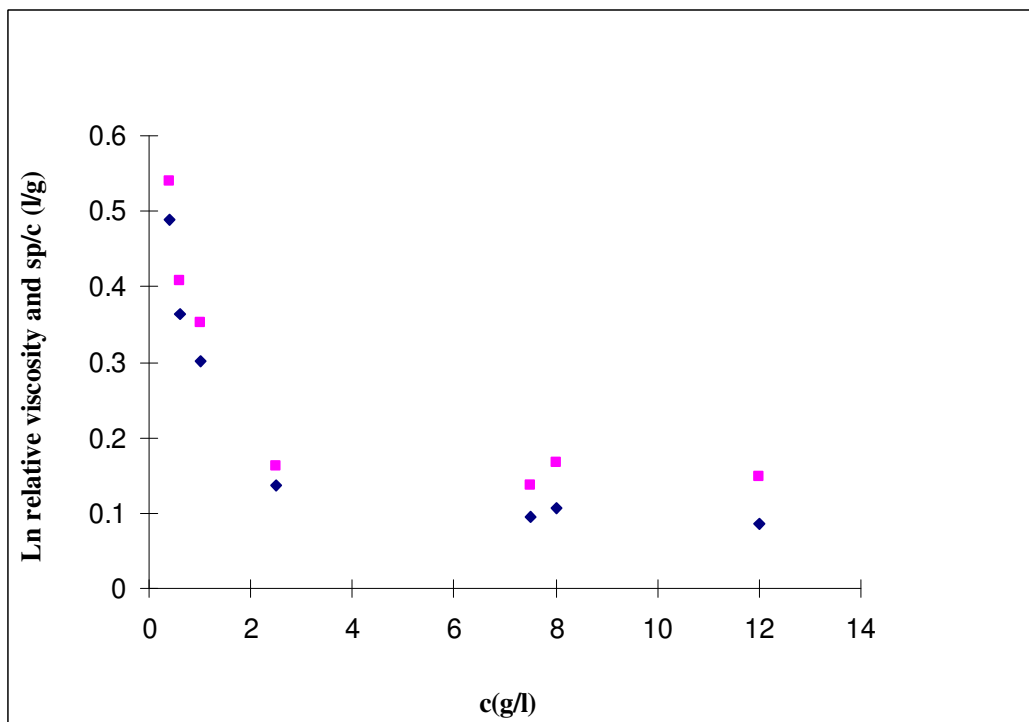
Figure 4.11 Intrinsic viscosity plot of PMMA 1095 in acetophenone at 25 $^{\circ}$C. (♦) ln relative viscosity/c and (■) specific viscosity/c. [η] = 0.16 l/g.

Values of intrinsic viscosity were obtained in the higher concentration linear regime $2t_0 < t < 4t_0$, $R^2 > 0.9$ and are given in Table 4.7, as well as calculated values of $c*$.

For comparison PMMA 909 in butanone which calculated through Mark-Houwink Equation where k=6.83 x 10^{-3} and a= 0.72 ,giving [η] = 1.3 dl/g .We measure [η] = 1.6 dl/g ,the diffrence being a result of the broad molecular weight distrubtion of the PMMA sample used[9].

Table 4.7 Summary of Intrinsic Viscosity ([η] +/- 10 %) and c* (+/- 10 %) using the Flory Approximation for PMMA and PS solutions at 25 °C.

Polymer	Solvent	[η] (dl/g)	c* (g/dl)
PMMA1390	γ-butyrolactone	1.9	0.5
PMMA 909B	Acetophenone	1.6	0.6
	Anisole	1.6	0.8
	γ-butyrolactone	0.7	1.5
	Butanone	1.3	0.7
PMMA 590	γ-butyrolactone	1.0	1.0
PMMA 395	γ-butyrolactone	0.6	1.7
PMMA 145	γ-butyrolactone	0.2	4.1
PS 320	γ-butyrolactone	0.6	1.6
PS 770	γ-butyrolactone	1.1	0.92
PS 1690	γ-butyrolactone		

It is well known in intrinsic viscosity determination that if t > 4t$_o$ deviation from ideality due to chain entanglement occurs and the flow times become progressively dominated by 'dimers' and increasingly higher 'mers'. Interestingly all PMMA dilute solutions, but not PS dilute solutions, reported here show a positive divergence from the Huggins and Kraemer equations at a very low concentration, t ≈ t$_0$ but not in the case of polystyrene. The relationship between η_{sp}/c and c at high dilution has been reported for neutral polymer solutions by several groups. In their study, Yang et. al.[10] focused on a better understanding of the viscosity behaviour of the neutral polymer

solutions poly(vinylalcohol) (PVA), poly(vinylpyrrolidone) (PVP) and poly(ethylene oxide) (PEO) in water. Their experimental results show that η_{sp}/c changes regularly with c, indicating that the accuracy of the flow time measurement of both pure solvent and dilute polymer solution is critical. It is noted that Yang et .al[10]. used an ubbelohde viscometer whereas a falling ball capillary was used in this study . In both cases it is believed that the phenomena are the same. The study showed that the abnormal viscosity behaviour of neutral polymer solutions at low concentrations appears because of the systematic errors arising from inappropriate techniques used for determining the viscosity of polymer solution. If that were the case here then would expect similar observations for both PMMA and PS solutions which is not the case. In their study of polyvinyl alcohol (PVA) in NaCl/Water[10] at 25 ^{o}C Ohrn et al reported a rapid increase of η_{sp}/c at low concentrations in η_{sp}/c vs. This they believed to be due to the adsorption of polymer molecules by the capillary walls, which decrease the effective diameter of viscometer capillary. Similar results have also been reported for solutions of polyelectrolyte[11], sodium salt of partially sulphuric acid-esterified poly(vinyl alcohol)(NaPVS)[11], where the relationship between η_{sp}/c and c at low concentrations is even much more complex.

4.3 References

1. L. Xu, W. W. Zhang and S. R. Nagel, *Physical Review Letters* **2005**, **94**, 184505.
2. A. F. M. Barton *Handbook of Solubility Parameters and Other Cohesion Parameters*, CRC Press, **1985**.
3. C. W. Macosko, *Rheology: Principles, Measurements, and Applications* 1 edition edn., Wiley-VCH, **1994**.
4. E. J. Regalado, J. Selb and F. Candau, *Macromolecules* 1999, **32**, 8580-8588.
5. A. Bhattacharya and P. Ray, *Journal of Applied Polymer Science*, **2004**, **93**, 122-130.
6. I. W. Hamley, *Introduction to Soft Matter: Synthetic and Biological Self-Assembling Materials*, 1st Edition edn., **2007**.
7. J. Burke, *AIC Book and Paper Group Annual.*, **1984**.
8. C. M. Hansen, *Hansen Solubility Parameters: A User's Handbook*, Second Edition ed edn., CRC Press, **2007**.
9. H. LWagner, *J. Phys. Chem. Ref. Data*, **1987**, **16**, 165-173.
10. H. Yang, Y. Yan, P. Zhu, H. Li, Q. Zhu and C. Fan, *European Polymer Journal* **2005**, **41**, 329-340.
11. K. Nishida, K. Kaji and T. Kanaya, *Polymer*, **2001**, **42**, 8657-8662.

Chapter Five

The effect of low molar mass H-bonding additives on the inkjet drop generation of polymer-containing fluids

This chapter discusses the effect of hydrogen bonding interactions on the drop generation of both acid and hydroxyl-containing polymer solutions with the aim of understanding whether polymer chain relaxation can be influenced through the use of appropriate polymer co-solvent interactions. Two polymer co-solvent systems of different types are considered.

1. Low molecular weight MMA/MAA co-polymers, Mn = 7 – 10 kDa, Mw = 11 – 15 kDa in a good non-H-bonding solvent, γ-butyrolactone, in combination with a miscible H-bonding co-solvent.

2. Medium molecular weight cellulose acetate butyrate (CAB2) supplied by Eastman, Mn = 30.7 kDa, Mw = 76.6 kDa, 1 wt-% Hydroxyl content in a good non-H-bonding solvent, γ-butyrolactone, in combination with a miscible H-bonding co-solvent.

5.1 Rheological behaviour of polymer solutions

5.1.1 Newtonian fluids

Figure 5.1 shows an element of liquid moving at a strain rate γ under an applied shear stress τ. The viscosity of a liquid is the ratio of the applied shear stress to the resultant strain rate (or equally, the ratio of the shear stress required to move the solution at a fixed strain rate to that of the strain rate). Depending on the change of strain rate versus the stress inside a material, the viscosity can be categorized as having a linear, non-linear, or plastic response.
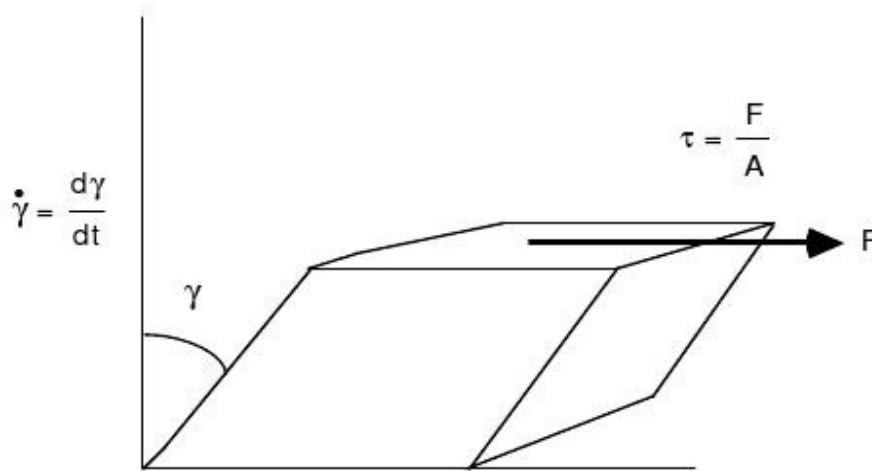
Figure 5.1 An element that deformed by shear [1]

When a material exhibits a linear response it is categorized as a Newtonian material and is defined as:

$$\tau = \eta \frac{du}{dx}$$ 5.1

where τ is the applied shear stress, η is the dynamic viscosity and $\frac{du}{dx}$ is the strain rate where u is the displacement in the x direction and shows linear shear stress – shear strain rate behaviour.

5.1.2   Polymers in solution

The behaviour of polymer chains in solution can be divided into three different regimes: dilute, semi-dilute and concentrated. These different regimes are highly dependent on the polymer mass concentration, and the ratio of the total mass of polymer dissolved in a solution.   Another dependent way is the volume fraction of polymer ϕ, the volume occupied by the polymer in solution ratios, and also the volume of the solution. The polymer density can create a relationship between these concentrations, as:

$$\phi = \frac{c}{\rho} = c\frac{V_{mon}}{M_{mon}}N_{AV}$$ 5.2

The density of the polymer in equation 5.2 indicates the ratio of monomer molar mass M_{mon} and $V_{mon}N_{av}$ is the monomer molar volume. Another important factor is termed the pervaded volume V, equation 5.3, which is the size of the polymer chain measurement.

$$V = R^3$$ 5.3

Where R^3 is the size of the polymer chain.

The pervaded volume is greater than the occupied volume of the polymer chain. Normally, for natural polymers, the dimension is less than 3 which means that the pervaded volume is covered either by the solvent or other chains. The overlap volume fraction $\phi*$, or overlap concentration $c*$, can be defined in this regime. If the volume fraction for a single molecule is inside the pervaded volume,

$$\phi* = \frac{Nv_{mon}}{V}$$ 5.4

Now in this regime, where $\phi = \phi*$, the polymer chains are just overlapping and the pervaded volume closely fills the space. Or, on the other hand, the polymer chains do not interact strongly but begin to overlap. This point is called the overlap concentration (c*) [2].

$$c^* = 1/ [\eta].$$ 5.5

This regime is termed a dilute solution, where the volume fraction is less than the overlap volume fraction $\phi < \phi*$ and here a large distance between each polymer chain occurs, which means that the polymer coils are very far from each other. In addition, the behaviour of the polymer chain here is most likely to be the same as for a pure solvent, as indicated in Figure 5.2.

When $\phi > \phi*$, the polymer chain solutions are termed semi-dilute, as in Figure 5.2 (B). In this regime, the concentration or volume fraction of the polymer chains is less than 1 and the solvent fills most of the occupied volume. The polymer coils behave with physical properties such as viscosity, which means that adding a small amount of polymer to the solvent can cause a dramatic change in the viscosity of the polymer coils and a weak interaction happens between each polymer coil as the entanglement is about to start.

Under a concentrated regime, the polymer chains overlap and the viscosity of the solution increases sharply. In this case, [c]>>>>[c*] (entangled). This is indicated in Figure 5.2 as C.
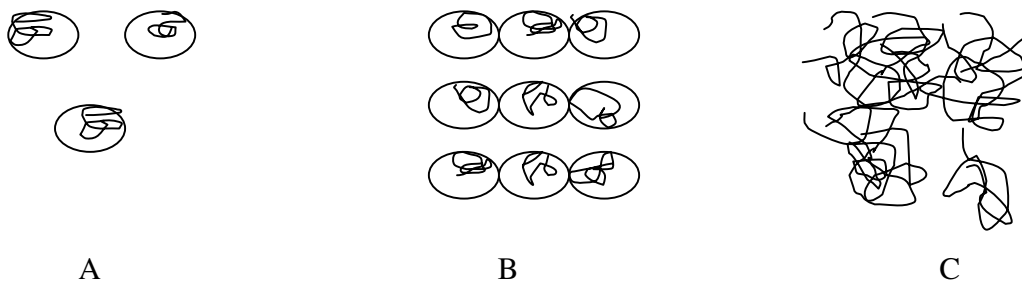
Figure 5.2 Solution regimes for flexible polymers

5.1.3   Non-Newtonian polymer fluids

A non-Newtonian polymer fluid is a fluid where the viscosity changes with a change in shear rate. Therefore, the viscosity itself has different values at different shear rates. An example of a non-Newtonian polymer fluid is a polymer with high molecular weight (polymer melt).
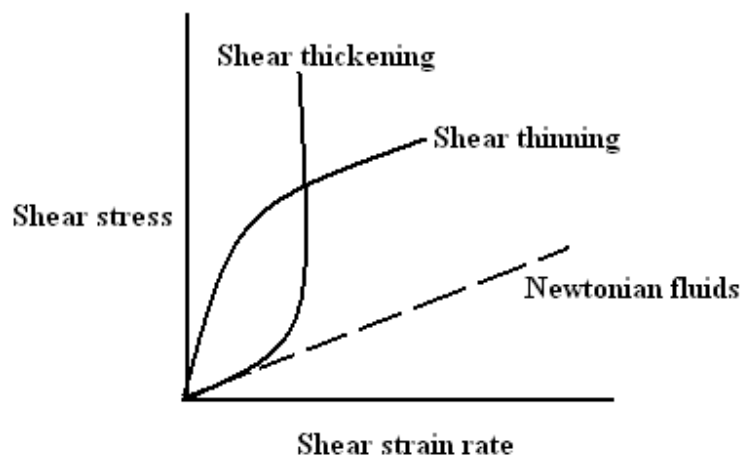
Figure 5.3 Behaviour of non-Newtonian fluids

The figure above shows non-Newtonian behaviour including: shear thinning (pseudoplastic); viscosity decreasing with increasing shear rate and shear thickening (dilatant); viscosity increased by increasing shear rate.

5.2   Polymer Viscoelasticity

In the early nineteenth century, Maxwell and Boltzmann   , became interested in studying viscoleasticity, and since then viscoleasticity has become an important part of polymer engineering.   A viscoleasticity material is one that has properties of being both viscous and elastic when it undergoes deformation. A good example that describes this behavior is bouncing putty where, if putty is rolled into a spherical shape, it can be bounced like a rubber ball[2].

A viscoelastic polymer can become Newtonian or non-Newtonian depending on the relationship between strain and stress over time. So, if the material has a linear response, a Newtonian material is present here, and this also indicates that the stress is linearly proportional to the strain rate. In another type, namely a non-Newtonian fluid, the material exhibits different types of behavior as the viscosity changes. If the viscosity decreases with increasing shear rate, the material exhibits a shear thinning behavior that is termed pseudoplastic. The third type is the

82

stressing-rate effect, a non-linear strain effect, with the curve increasing rapidly with time. The fourth type is the straining-rate effect; the curve decreases with time but it increases as a higher strain rate is applied.

5.2.1   Time–dependent behaviour

The time taken for the material to reach a certain state The time of the material depends on the applied stress and strain. So, there are four different types of viscoelastic material behaviour that depend on time. The first phenomenon is called creep and this happens when the stress is constant at t=0 and strain increases rapidly and decreases slowly over a long time. The second behavior is called relaxation where the strain is held constant and the stress decreases slowly until it decays with time.

5.2.2   Viscoleasticity: mechanical model

According to the four different phenomena mentioned, a stress or strain interaction can be obtained by modelling the viscoelastic material. These models are the Maxwell, Kelvin-Voigt and Standard linear solid models. Viscoelastic behaviour under deformation has an elastic component and a viscous component, as described by Hookes's and Newton's laws. Hookes suggested that the elastic behaviour can be modelled as

$$\sigma = Ee \quad \text{or} \quad \sigma = E\frac{de}{dt} \qquad\qquad 5.6$$

Where E is the elastic modulus and σ is the stress. Newton's law describes it as

$$\sigma = \eta\frac{de}{dt} \qquad\qquad 5.7$$

Where η is the viscosity and $\frac{de}{dt}$ indicates the strain rate.

The problem with Hookes's and Newton's laws is that they only apply at small strains. There are different other models that can describe theses two Hookes   and Newtonians and called a viscoelastic models which are : Maxwell ,Kelvin –voigt and standard linear solid models.

5.2.3   Maxwell Model

This model proposed by Jamws Maxwell in 1867. This model concentrates on the material under constant strain and the gradual relaxation following.

  its obtained by two components the first is a elastic element(Spring)
and second component is the viscous element(damper).

The first compenent which is the elastic component occurs instantaneously which corresponds to the spring and it relaxes immediately after removing the applied stress. The second component which is the viscous component grows more as long as the stress is not removed.

This Model predict an important factor for most of the polymers in the fact that the stress decay exponentially with constant stress conditions. The limitation of this model is that its not capable of predicting creep accurately. Applying this model to soft solids can be done.

5.2.4   Kelvin-Voigt model

This model is composed of two components , the Newtonian damper and the Hookean elastic spring connected in parallel. In contrast to the Maxwell model, This model is used to explain the creep behaviour of different polymers. This model uses linear first order equation and thus,represents a solid underdoing reversible viscoelastic strain. One of the limitation of this model is that its not accurate regarding the relaxation states of polymers which is the opposed in the Maxwell model. This model is applied in many different fields such as organic polymers,rubber and wood.

5.2.5 Standard linear solid model

This model combines the Maxwell model and the Hookean spring in parallel. This model is based on the viscous material as a spring and the dashpot in series with each other and both are in parallel with the lone spring. This model is more accurate that the Maxwell and Levin-voight models in predicting the material effect its only limitation is that it can be difficult to calculate.

5.3 Shear rate dependency of polymer solutions

In general, a decrease in the viscosity while the shear rate increases is called shear thinning. Also, the fluid is referred to as being pseudoplastic. These phenomena can have a dramatic effect on decreasing the viscosity. Many examples show this effect for pseudoplastic fluids, such as a solution of carboxymethyl cellulose (CMC) in water, polyacrylamide in water, and glycerine. Moreover, all the polymer solutions that undergo shear-rate and depend on viscosity are also good examples. On the other hand, some fluids behave in an opposite way such that viscosity increases as shear-rate increases and this phenomena is known as dilatancy or shear thickening, the reason for this behaviour probably being due to a suspension of very small particles in the solution. One example of shear thickening is a starch in ethylene glycerol/water mixtures.

5.3.1 Shear thickening

This theory is seen as an extension of Flory's theory of the expansion parameter to the case where macromolecules would contain segments that associate in an intermolecular fashion. This theory describes the rheological properties of shear-thickening polymer solutions. By using this theory we were able to determine the association constant. Flory also proposed that, when macromolecules with associating groups are placed in an elongational flow field at a sufficiently high strain rate, they will extend, which in return will break the intramolecular associations and allow the formation of intermolecular associations to an extent that is determined by the association constant.

Figure 5.4 Transition from random coil to extended state at a high strain rate[3]

5.3.2 The dynamics of associating chains

In a study that was carried out by Odell and Keller[3] it was found that a macromolecule that is in an elongational flow field undergoes a transition from a random coil to a fully extended state at a sufficiently high rate of strain. Switching off the strain would result in returning the extended macromolecule to a stable state thermodynamically.

This suggests a qualitative model for the phenomenon of shear thickening. In the resting state, the associated macromolecules are in solution as random coils and have different numbers of transient intramolecular associations. Applying a large elongational strain at a sufficiently high rate a sufficient rate will result in extending the macromolecules. The extended chains will face shear, turbulence and Brownian motion which will result in the reformation of the associations. A gel network will be formed as a result of the intermolecular associations which act as crosslinks[3].

5.3.3 Rheology of FM9

FM9 is a polymer formed from t-butylstyrene and methacrylic acid, it contains 11.6 mol % carboxyl groups and has a molecular weight of Mw= $(10 +-2) \times 10^6$ g mol^{-1}; this molecular weight was determined by scattering light in a variety of solutionsAs described in the literature, FM9 exhibits shear thickening and that is why so much attention been given to the study of FM9. Peng and Landel studied the shear thickening effect on FM9 in organic solvents and they found that there is no effect on the threshold strain rate value. However, the shear thickening happens beyond this point and also FM9 solutions show a time-dependent threshold of a shear thickening type.

The beginning of the shear thickening effect was observed and it coincided with normal stress measurements. Their explanation for this particular polymer solution is that the shear thickening increases due to induced hydrogen bonding when molecules are sheared[4]. So, polymer molecules behave in this regime as intramolecular interactions at below a critical rate which depends to a large degree on the concentration. When shear applies, these intramolecules may convert to intermolecules, the interaction being due to hydrogen bonding interactions between polymer chains and polymer coils which are entangled with each other, possibly forming a network between the hydrogen bonds. This change of macromolecules agrees with the Wolff and Dupuis theory.

M.J. Ballard and colleagues studied FM9 and looked at shear thickening under elongational flow. Here is some background about FM9.. Chemically, FM9 is a homogenous copolymer and it does not show systematic variation of molecular weight with the refractive index of the solvent. The dimension of FM9 in the theta-state is unknown. FM9 in kerosene is close to its theta dimension and in a mixture of kerosene/butanol the radius by light scattering is 107 nm, which in return suggests that α =1.30 in the solvent. Kerosene has a density of 780 g dm^{-3} and has a molar volume of approximately 0.218 dm^3 mol^{-1}.

When FM9 is dissolved in a decalin/acetic acid mix (at a ratio of 97/3), the latter will suppress the hydrogen bonding and will be subjected to an elongational flow field, having a relaxation time of 620 microseconds.

The two main differences between these methods are that the hydrogen-bonded FM9 expansion factor is small and that decalin is a more viscous solvent than kerosene. By knowing this we can predict that the hydrogen-bonded FM9 in kerosene should have a critical elongational strain rate. Something that also has a minor effect is the solvency difference between kerosene and decalin. The thermodynamics of FM9 are such that, when FM9 is dissolved in kerosene alone, the hydrogen bonds are switched on and the chains would have contracted to an expansion parameter of 1[3].
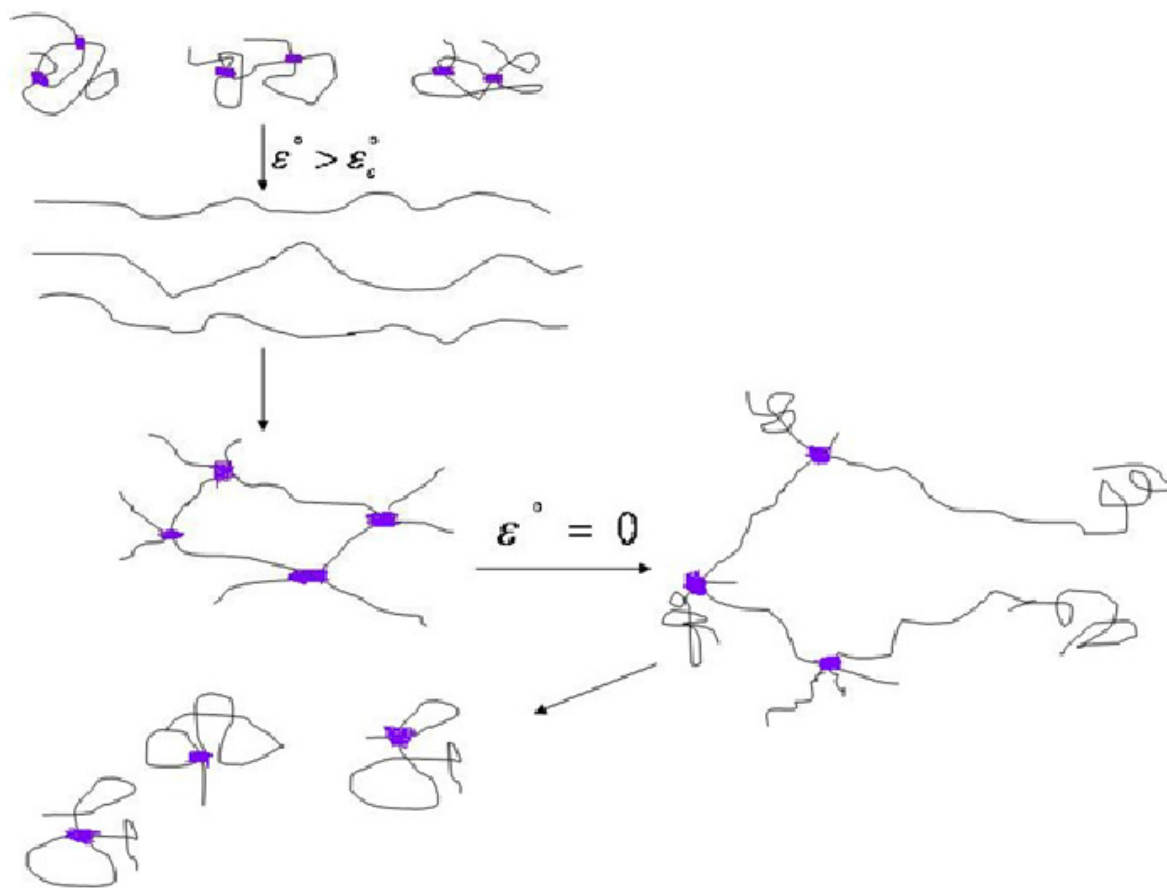
Figure 5.5 Shear thickening mechanism of PMMA/MAA copolymer solutions in hydrocarbon solutions under elongational flow[3].

5.4 Effect of low molar mass H-bonding additives on the inkjet drop generation of fluids containing low molecular weight carboxylic acid polymers

The aim of the study is to look at the effect on chain elongation, during the inkjet process, of functional groups with a polymer backbone having the ability to undergo inter-conversion from intra- to inter-molecular hydrogen bonding. Two polymers were studied, the details of which are given in Table 5.1. γ-butyrolactone was chosen as a solvent due to its high boiling point (204 °C)

which prevents the drying of polymer solutions during the printing process, thus avoiding nozzle blockage.

Table 5.1 Polymers used in the inkjet study

	MMA (wt-%)	MAA (wt-%)	Mn	Mw	c* (g/dl)
Ka 1/59	100	0	7500	11400	15.1
Ka 1/63	92	8	9500	14500	22.7

The following waveform was used in the Microfab printhead.

Table 5.2 Microfab waveform used

	Time (µs)	Voltage (V)	Source	PC Trig.
Idle		0	Mode	Continuous
Rise	10		Drops/Trigger	1
Dwell	25	variable	Frequency	4000 Hz
Fall	5		Strobe Driver	1
Echo	5	0	Strobe Enable	on
Final Rise	5		Strobe Delay	0 µs

Results were repeated at least two times and found to essentially over the whole voltage range, although some variability was occasionally observed but was consistent with the trends discussed. Figure 5.9 as example.

5.4.1   Characteristic behaviour of an inkjet printing Newtonian fluid

For reference, the behaviour of a Newtonian fluid has been evaluated under the drop-on-demand conditions used in this study. The Newtonian case serves as an important inelastic baseline from

which to compare the elastic effects of the polymers. Due to its low viscosity it was not possible to reproduce pure γ-butyrolactone under these inkjet conditions, so a water/glycerol/isopropanol mixture at 35/60/5 % v/v was used having a viscosity of 4.8 cP and a static surface tension of 36.0 mN/m. Figure 5.6 shows photo sequences for the fluid at 40, 50 and 60 V applied voltage as a function of time, t. Results are shown where the data has been shifted by t_d, being the delay between the initial voltage rise and the appearance of an outwardly moving meniscus.

40V						
50V						
60V						
t-t$_d$ (μs)	10	20	30	45	60	100
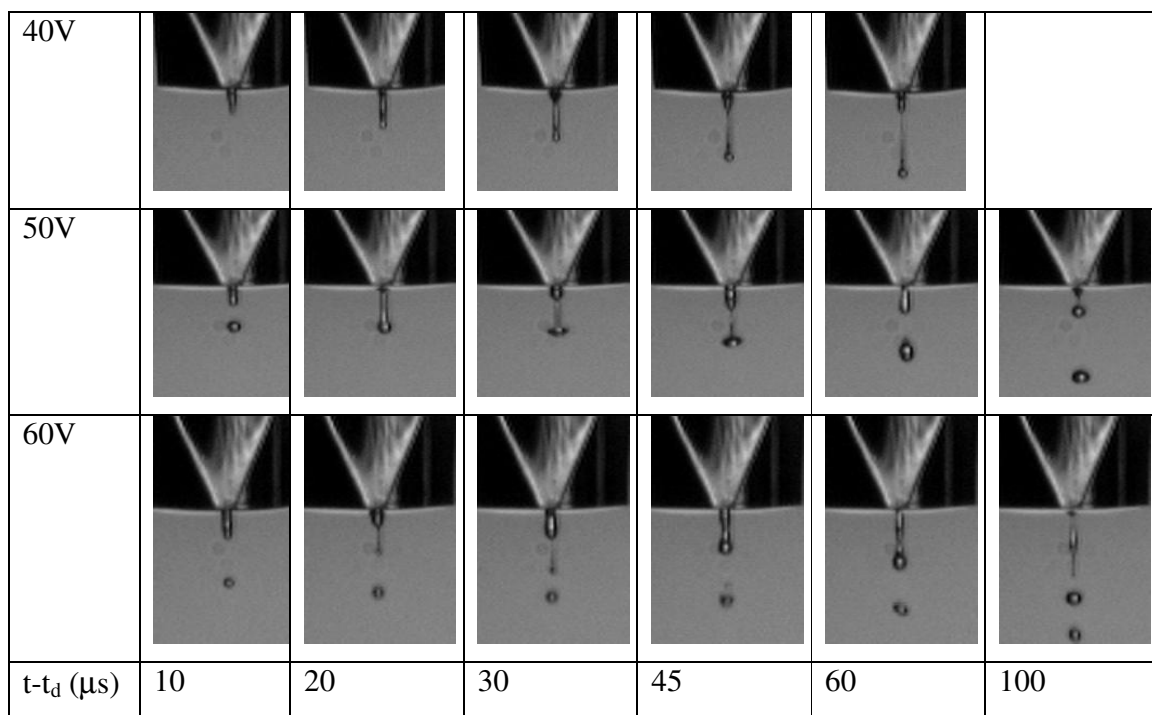
Figure 5.6 Photo sequences of the formation of a Newtonian droplet consisting of water/glycerol/isopropanol with an applied voltage of 40, 50 and 60 V at 25 °C[5]

From the photo sequences, the distance travelled L by the primary droplet, defined as the distance between the underside of the primary droplet and the nozzle plate, as a function of time, can be determined as shown in Figure 5.7. Qualitatively, at a low applied voltage (40 V) we can see rapid conical necking to form a large primary droplet and a long thin ligament tail. Pinch-off occurs close to the nozzle after 60 μs with subsequent droplet and ligament coalescence into a single drop after 105 μs. Increasing the applied voltage leads to instability in the ejected ligament with multiple pinch-off events as shown for both 50 V and 60 V. This fluid exhibits many of the

features previously reported for low-viscosity Newtonian fluids and is typical of the previously discussed regime1[5-7].
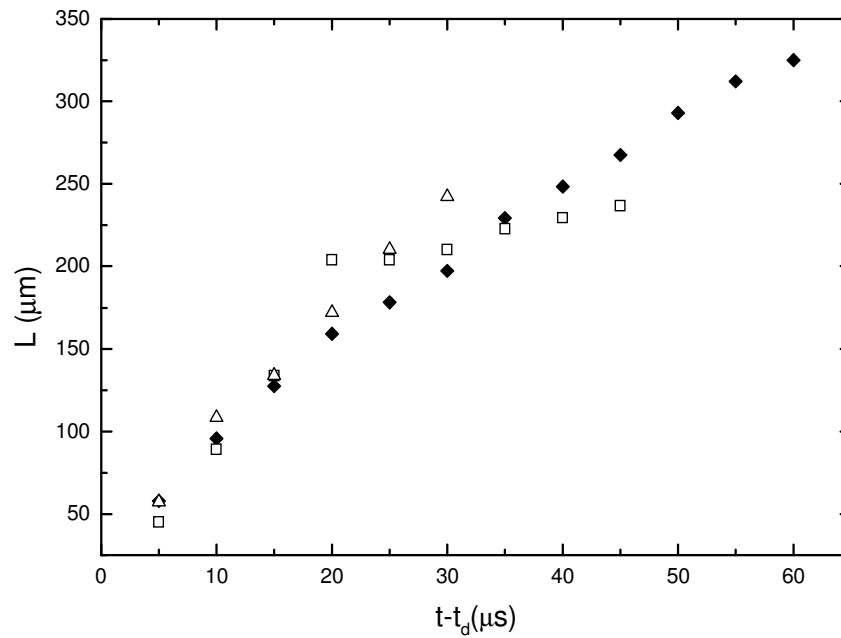
Figure 5.7 Distance travelled L as a function of time t–td to first break-off at (♦) 40 V, (□) 50 V and (Δ) 60 V for water/glycerol/isopropanol at 25 $^{\circ}$C. LSTD. = 1 μm and (t-td)STD. = ± 0.5 μs [8]

.

5.4.2 Characteristic behaviour of an inkjet printing Ka 1/59 low molar mass PMMA

Table 5.3 Physical properties of PMMA (Ka 1/59) solutions in γ-butyrolactone at 25 $^{\circ}$C

Concentration (g/dl)	c/c*	Viscosity (cP)	Surface tension (mN/m) +/- 1
8	0.5	3.	39
15	1	6	37
23	1.5	11	36

All concentrations showed qualitatively similar behaviour with drop break-off near to the nozzle tip with a primary droplet attached to a thin ligament. The delay time between the initial voltage rise and the appearance of an outwardly moving meniscus was in the range 33 +/- 3μs for all three fluids.

Figure 5.8 shows the photo sequence for c/c* = 0.5 at 25 V applied voltage as a function of time, t-t_d for Ka 1/59 (PMMA). The different stages of the drop ejection process are clearly visible (i.e. drop development, elongation and break-up). During flight, each drop then split into a primary droplet and smaller satellite droplets which did not coalesce within 1 mm of the nozzle tip. Although the pulse employed and the overall timescale of drop ejection is the same as that shown for the Newtonian fluid in Figures 5.5 and 5.6, the drop formation process is qualitatively different. All fluids show pinch-off near to the nozzle tip with a primary droplet attached to a thin ligament. From the obtained photo sequences the distance traveled L by the primary droplet as a function of time was determined as shown in Figure 5.9 and 5.10 for c/c* = 0.5 and 1.5 for a range of applied voltages.

| 0 μs | 30 μs | 65 μs | 78 μs |
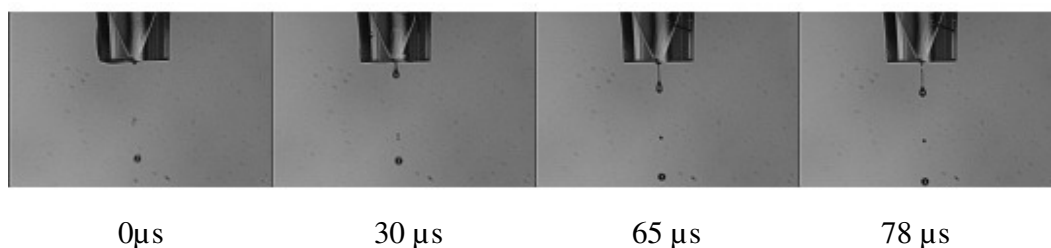
Figure 5.8 Drop formation for Ka 1/59 at c/c* = 0.5 in γ-butyrolactone at 25 ^{o}C and an applied voltage of 40 V

From the *L-t* data we can identify two distinct regimes[4]. At short time intervals, t-t_d < 20 μs, the stretching is determined by the interplay of inertia and surface tension and is therefore independent of polymer concentration and molecular weight. At long time intervals, the distance travelled increases linearly with time and the velocity becomes constant, implying that frictional force on the droplet can be ignored and the ligament properties are determined by the rheological properties of the fluid. Similar behaviour has been reported for PEO in glycerol water[4] polystyrene in acetophenone[8] and cellulose ester butyrate in γ-butyrolactone[9].
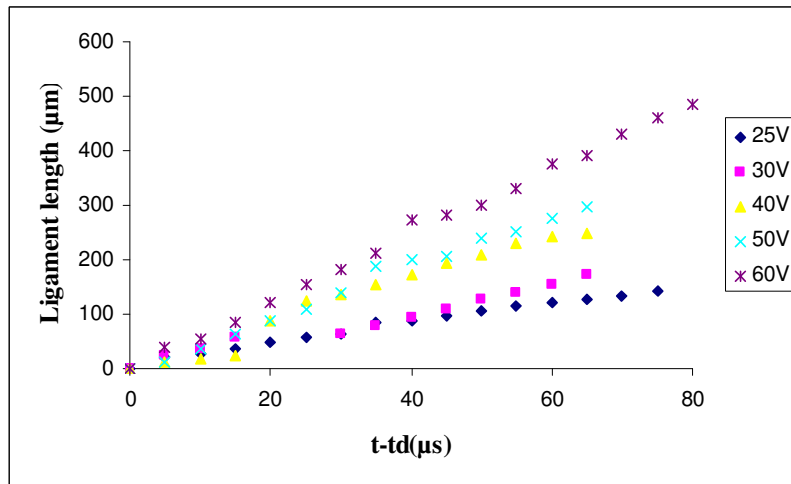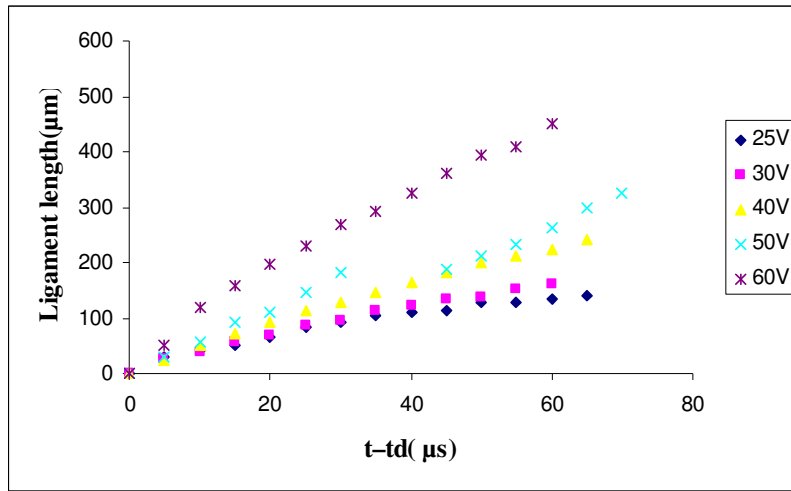
Figure 5.9 Distance travelled, L, as a function of time, t–td, to first break-off point for Ka 1/59 in γ-butyrolactone at c/c* = 0.5 at 25 °C (upper Figure is first repeat) (lower Figure is second repeat).
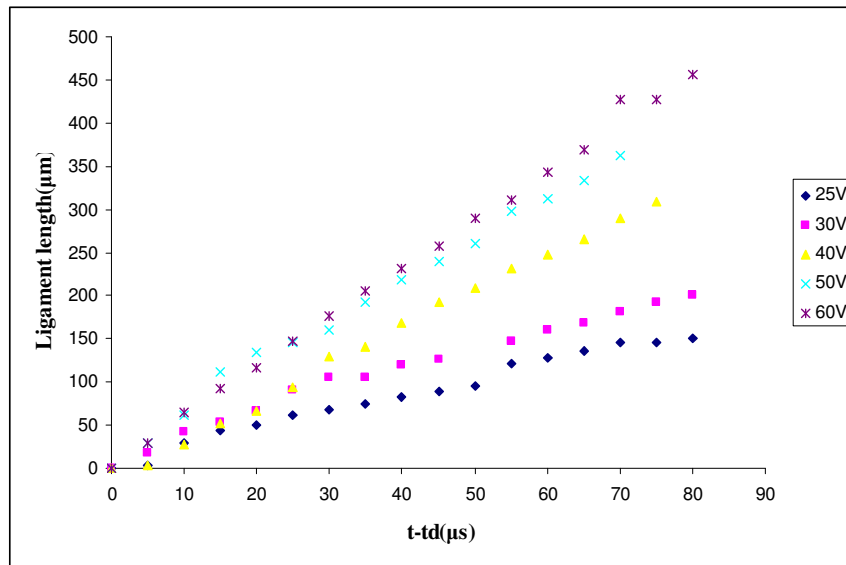
Figure 5.10 Distance travelled, L, as a function of time, t–td, to first break-off point for Ka 1/59 in γ-butyrolactone at c/c*=1.5 at 25 ^{o}C

Increasing the applied voltage results in a longer ligament at rupture due to increasing kinetic energy applied to the meniscus. The slope in stage II increases with applied voltage, indicating that droplet velocity is increasing, again due to the increased amount of kinetic energy given to the fluid. The rupture time remains constant due to the constant viscoelastic nature of the fluid. The effect of reduced concentration on ligament length at rupture is shown in Figure 5.11.

Figure 5.11 Distance travelled, L, as a function of time, t–td, to first break-off point for Ka 1/59 in γ-butyrolactone, at reduced concentrations of 0.5, 1.0 and 1.5. at 50V

It has been proposed that drop break-up behaviour is in part related to the strain hardening resulting from the presence of polymer at a high strain rate[6-8,10]. The micro-rheological explanation for strain hardening is a sudden transition of the polymer chain from a coiled to a stretched state, which is accompanied by a strong increase in the hydrodynamic drag. The coil-stretch transition for linear polymers occurs at a critical Weissenberg number:

$$W_{ecrit} = \varepsilon_{crit} . \tau_1 \qquad\qquad 5.8$$

where τ_1 denotes the longest relaxation time and ε_{crit} the critical elongation rate[11, 12]. The longest polymer chain relaxation time is typically described by the Zimm non-free-draining relaxation time, λ_z[5, 13].

$$\lambda_z = \frac{\eta_s [\eta] M}{RT} \qquad\qquad 5.9$$

For the inkjet process, the strain rate at the nozzle tip is such that the critical Weissenberg number is exceeded for all polymer molecular weights at the pinch region, which is the point at which the ligament is attached to the nozzle tip meniscus[4, 9]. When the strain is removed, the extended polymer chain then returns to the more thermodynamically stable coiled state.

The data indicates that, going through c/c* = 1, the ligament length does not fall off, as previously reported for high molar mass cellulose esters in γ-butyrolactone[7], but continues to rise gently. For Ka 1/59 we calculate λ_z from Equation 5.9 to be of the order of 0.05 μs at 25 $^{\circ}$C, which is short on the timescale of the experiment. Given the low molecular weight of the polymer, the extent of entanglement between the chains is small and hence it is not surprising, over the concentration range studied, that we see little difference in drop break-up behaviour. In their study of four different PMMAs (linear and star) with different high and low molecular weight, Schubert et al found that the distance travelled L for a droplet as a function of time gave a single curve when c/c*=1, but beyond this point the ligament for different PMMAs collapsed. This was caused by the fact that, whereas when droplets travel for a short time an interplay of inertia and surface tension can play an effective role in obtaining ligament stretch in this region,

which means that the rheology of the polymer is independent and does not affect the droplet, at longer times the distance travelled increases linearly with time.

5.4.3 Inkjet printing by methacrylic acid containing copolymer

The study focused on the effects of carboxylic comonomers, based on polymer Ka 1/63 92/8 MMA/MAA, printing in γ-butyrolactone at c/c* = 0.5, 1.0 and 1.4 (Table 5.5).

Table 5.4 Physical properties of PMMA (Ka 1/63) solutions in γ-butyrolactone at 25 ^{o}C

Concentration (g/dl)	c/c*	Viscosity (cP)	Surface tension (mN/m) +/- 0.5
7.5	0.5	3.1	38.7
15.1	1	6.2	36.1
22.6	1.5	11.2	37.5

Figure 5.12 shows the photo sequence for c/c* = 0.5 at 25 V applied voltage as a function of time, t-t_d. All concentrations showed qualitatively similar behaviour with drop break-off near to the nozzle tip with a primary droplet attached to a thin ligament, as already seen for Ka 1/59. The delay time between the initial voltage rise and the appearance of an outwardly moving meniscus was in the range 33 +/- 3μs for all three fluids.

| 0μs | 20 μs | 65μs | 85 μs |
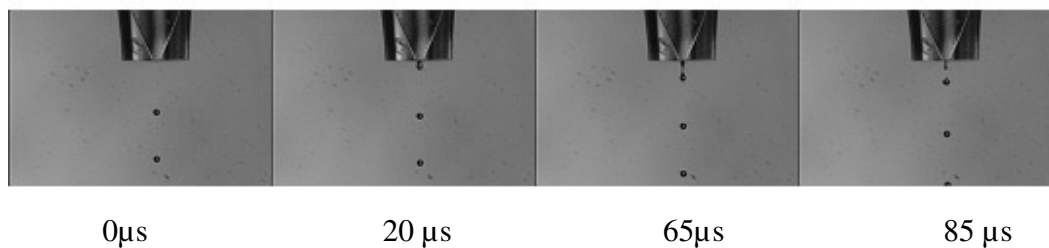
Figure 5.12 Drop formation for Ka 1/63 at c/c* = 0.5 at 25V

Again, from the *L-t* data we can identify two distinct regimes, as in Figure 5.13[9]. At short time intervals, t-t_d < 20 μs, the stretching is determined by the interplay of inertia and surface tension and is therefore independent of polymer concentration and molecular weight. At long time intervals, the travelled distance increases linearly with time and the velocity becomes constant,

implying that frictional force on the droplet can be ignored and the ligament properties are determined by the rheological properties of the fluid.
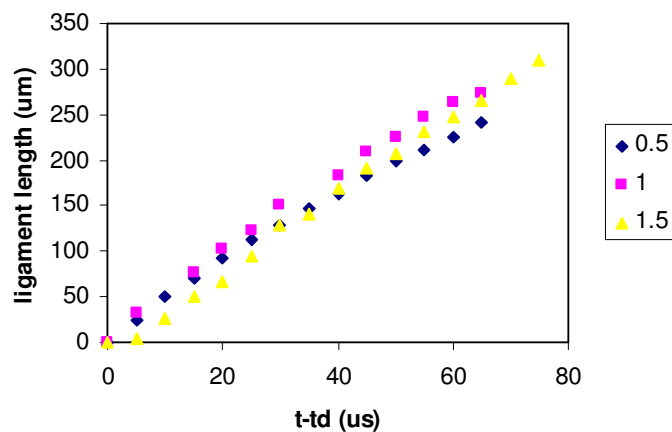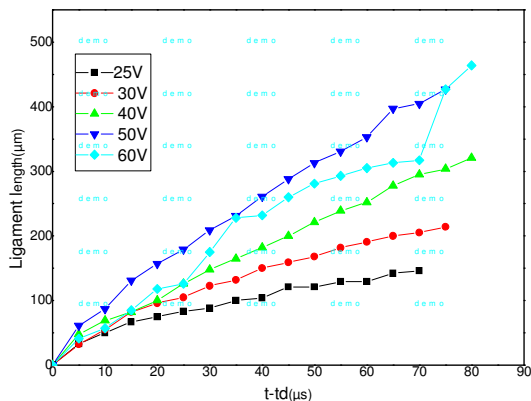

Figure 5.13 Distance travelled, L, as a function of time, t–td, to first break-off point for Ka 1/63 in γ-butyrolactone at c/c*=1

On going through c/c* = 1 the ligament length does not fall off, as previously reported for high molar mass cellulose esters in γ-butyrolactone[7], but continues to rise gently. For Ka 1/63 we again calculate λ_z from Equation 5.9 to be of the order of 0.04 μs which is short on the timescale of the experiment. Given the low molecular weight of the polymer, the extent of entanglement between the chains is small and hence it is not surprising, over the concentration range studied, that we see little difference in drop break-up behaviour. Both Ka 1/59 and 1/63 show the same overall drop break-up behaviour with the only difference being the longer ligament length at rupture for the acid-containing polymer when compared with the PMMA homopolymer, Figures 5.14 – 5.15.
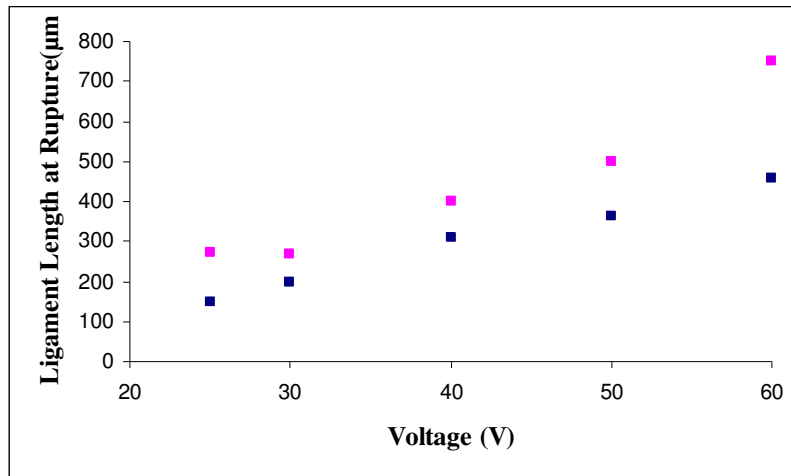
Figure 5.14 Ligament rupture length (µm) as a function of applied voltage (V) at c/c* = 1.5 in γ-butyrolactone. ■ represents Ka1/59 and ■ represents Ka1/63.
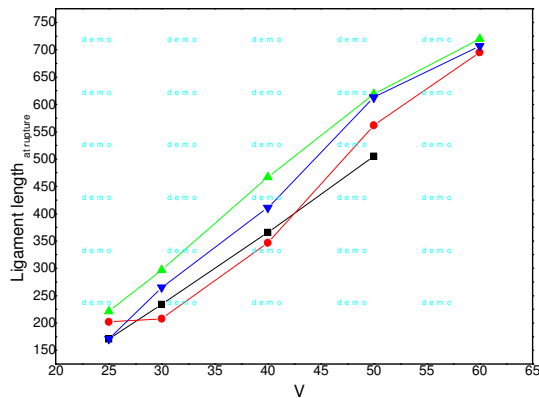
Figure 5.15 Ligament rupture length (µm) as a function of applied voltage for Ka 1/59 and Ka 1/63. Ka 1/59 (■) at c/c*=0.5 and Ka 1/63 at c/c*=0.5 (▲), Ka 1/59 (●) and for Ka 1/63 (▼) at c/c*=1

Given the similar molecular weights and comparable Zimm relaxation times, this is possibly weak evidence for the presence of inter-chain hydrogen bonding leading to greater viscoelasticity. This is in part supported by the higher overlap concentration for Ka 1/63 (with acid), which could suggest that the polymer chain is less swollen due to internal H-bonding when in the relaxed state.

5.4.4 Effect of low molar mass H-bonding additives on the inkjet drop generation of fluids containing low molecular weight carboxylic acid polymers

It is well known that, in the case of elongation flow, macromolecules will convert from the coiled to the fully extended state, as mentioned earlier. These polymers behave as weakly-associating polymers; therefore, while the polymer chain is extended, there is the [3]possibility of converting from intra-molecular to inter-molecular association However, the way to reduce or stop these interactions is to add H-bonding co-solvents[14] solution[3]. To explore this further, Ka 1/63 at c/c* = 1 was formulated with increasing amounts of t-butanol to see if this might influence the proposed inter- and intra-molecular H-bonding.

The effect of t-butanol on the overlap concentration in γ-butyrolactone/t-butanol solvent blends is shown in Figure 5.16 for Ka 1/63. On going from 100/0 to 80/20 γ-butyrolactone/t-butanol, c* decreases with increased t-butanol concentration by 15%, indicating that the polymer coil is getting bigger and hence the co-solvent mixture is a better solvent or, more probably, partial or complete MAA/t-butanol H-bonding has occurred.
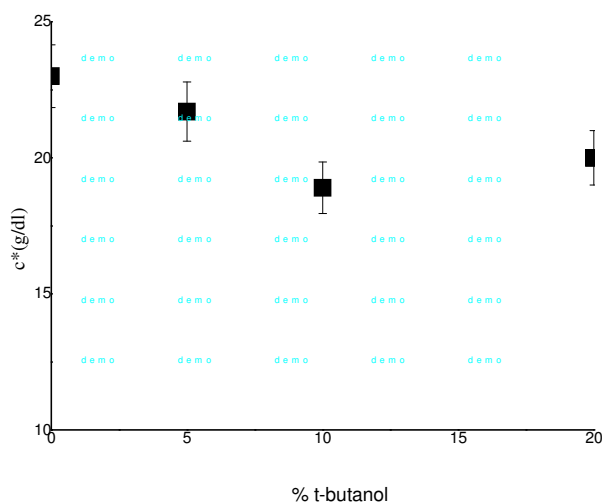
Figure 5.16 Effect of γ-butyrolactone/t-butanol solvent ratio on c* for Ka 1/63

The following formulations were created, representing molar ratios of t-butanol/MAA of 4.7:1, 9.4:1 and 14:1 respectively. Only the two lower t-butanol formulations could be jetted (see Table 5.6).

Table 5.5 Physical properties of Ka 1/63 in γ-butyrolactone / t-butanol at c/c* = 1

γ-butyrolactone : t-butanol (w/w)	Mole ratio Carboxylic acid: t- butanol	Ka1/63 (g/dl)	Viscosity (cP)	Surface tension (mN/m)
95/5	4.7:1	15	14	39.1
90/10	9.4:1	18	14	34.3
80/20	14.1:1	15	high	Not determined

| 0μs | 20 μs | 65 μs | 75 μs |

| 0μs | 40μs | 70μs | 100μs |

| 0μs | 40μs | 70μs | 103μs |
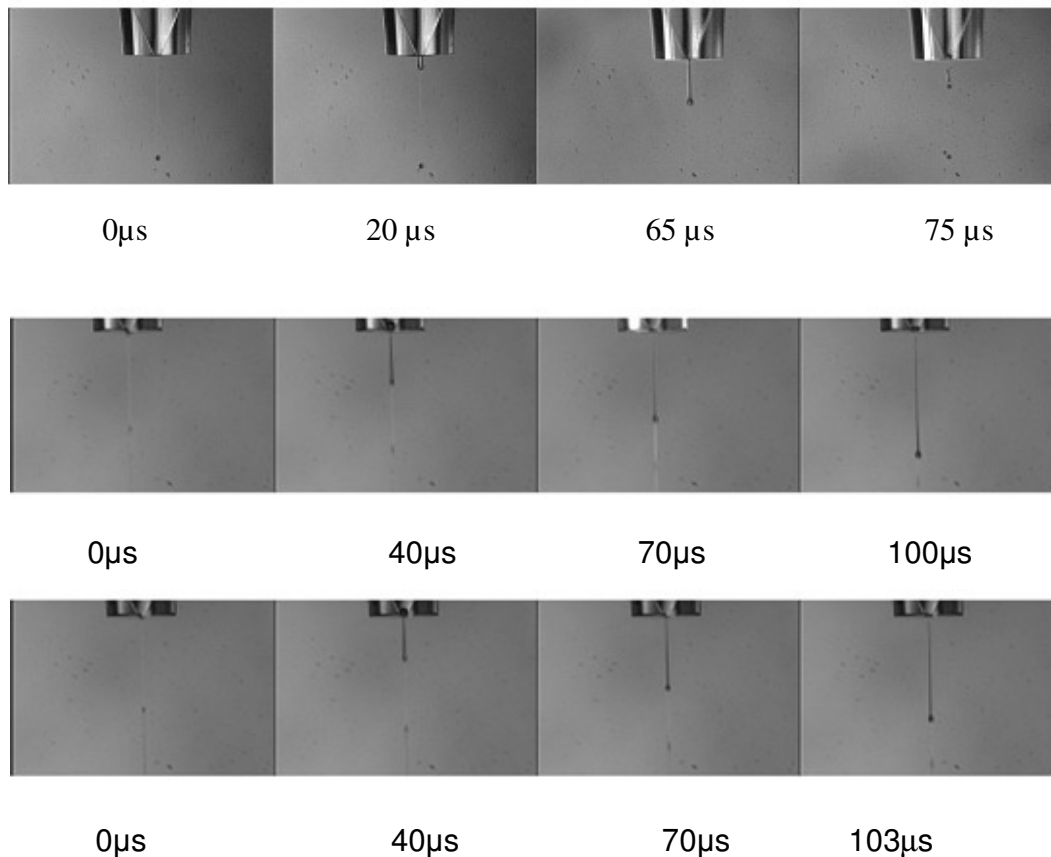
Figure 5.17 Drop filament formation through the inkjet process for (top to bottom) γ-butyrolactone / t-butanol 100/0, 95/5, 90/10 at an applied voltage of 50 V for Ka 1/63

From Figure 5.17 we observe that the ligament at rupture is much longer in the presence of t-butanol and that the time to rupture has increased by approximately 33%. We had expected the t-butanol to disrupt any transient network formation occurring upon elongation. If this had been

the case, a decrease in ligament length may have been expected. That we do not see this is maybe due either to stabilization of the extended state, which is unlikely, or the 'solvation state' of the polymer changing on jetting, with the polymer becoming more swollen and thus increasing the non-elongational viscosity. This may result from breaking intra-molecular MAA/MAA H-bonding on extension and replacing it fully with MAA/t-butanol H-bonding on relaxation, as in Figure 5.15. This is possible given the large molar excess of t-butanol to the available MAA.

5.5 Effect of low molar mass H-bonding additives on the inkjet drop generation of fluids containing medium molecular weight cellulose acetate butyrate (CAB2)

In this study we have focused on the effect of H-bonding miscible co-solvents on the inkjet printing of a specific cellulose ester polymer (CAB2). CAB polymers are the reaction product of combining acid anhydrides and organic acids with the hydroxyl groups found on the anhydroglucose repeating units of a cellulose molecule (see Figure 5.18[15]). Eastman CAB polymers are synthesised from cellulose, which is a natural polymer and a major component of plant-cell walls[16, 17].
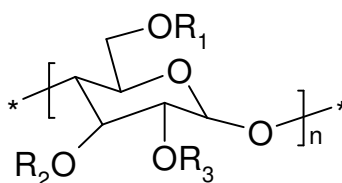
Figure 5.18 Chemical structure of cellulose ester (CAB2) where R_1, R_2 and R_3 are Acetyl, Butyryl or H; 2 wt-% acetyl, 52 wt-% butyryl, 1 % hydroxyl, Mn = 30.7 kDa, Mw = 76.6 kDa

CAB polymers have a helical coil structure in solution and are considered to be weak rod-like polymers[18]. These polymers are of interest since they contain segments which are capable of H-bonding and segments which are hydrophobic. It has been shown that such polymers may undergo shear thickening, or strain hardening, arising through a change from primarily intramolecular to intermolecular association[3,14,19,20] .CAB2 was chosen since its jetting behaviour

in γ-butyrolactone has been extensively studied over a broad range of concentrations c/c* = 0.2 – 3.0.

Acetic acid and t-butanol were chosen as prospective H-bonding additives and formulated in γ-butyrolactone at between 1:1 – 1:5 additive (CO_2H/OH) : CAB2 OH group mole ratio at a polymer concentration c/c* = 1. The effect of the additive on polymer overlap concentration was determined and tabulated in Table 5.6, with ink formulations given in Table 5.7.

Table 5.6 Intrinsic viscosity results for CAB2 in γ-butyrolactone plus H-bonding additives determined at 25 ^{o}C.

Mole ratio CAB2 OH: solvent	CAB2	Additive	Ubbelohde	
			$[\eta]$ / dl/g	c* / g/dl
	100	0	0.063 +/- 0.006	15.8
1:1		Acetic acid	0.057 +/-0.006	17.5
1:2			0.060 +/- 0.005	16.6
1:5			0.073 +/- 0.007	13.6
1:1		Butanol	0.064 +/- 0.006	15.6
1:2			0.058 +/- 0.006	17.3
1:5			0.072 +/- 0.007	13.9

Table 5.7 Ink formulation data for CAB2 inks at constant c/c* = 1

	Ink formulation (g)				η (m.Pa.s)	γ (mNm^{-2})
	CAB2	γ-B	t-butanol	Acetic acid		
γ-Butyrolactone /acetic acid 1:1	17.5	100		0.0995	4.7	34
γ-Butyrolactone /acetic acid 1:2	16.6	40		0.199	4.5	33
γ-Butyrolactone /acetic acid 1:5	13.6	40		0.398	4.8	34
γ-Butyrolactone /t-butanol 1:1	15.6	100	0.123		4.82	34.4
γ-Butyrolactone /t-butanol 1:2	17.3	40	0.246		4.77	33
γ-Butyrolactone /t-butanol 1:5	13.9	40	0.492		5	33.3

Table 5.8 Effect of OH-group on t-butanol and Acetic acid ratio on ligament rupture for CAB2 at c/c* =1

V	CAB OH : t-butanol (mol/mol)							
	1:0		1:1		1:2		1:5	
	t_{rup} (μs)	L_{rup} (μm)	t_{rup} (μs)	L_{rup} (μm)	t_{rup} (μs)	L_{rup} (μm)	t_{rup} (μs)	L_{rup} (μm)
40V	70	171	80	208	75	170	75	186
50V	85	360	80	337	75	217	75	261
60V	85	537	80	398	78	233	80	272
	CAB OH : acetic acid (mol/mol)							
40V	70	171	77	210	75	118	70	112
50V	85	360	81	347	75	189	70	187
60V	85	537	80	518	75	233	70	242

Table 5.8 above shows the ligament length of CAB2 at the time of rupture with two different solvents at a polymer concentration of c/c* = 1. Acetic acid as a co-solvent shows a decrease of ligament length due to polymer chain entanglement for the extended state; also, the relaxation time will be longer than in the Zimm model calculation. However, with regard to Keller's theory, some of the polymer is weakly associating and that should break the chain in the case of an increase in relaxation time, forming an intermolecular association that will create a transit gel with high viscosity, so that the h-bonding of the co-solvent might interact as well and form another network with the polymer chain becoming more swollen. In the case of t-butanol, as we can see from Table 5.8, there is not all that much happening to the ligament at the rupture time.

Figures 5.19 - 5.22 show the effect of adding two different solvents (t-butanol and acetic acid) to CAB soluble in γ-butyrolactone with different molar ratios of these additives. Also, the study is concerned with ligament length re time. A theory that can explain the behaviour of a random polymer coil and its extension in elongational flow was suggested by Odell and Keller, who say that macromolecules can undergo change from coiled polymer to extended state under high strain rates. So, in our case, we have three examples that are of interest and fully explained..
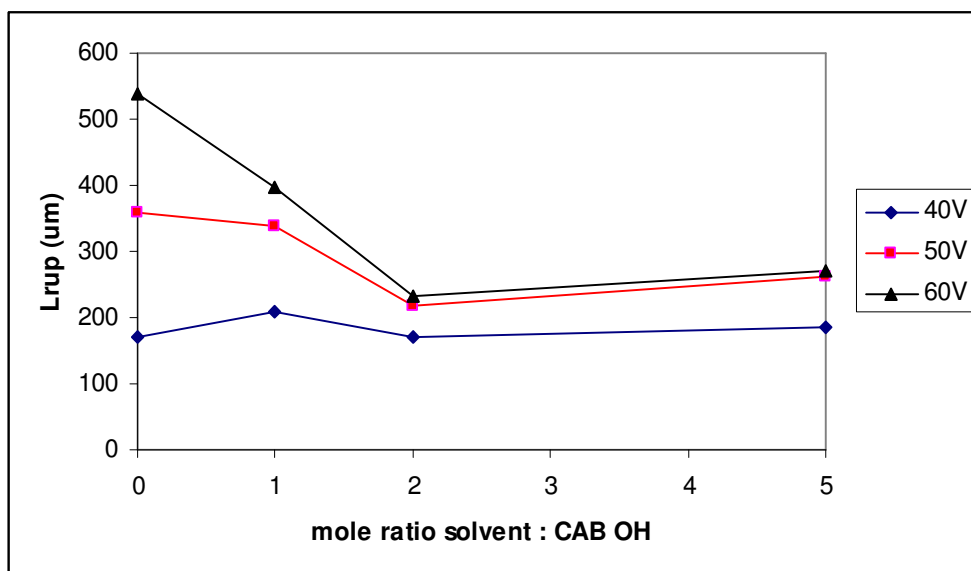
Figure 5.19 Effect of t-butanol on ligament length at rupture for CAB2 in γ-butyrolactone at c/c/* = 1 and 25 $^{\circ}$C, using a MicroFab printhead, as a function of drive voltage

| 0 µs | 30 µs | 60 µs | 90 µs |
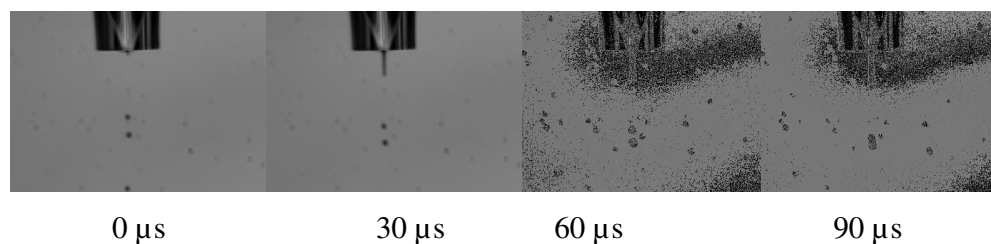
Figure 5.20 Photo sequence of drop formation for CAB2 in (1:2 γ-Butyrolactone: t-butanol) at c/c*=1
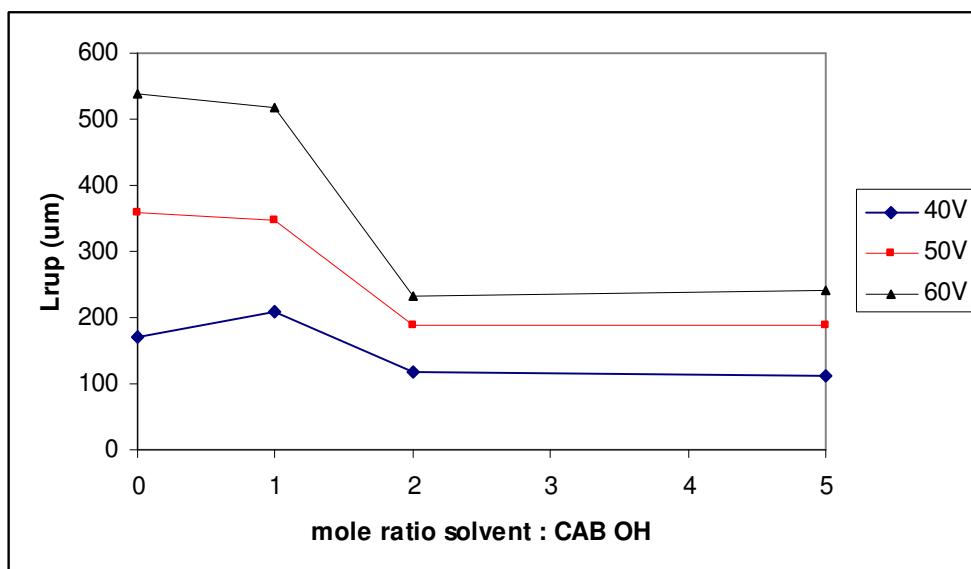
Figure 5.21 Effect of acetic acid on ligament length at rupture for CAB2 in γ-butyrolactone at c/c* = 1 and 25 $^{\circ}$C, using a MicroFab printhead, as a function of drive voltage

| 0 µs | 30 µs | 50 µs | 79 µs |
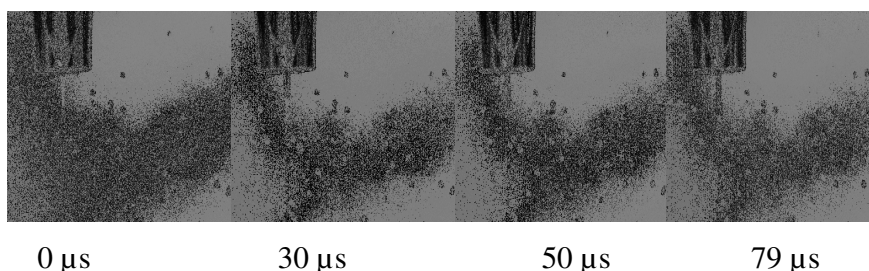
Figure 5.22 Photo sequence of drop formation for CAB2 in (1:4 γ-Butyrolactone: Acetic Acid) at c/c*=1

a. Cellulose ester (CAB2) in γ-butyrolactone

Before jetting, the polymer coils are in the solution and behave as intra-chain associations. When an elongational shear is applied the polymer chain will extend and form inter-chain H-bonds which rapidly create a gel as previously observed for FM9[4] . After the shear is removed the chains will relax back to the coiled state more slowly than the calculated Zimm relaxation rate due to the need to break the formed inter-molecular H-bonds.

b. Cellulose ester (CAB2) in γ-butyrolactone with either t-butanol or acetic acid at 1: mole ratio

In this case, an equal combination of CAB2 and CAB2/additives is considered, so the intra-chain of this combination is extended and the additive, for example t-butanol, will react, either H-bonding with CAB2 or directly with CAB2 itself. The inter-chain that would be produced for either t-butanol H-bonding with CAB2. CAB2 has a large viscosity due to performing a network of both inter-chain forms. The hydrogen bonding here is not strong enough for the remaining gel. The effect of adding the same molar amount of additive to CAB2 would allow us to predict that there is not a big change either in the ligament length at rupture or the time of rupture.

c. Cellulose ester (CAB2) in γ-butyrolactone with either t-butanol or acetic acid at a molar excess ≥ 2:1

In this regime, co-solvent was added such that it was in ≥ 2:1 excess over the hydroxyl groups on the polymer chain. As shown in both Figures 5.21 and 5.22, there was a decrease in the ligament length which can be explained as a case of the intra-chain of a combination of double the amount of t-butanol H-bonding or acetic acid H-bonding strongly reacting with CAB2 H-bonding while extended. After some time these intra-chains will reform as inter-chain associations with very large viscosity and form a network that will decay by the time of the chain returning when the elongational force is switched off. But as to what leads to a decrease in the ligament length, the answer would be that additional amounts of co-solvent would disrupt any network formed during the elongation as it mention in figure 5.5.

5.6 Conclusions

The theory covering shear-thickening polymer solutions predicts a transition from the smooth shear thickening of a low polymer concentration to abrupt thickening at high concentrations.

The theory agrees with the experimental results on the constancy of the critical stress but the differences in the values arise from different definitions of the critical strain rate.

In a different study into the same matter that was carried out by J.A. Odell et al, we can note the increasing concentration shift in the curves of the strain rate towards lower sigma values. Through observing different concentrations we can see that the extension of the chains occurs at lower strain rates than would be expected from the network effect. The theory predicts that at higher concentrations the entanglement effects will be dominant, so the extension of the chain might be suppressed by the network effect. The main focus of Odell et al's study was the delocalization of the birefringent zone within the flow field in the form of the flare effect. Odell and his colleagues show the sudden appearance of the localized birefringement line at the critical strain rate. Therefore, PMMA/MMA in co-solvents of t-butanol and γ-butyrolactone could have the same influence from FM9 where the hydrogen bonding can be suppressed by the addition of glacial acetic acid. In this additional case In this case of addition, the solution behaves like atactic polystyrene; the elongational viscosity at low strain rates is completely suppressed.

In theory, there is a method that assesses the lifetime of transient chemical bonds. The shear-thickening theory suggests that the system will acquire the characteristics of a permanent network according to conventional criteria, and then it will appear as a gel. This gel form represents the distant end of the spectrum of transient networks.

5.7 References

1.   http://www.ias.ac.in/initiat/sci_ed/resources/chemistry/Viscosity.pdf. (02/01/2010),
2.   Rubinstein, M.; Colby, R. H., *Polymer Physics*. Oxford University Press: Oxford: **2003**.
3.   Ballard, M. J.; Buscall, R.; Waite, F. A., *Polymer* **1988,** 29, (7), 1287-1293.
4.   Choplin, L.; Sabatiè̀l, J., *Rheologica Acta* **1986,** 25, (6), 570-579.
5.   de Gans, B. J.; Duineveld, P. C.; Schubert, U. S., *Advanced Materials* **2004,** 16, (3), 203-213.
6.   Christanti, Y.; Walker, L. M., *Journal of Non-Newtonian Fluid Mechanics* **2001,** 100, (1-3), 9-26.
7.   Cooper-White, J. J.; Fagan, J. E.; Tirtaatmadja, V.; Lester, D. R.; Boger, D. V., *Journal of Non-Newtonian Fluid Mechanics* **2002,** 106, (1), 29-59.
8.   De Gans, B. J.; Kazancioglu, E.; Meyer, W.; Schubert, U. S., *Macromolecular Rapid Communications* **2004,** 25, (1), 292-296.
9.   Xu, D.; Sanchez-Romaguera, V.; Barbosa, S.; Travis, W.; Wit, J. d.; Swan, P.; Yeates, S. G., *Journal of Materials Chemistry* **2007,** 17, (46), 4902-4907.
10.   Christanti, Y.; Walker, L. M., *Journal of Rheology* **2002,** 46, (3), 733-748.
11.   De Gennes, P. G., *The Journal of Chemical Physics* **1974**, 5030-5042.
12.   De Gans, B. J.; Xue, L. A., U. S.; Schubert, U. S., *Macromolecular Rapid Communications* **2005,** 26, (4), 310-314.
13.   Doi, M. R.; Edwards, S. F., *The Theory of Polymer Dynamics*. Oxford University Press: **1986**.
14.   Odell, J. A.; Keller, A.; Miles, M. J., *Polymer* **1985,** 26, (8), 1219-1226.
15.   Koleske, J. V., *Paint and Coating Testing Manual*. Fourteenth Edition ed.; **1995**.
16.   BUCHANAN, C., M ; WO1991/014709, **1991**.
17.   Eschbach, P. Eastman Features Cellulose Esters Technologies at INDEX 2005. (12/08/2010),
18.   Vyas, N. G.; Shashikant, S.; Patel, C. K.; Patel, R. D., *Journal of Polymer Ccience. Part A-2 Polymer Physics* **1979,** 17, (11), 2021-2029.
19.   Peng, S. T. J.; Landel, R. F.; , *Journal of Applied Physics* **1981,** 52, (10), 5988-5993.
20.   Savins, J. G., *Rheologica Acta* **1968,** 7, (1), 87-93.

Chapter Six

Flow-Induced Polymer Degradation during Ink-Jet Printing of Poly(methylmethacrylate) and Polystyrene

6.1 Introduction.

Ink-jet printing has developed as an important technology for the defined spatial deposition of polymer solutions in applications as diverse as graphics, textiles, digital electronics and displays[1-4].It has long been recognised that the addition of polymer to an ink has a strong impact on the nature of the drop generation and ejection process, with the drop break-up behaviour being in part related to the strain hardening resulting from the presence of polymer passing through a strong elongational flow field[5-9]. The micro rheological explanation for strain hardening is the sudden transition of the polymer chain from a coiled to a stretched state, which is accompanied by a strong increase in the hydrodynamic drag. The coil-stretch transition occurs for linear polymers at a critical strain rate (ε_{crit}) where the rate of deformation of the chain exceeds its rate of relaxation so that it passes from a slightly distorted random coil to an extended state, This critical condition is achieved when the critical Weissenberg-number ($W_{ecrit} = \varepsilon_{crit}.\tau_{1)} > 0.5$, where τ_1 denotes the longest relaxation time[6, 10] . For the inkjet process the strain rate at the nozzle tip is typically greater than 50,000 s^{-1}, and as a consequence the critical Weissenberg-number is exceeded for all polymers having Mw > 50 kDa at the pinch region, the point at which the ligament is attached to the nozzle tip meniscus[6, 8] .

Flow induced deformations can also lead to irreversible changes in the structure of a complex fluid. The mechanical degradation of polymers in elongational flow fields has long been recognised and can lead to a reduction in average polymer molecular weight [11-13]. The passage through an elongational flow field exerts strong hydrodynamic forces upon a coiled polymer molecule in solution as it stretches orients and extends in the direction of flow. If the

elongational forces on the molecule are sufficiently strong, and the rate of chain stretching far exceeds the rate of chain relaxation, the polymer backbone can be broken[14].

6.2 Mechanical degradation of polymers in elongational flow

In a studies that focused on flow-induced scission of isolated macromolecules in well characterized uniaxial or two dimensional extensional flow fields Odel and Keller showed that it was possible in strong extensional flow fields to completely stretch isolated macromolecules[12]. Both high molecular weight Atactic polystyrene and polyethylene oxide were shown to undergo polymer chain scission that was close to the centre of the molecules[12]. This was explained in terms of stress build up from chain ends towards the chain centre. The system was composed of cross slots that allowed for planar flow as shown in Figure 6.1, with polymer solution going through two opposed channels and being pulled out from two orthogonal opposed channels. The centre of the flow field which is marked as (X) is a stagnation point where the velocity of the fluid flow is zero.

A   B
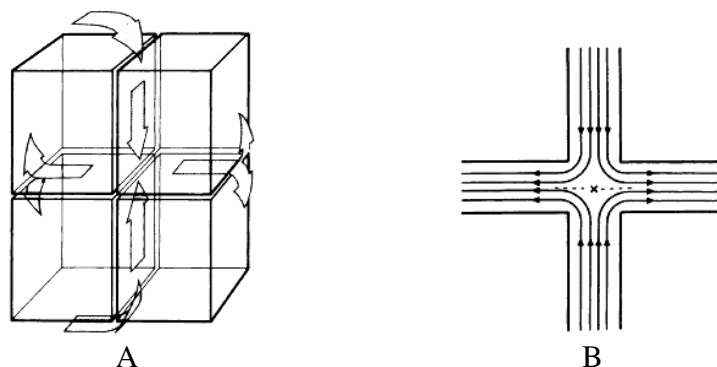
Figure 6.1 shows the planar elongational flow which are made by the cross slot and the stagnation point which appears as (X) is marked[12].

 Subsequently Muller et al studying the degradation of atactic polystyrene Mw = 580 kDa and elongational showed that in both the dilute and moving into the semi-dilute regimes that chain scission was essentially centro-symmetric[15].

Moving into the semi dilute regime beyond a critical concentration point Keller et al showed that the interaction of extended polymer chains in solution under different flow fields can alter the mechanism of chain scission [16]. At the low strain rates the polymer chain behave as if in the dilute regime which means that stretching of the polymer chains can proceeded and subsequently separate from each other as long as they have the same relaxation time and hence scission is essentially centro-symmetric. This result was explained by a Thermally Activated Barrier to Scission (TABS) model, based on the fact that molecules extend and in it calculates the combined effect of the accumulating molecular stress and temperature. The theory is then used to predict the frequency of a scission. If a high strain rate is applied a transient network can occur making it difficult for the polymer chains to relax. This can lead to almost random scission along the chains inferring that the forces required to break the chain are transmitted either by valence bonds, i.e. network chains and junctions or discrete entanglements rather than by hydrodynamic interaction[16].

Recent studies on transient elongational flows imposed by sudden contractions have been reported to lead to molecular weight degradation of the whole distribution after a single pass,

under a continuously applied pressure, for solutions of polyethylene oxide, polyacrylamide and polystyrene in the semi-dilute regime, c/c* = 1.5 – 20, Figure 6.2[17-20]. Such configurations are characterised by both a high contraction ratio, typically > 35:1, long residence time in a typical elongational flow field of 45,000 s^{-1} giving a Deborah number (De) on the order of 550[11, 20] indicating the polymer chains are being stretched much more rapidly that they can relax.

Deborah number (De) is the ratio of structural relaxation time scaled to the characteristic flow time of the system and it was first introduced by Reiner [21] to see how fluid a material is . De = t_c/t_r [20] where t_c is the relaxation time of the material and t_r is the time observation time for the experiment. So, when $t_c > t_r$ the material behaves like a solid and when $t_r > t_c$ the material behaves as a fluid. In the dilute solution regime at low shear rates the polymer has the viscosity essentially that of the solvent and a low Deborah number the polymers being in the random coil conformation. At high strain rate the polymer solutions may become viscoelastic dependant on molecular weight and concentration exhibiting a high Deborah number as the polymer chains easily extends and the hydrodynamics size of polymer becomes larger and are slow to relax having a high Zimm relaxation time[22] .

Transient elongational flows imposed by sudden contractions have been reported to lead to molecular weight degradation of the whole distribution after a single pass, under a continuously applied pressure, for solutions of polyethylene oxide, polyacrylamide and polystyrene in the semi-dilute regime, c/c* = 1.5 – 20[17, 18, 23, 24] . Such configurations are characterised by both a high contraction ratio, typically > 35:1, long residence time in a typical elongational flow field of 45,000 s^{-1} giving a Deborah number (De) on the order of 550[11] as shown in Figure 6.2.
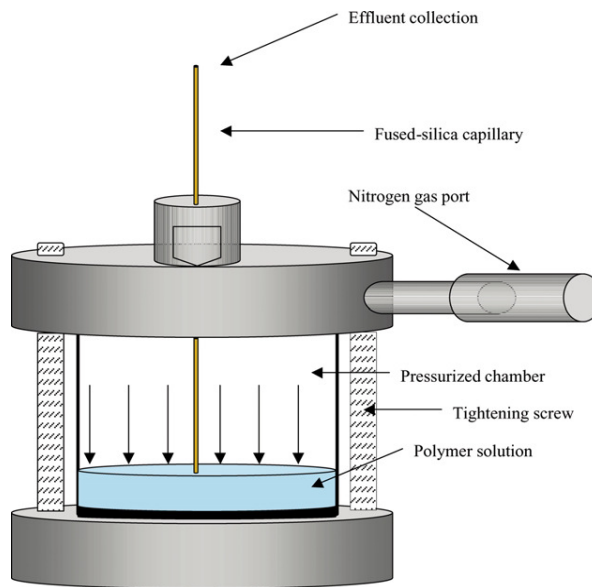
Figure 6.2 Aluminum pressure device with a capillary the used for in jetting multi-passes of polymer solutions[11].

The is a dimensionless number, used in rheology to characterize how "fluid" a material is. Even some apparent solids "flow" if they are observed long enough. Formally, the Deborah number is defined as the ratio of a relaxation time, characterizing the intrinsic fluidity of a material, and the characteristic time scale of an experiment (or a computer simulation) probing the response of the material. The smaller the Deborah number, the more fluid the material appears. and is given by:

$$De = t_c/t_p \qquad\qquad 6.1$$

where t_c refers to the stress relaxation time (sometimes called the Maxwell relaxation time), and t_p refers to the time scale of observation.

Nghe et al showed that in certain microfluidic device geometries it is possible to induce polymer chain degradation monitored by decease in viscosity between entrant and exiting solution, Figure 6.3[25]. A small scale flow geometry was used to minimize the Reynolds number which resulted in the suppression of the inertial instabilities which was noticed had an effect on the polymer degradation process. The constriction of the device in the upstream zone is a unique as it goes from 500 μm to 20 μm. Based on, Newtonian fluids the characteristic of the upstream zone is that it generates a strong extensional component in the direction of the flow. On the other hand, the solution is to shear and the progressive exit manages to minimize the strong extensional

116

event from generating. An illustration of the potential of this device was shown by applying it to a series of 15 different concentration (0.05 to 0.8 wt-%, c/c* = 0.1 - 0.1 of aqueous polyethylene oxide solutions having an average weight average molecular weight from 600 – 800 kDa,.
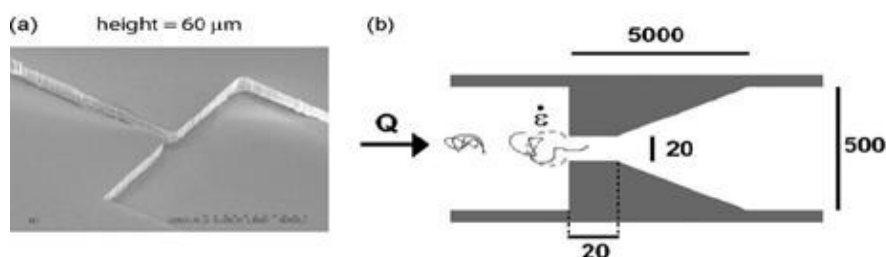
Figure 6.3 Microfluidic 60 µm planar device [25].

This study achieved two purposes that were useful for further explorations. The new design of the micro fluidic device is useful for screening the degradation of polymers in solution and would also helps in the study of the molecular weight and concentration dependence on polymer degradation. By using the micro fluidic it was able to reduce the magnitude of the necessary volume of solution required by two orders. Also the sample preparation time was reduced by the same factor. This helped significantly in exploring different degradation conditions and polymer formulations.

In summary, studies to date in different device geometries have observed polymer degradation under elongational shear when c >c*, Mw > 100 kDa and the residence time in the elongational flow is longer than the polymer relaxation time.

Here we report the first time observations of and conditions for the mechanical degradation of polymer molecular weight under conditions of drop on demand inkjet printing. These observations have implications with respect to the printing of functional and biological materials where retention of polymer composition is critical.

6.3   Results and Discussion

6.3.1   Inkjet Printing of Polymer Solutions

Anisole, acetophenone and γ-butyrolactone are all good solvents for both PMMA and PS having relative Energy Difference (RED) numbers[26] in the range 0.35 – 0.9 giving in all cases clear miscible solutions. Boiling points are in the range 152 – 204 ^{o}C enabling sustained inkjet printing at room temperature without significant nozzle blockage. For each polymer - solvent combination the overlap concentration c* was defined as previously discussed using the classification of Flory[27] for a flexible polymer in solution, $c* = 1/[\eta]$ and polymer concentration expressed as a reduced concentration [η].c or c/c*[28].

Solutions of PMMA and PS having low polydispersity index (PDi) ≤ 1.3 (M_w 123 – 2000 kDa) and broad PDi = 1.8 – 1.9 (PMMA M_w = 909 and PS Mw = 900 kDa) in γ-butyrolactone were prepared at reduced concentration = 0.15, 0.33, 0.5, 0.75, 1.0. For all fluids low shear viscosity and surface tension were in the range 1 – 10 cP and 29 – 40 mN/m at 25 ^{o}C respectively, indicating that they are suitable for inkjet printing[29]. Despite this it was not possible to inkjet print all fluids. It should be noted that both PMMA and PS showed comparable behaviour at equivalent molecular weight. Figure 6.4 shows a composite plot for all PMMA and PS fluids in γ-butyrolactone, and shows the maximum reduced concentration at which jetting was achieved as a function of weight average molecular weight with representative jetting behaviour in the Microfab printhead shown in Figures 6.5 – 6.9. It should be noted that the maximum reduced concentration evaluated was unity and it is probable that for lower molecular weight polymers the threshold concentration will indeed be higher. We observe that as molecular weight increases it become increasingly more difficult to jet higher concentration fluids, being a function of both drive voltage and printhead architecture[22].

118
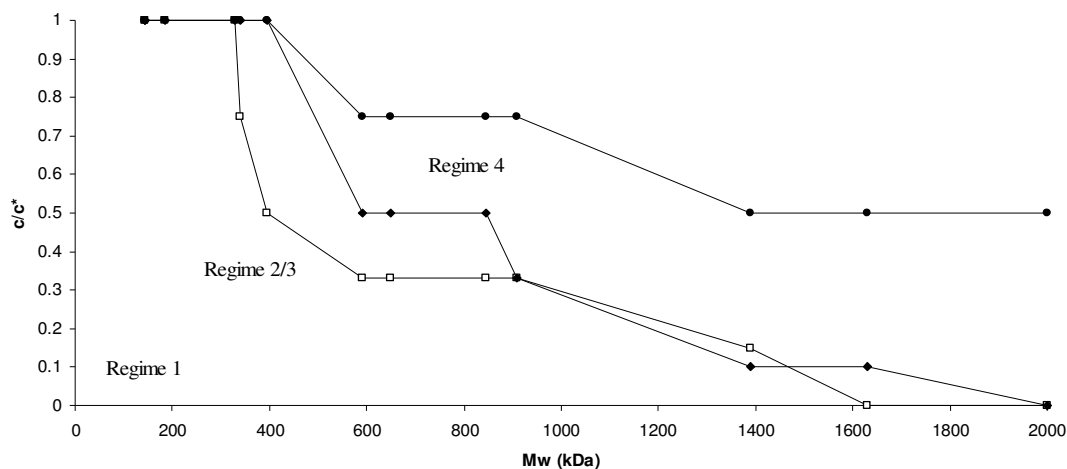
Figure 6.4 Maximum reduced concentration (c/c*) at which inkjet printing was observed for PMMA and PS in γ-butyrolactone at 25 °C using respectively a Microfab Printhead at 30 V (□) and 50V (•) and Dimatix a 10pl printhead (♦).

Regimes 1 – 4 were defined by drop visualization using the Microfab print head as shown for selected fluids in Figures 6.5 – 6.9 and are consistent with regime characterization used by Meyer et al[30],who studied the effect of different polyacrylamide molecular weight staring from 500000 to 6 x 10^6 on drop generation, Mun et al on high molecular weight polyethylene oxide[31], Clasen et al on high molar mass polystyrene in diethylphthalate[32], and Xu et al on cellulose esters in γ-butyrolactone [5].

| 81 kDa | 590 kDa | 909 kDa |
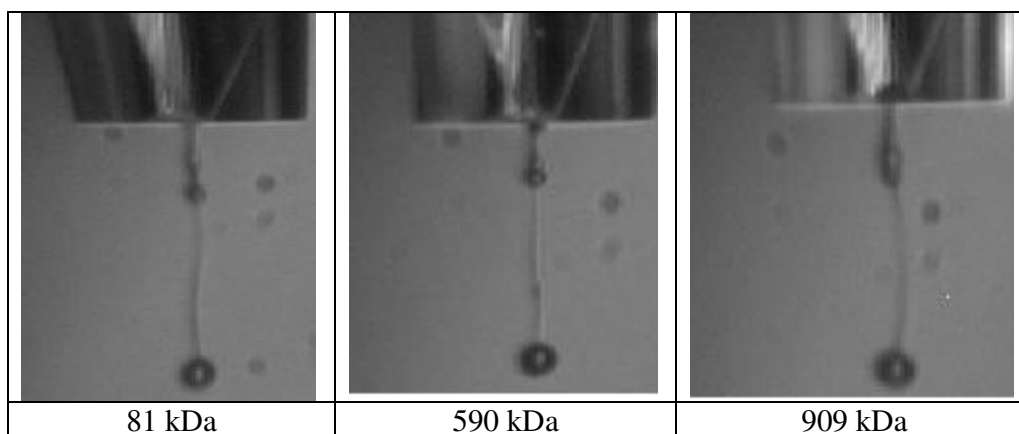
Figure 6.5 Drop formation at 50 V in Microfab printhead for various molecular weight PMMA samples in γ-butyrolactone at c/c* = 0.15.

119

	350 kDa	1200 kDa
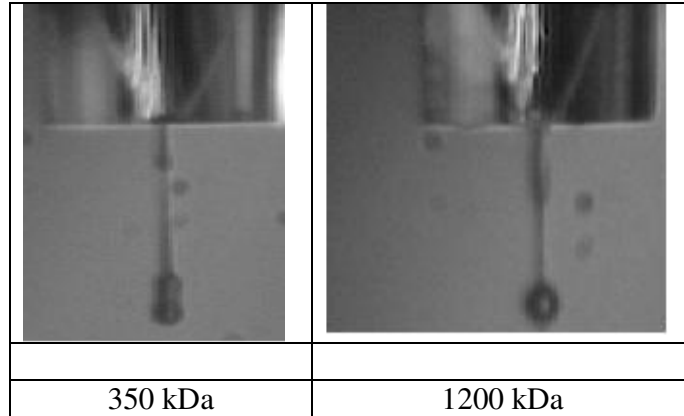
Figure 6.6 Drop formation at 50 V in Microfab printhead for various molecular weigh PMMA samples in γ-butyrolactone at c/c* = 0.5.

c/c*	0.5	0.75	1
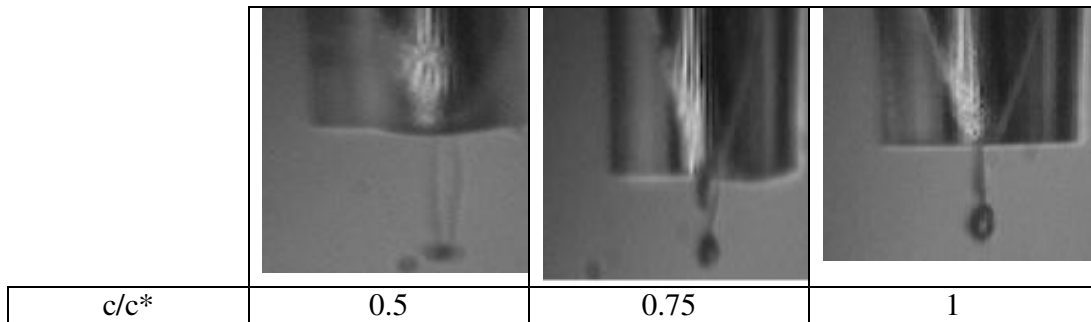
Figure 6.7 Drop formation of different reduced concentration c/c* at 30 V for PS 340 k Da.

c/c*	0.5	0.75
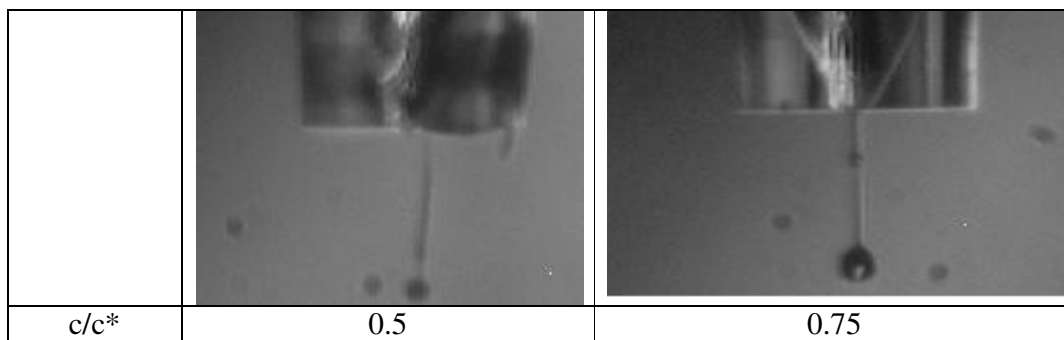
Figure 6.8 Drop formation of different reduced concentration c/c* at 50 V for PS 340 kDa.

| c/c* | 0.75 | 0.75 |
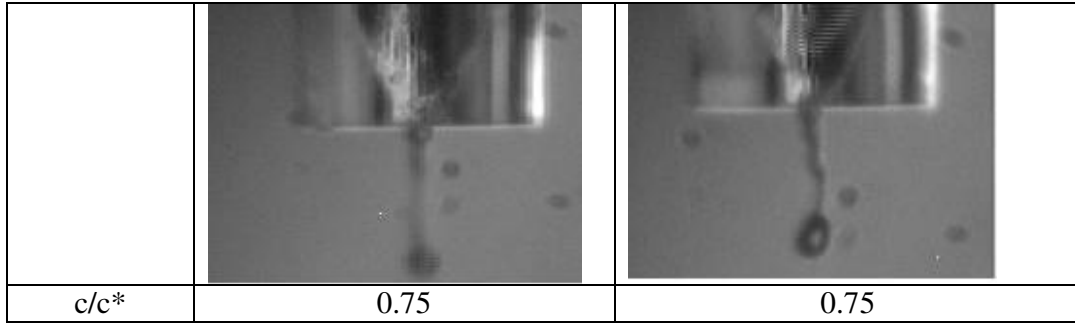
Figure 6.9 Drop formation of PS 840k Da at 30Vand 50 V .

The jettability of the respective polymer solutions can be addressed by considering the polymer relaxation times. The maximum relaxation time for linear polymer can be calculated from using the Zimm equation:

$$\lambda z = \eta_s[\eta]M_w/RT \qquad\qquad 6.2$$

where η_s denotes the viscosity of solvent (the gas constant) and T the temperature and [η] is the intrinsic viscosity of polymer solution, M_w is the molecular weight. The apparent universality of Zimm behaviour is believed to arise either from the fact that elongational flow experiments only probe the dynamics of the partially stretched coil[33], or that the coil-stretch transition is essentially non-equilibrium since molecules only experience a finite residence time in the flow field [34]. Since the critical strain rate (ε_{crit}) for deformation from a slightly distorted random coil to an extended state is exceeded for particularly molecular weight polymers studied then strain hardening results in a rapid increase in fluid viscosity. For polymers having $M_w > 250$ kDa the maximum relaxation time (λ_z) with a concomitant reduction in ligament viscosity is > 100 μs with De > 1, which is greater than the time scale for ligament detachment from the nozzle tip meniscus in the Microfab printhead which is between 80 – 90 μs irrespective of applied voltage. The residual viscoelasticity within the ligament therefore resists drop break-up being amplified for very high molecular weight polymer at lower than overlap concentration where resultant chain entanglement of the partially relaxed chains can fully damp out fully drop break up, De $>$ 40.

6.3.2 Molecular weight Degradation

For each fluid, drop ejection velocity (v) was determined stroboscopically[5], and the strain rate at the nozzle tip (ε) calculated using $\varepsilon = v/D$ where D is the nozzle diameter [35]. Molecular weight and distribution for all samples were determined before and after printing. Unless specified otherwise all results are for polymer in γ-butyrolactone with equivalent results being observed in both acetophenone and tetralin.

6.3.2.1 Microfab printhead.

Fluids were jetted through the Microfab single nozzle glass capillary, 50 μm internal diameter, at 50 V with drop velocity between 2.5 – 5.5 ms^{-1} giving a calculated elongational strain rate at the nozzle tip between 50,000 – 110,000 s^{-1}, Table 6.1 and 6.2.
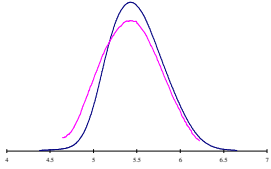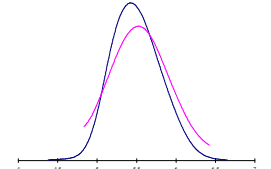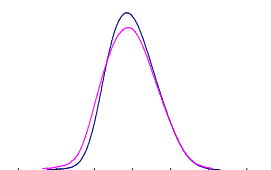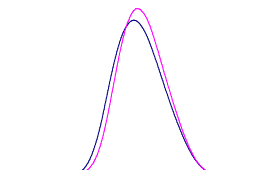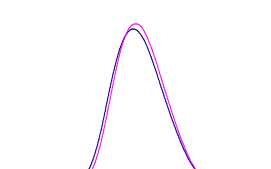
Table 6.1 Drop velocity, shear rate data for polymethyl methacrylate in γ-butyrolactone jetted using MicroFab print head.

Polymer	c/c*	Velocity (m/s) +/- 0.1	Shear rate (1/s)
PMMA 142 kDA	0.5	4.3	85000
PMMA 350 kDA	0.15	7.4	148000
PMMA 375 kDA	0.5	2.7	53000
PMMA 400 kDA	0.75	2.9	57000
PMMA 370 kDA	0.9	2.9	57000
PMMA 400 kDA	1.1	2.5	49000
PMMA 590 kDA	0.5	4.2	84000
PMMA 909 kDA	0.21	4.3	85000
PMMA 909 kDA	0.35	5.6	111000
PMMA 909 kDA	0.5	3.4	68000
PMMA1360 kDA	0.5	2.5	49000
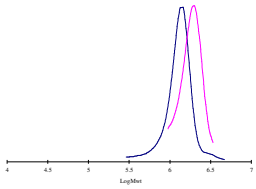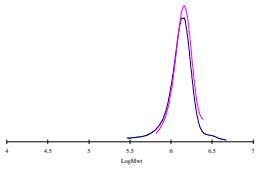
Table 6.2 Drop velocity, shear rate data for Polystyrene in γ-butyrolactone jetted using MicroFab print head.

Polymer	c/c*	Velocity (m/s) +/- 0.1	Shear rate (1/s)
PS 304 kDa	0.5	2.3	46000
PS 304 kDa	0.75	5.3	105000
PS 304 kDa	1	4.4	88000
PS 304 kDa	1.5	3.3	65000
PS 304 kDa	2	4.1	82000
PS 750 kDa	0.5	3.5	70000
PS 750 kDa	0.75	X	X
PS 750 kDa	1	X	X
PS 1630 kDa	0.5	3.2	63000

.

All polymers having a PDi $\leq$ 1.3, whether polystyrene or polymethacrylate showed no change in molecular weight and distribution. Representative data is given in Figures 6.10 – 6.11.

c/c*	Before and after jetting	Mw	PDi
0.15		363	1.9
0.33		473	1.9
0.5		381	1.9
0.75		422	1.6
1		415	1.6

Figure 6.10 Example of PMMA 350 kDA in γ-butyrolactone ink jetted using Microfab before (blue line)and after(pinky line) jetting at 50 V.

c/c*	Before and after jetting	Mw	PDi
0.15		1894	1.1
0.5		1402	1.1

Figure 6.11 Example of PMMA 1200 kDA in γ-butyrolactone ink jetted using Microfab before (blue line)and after(pinky line) jetting at 50 V.

However both PMMA 909 kDa, PDi = 1.9 and PS 900 kDa, PDi = 1.8 show reproducible broadening in molecular weight distribution and a shift to lower molecular weight the nature of which is dependant upon the reduced concentration of the fluid, Figure 6.12 – 6.13.

Molecular weight degradation is more pronounced at low reduced concentration with no degradation being observed at c/c* = 0.5 at 50 V for PS 900 and at c/c* = 0.75 for PMMA 909. It is noted that not all the distribution appears to undergo molecular weight degradation and repetitive jetting of PMMA 909 kDa at c/c* = 0.33 shows no significant reduction in molecular weight although a slight broadening to low molar mass was observed, as it shows in Figure 6.14.
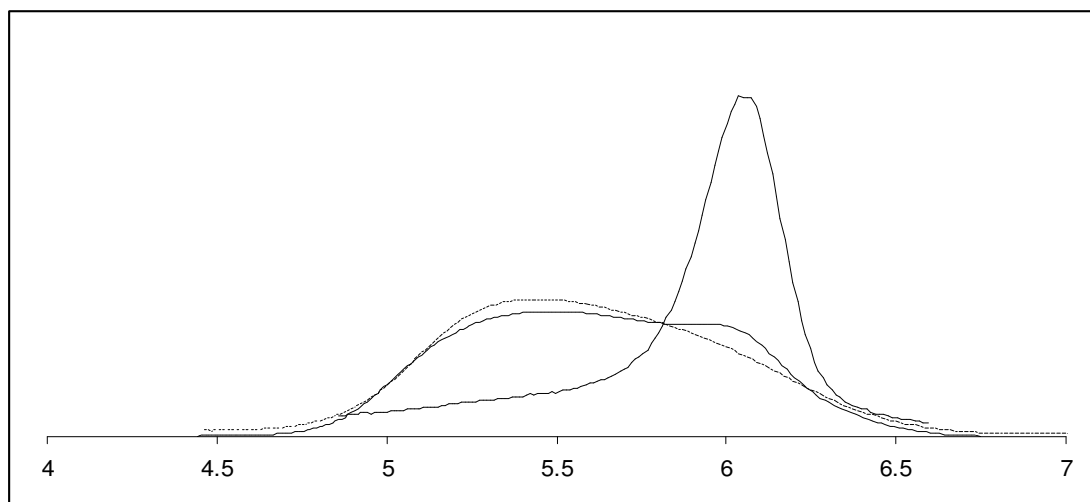
Figure 6.12 Effect of reduced concentration on molecular weight distribution (WF/dLogMwt against log mol wt) before and after single pass jetting for PMMA 909 kDa in γ-butyrolactone jetted at 50 V using a Microfab Printhead at 25 oC. Before jetting (—). After jetting c/c* = 0.15 (– · –), c/c* = 0.33 (– –), c/c* = 0.5 (— —).
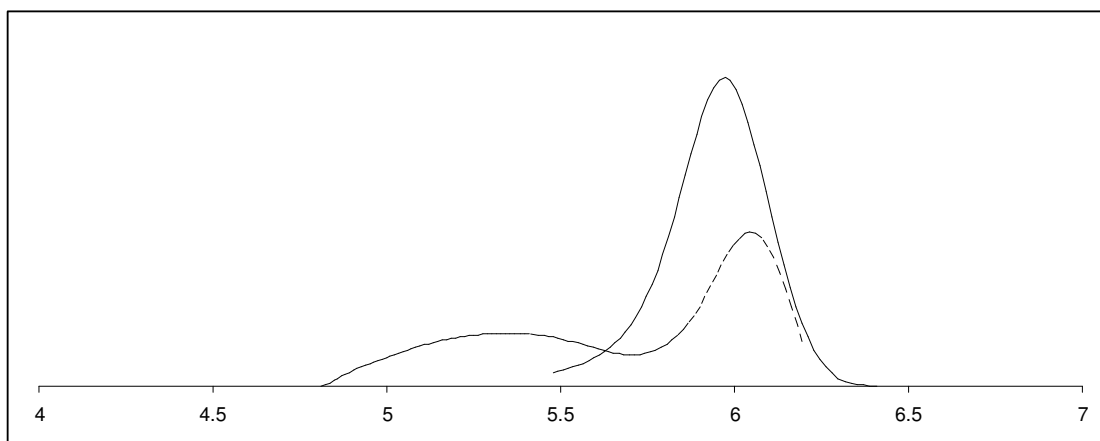
Figure 6.13 Effect of number of sequential passes on the molecular weight distribution (WF/dLogMwt against log mol wt) for PS900K in γ-butyrolactone at c/c* = 0.33 jetted at 50 V using a Microfab Printhead at 25 oC. Before jetting (—). Single pass (– –), double pass (– · – · –).
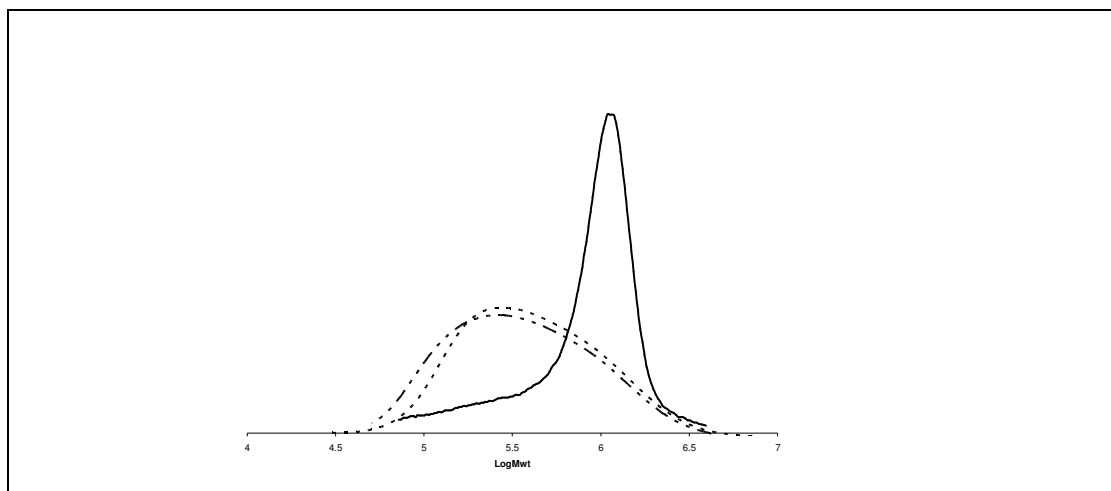
Figure 6.14 Effect of number of sequential passes on the molecular weight distribution (WF/dLogMwt against log mol wt) for PMMA 909K in γ-butyrolactone at c/c* = 0.33 jetted at 50V using a Microfab Printhead at 25 °C. Before jetting (—). Single pass (– –), double pass (– · – · –).

6.3.2.2 Dimatix print head.

When ink jet printed through a Dimatix DMP-2800 10 pl nozzle, 23 μm internal diameter droplet velocities were between 6.0 – 10.0 ms^{-1}. As a consequence of the smaller nozzle diameter higher elongational strain rates are experienced; 200,000 – 300,000 s^{-1}. Only single pass experiments were performed and for low polydispersity PMMA and PS we observe molecular weight degradation for polymers having M_w = 145 – 590 kDa, M_w = 290 – 650 kDa for concentration between c/c* = 0.15 – 0.5 except for PS 770 kDa which only degraded at c/c* = 0.15., Table 6.3, 6.4 and Figure 6.15. The highest molecular weight sample tested PMMA 1390 kDa, PDi = 1.16 did not show molecular weight degradation under any of the conditions tried. In all cases the polymer chains break essentially centro symmetrically leading to a halving of molecular weight, with for example for PS 770 kDa seeing a reduction in molecular weight at c/c* of Mw = 772 kDa, Mn = 659 kDa, PDi = 1.17 to Mw = 380 kDa, Mn = 340 kDa, PDi = 1.11. PMMA 909 kDa, PDi = 1.9 and PS 900 kDa, PDi = 1.8 showed reproducible broadening in molecular weight distribution and a shift to lower molecular weight only at c/c* = 0.15, because as shown in Figure 6.4 higher concentrations are at the limit of jet ability.

Table 6.3 PMMA solutions in γ-butyrolactone using Dimatix DMP printer 10pl drop size at 25 ^{0}C.

PMMA	c/c*	Velocity (m/s)	Shear rate (1/s)
PMMA 350 kDA	0.15	7.4	148000
PMMA 350 kDA	0.3	4.3	85000
PMMA 350 kDA	0.5	2.7	53000
PMMA 350 kDA	0.75	2.9	57000
PMMA 350 kDA	0.9	2.9	57000
PMMA 909 kDA	0.15		
PMMA 996 kDA	0.3	5.6	111000
PMMA 909 kDA	0.5	3.4	68000
PMMA 1200 kDA	0.15	2.3	48000
PMMA 1200 kDA	0.5	2.5	49000

| PS 170 kDa | PS 290 kDa | PS 650 kDa | (a) | (b) |
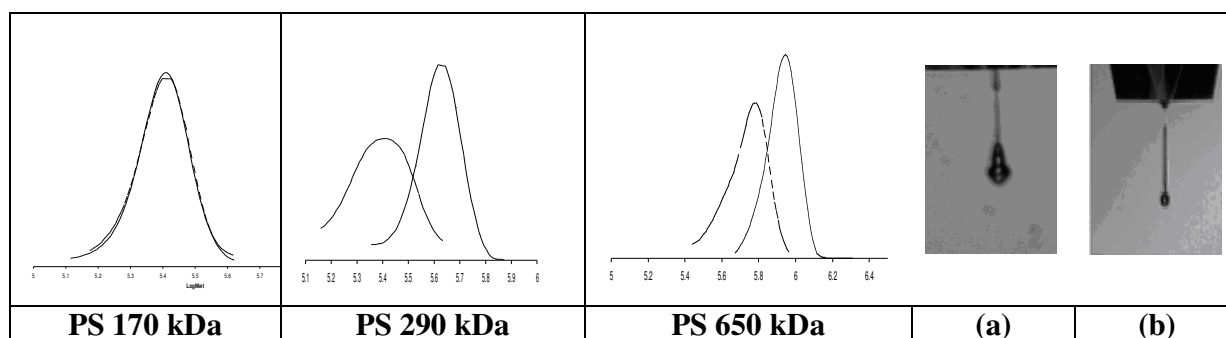
Figure 6.15 (WF/dLogMwt against log mol wt) before and after single pass jetting for low polydispersity PS in tetralin at c/c* = 0.15 jetted at 18-26 V using Dimatix 10pl DMP Printhead at 25 ^{o}C. Before jetting (—). Single pass jetting (– –). (a) Drop shape in Microfab at drop break off for 650 kDa at c/c* = 0.15 and c/c* = 0.33.

Table 6.4 Polystyrene solutions in γ-butyrolactone using Dimatix DMP printer 10pl drop size at 25 ^{0}C.

PS	c/c*	V	Velocity (m/s)	Shear rate (1/s)
PS 152 kDA	0.15	20	7	219000
PS 152 kDA	0.3	20		
PS 152 kDA	0.5	20	8	250000
PS 200 kDA	0.15	21	11	347000
PS 200 kDA	0.3	21	11	344000
PS 200 kDA	0.5	21		
PS 290 kDA	0.15	23	10	313000
PS 290 kDA	0.3	23		
PS 290 kDA	0.5	23		
PS 340 kDA	0.15	20	7	219000
PS 340 kDA	0.3	21	6	188000
PS 340 kDA	0.5	20	6	188000
PS 400 kDA	0.15	23	12	375000
PS 400 kDA	0.3	25	11	344000
PS 400 kDA	0.5	25		
PS 575 kDA	0.15	18	8	25000
PS 575 kDA	0.3			
PS 575 kDA	0.5	24	7	219000
PS 650 kDA	0.15	22	8	250000
PS 650 kDA	0.3	21		
PS 650 kDA	0.5	22	9	281000
PS 900 kDA	0.15	21	11	328000
PS 900 kDA	0.3	23	12	375000
PS 900 kDA	0.5	X	X	X
PS 2000 kDA	0.15	X	X	X
PS 2000 kDA	0.3	X	X	X
PS 2000 kDA	0.5	X	X	X

6.3.2.3 Discussion.

As previously discussed the mechanical degradation of polymers in elongational flow fields generated by several different geometries has long been recognised and can lead to a reduction in average polymer molecular weight [11-13]. Early work on cross-slot devices, which generate an opposing-jets geometry, require a large number of passes through the system to observe chain-scission since only a small percentage of the polymer solution passes through the stagnation point at any one time [13, 15, 16, 36, 37]. Conversely transient elongational flows imposed by sudden contractions have been reported to lead to molecular weight degradation of the whole distribution after a single pass, under a continuously applied pressure, for solutions of polyethylene oxide, polyacrylamide and polystyrene in the semi-dilute regime, $c/c^* = 1.5 - 20$ [17, 18, 23, 24]. Such configurations are characterised by both a high contraction ratio, typically $> 35:1$, long residence time in a typical elongational flow field of $45,000$ s^{-1} giving a Deborah number (De) on the order of 550 [11, 20] indicating the polymer chains are being stretched much more rapidly that they can relax.

We can consider the inkjet printhead as a short residence time contraction in that the fluid is forced from the large diameter ink chamber through the nozzle constriction. The Microfab glass capillary represents a constriction ratio on the order of 10:1, whist for the Dimatix head the constriction ratio is unknown but believed to be of the same order of magnitude. Based upon average measured drop velocities the residence time of the fluid in the constriction is short, on the order of 10 μs, after which the fluid begins to relax as the ligament and subsequent ejected droplet form [5]. It is noted that Deborah numbers are calculated based upon the residence time within the nozzle.

In the case of low polydispersity polymers we only observe molecular weight degradation at elongational shear rates $> 200,000$ s^{-1}, for PMMA and PS having $M_w = 145 - 590$ kDa $M_w = 290 - 650$ kDa respectively which corresponds to De on of the order $2 - 20$ but only for $c/c^* = 0.15 - 0.5$. From drop visualisation these fluids show characteristic Newtonian drop generation behaviour at $c/c^* = 0.15$, Figure 6.15a, whilst higher concentrations show drop generation behaviour consistent with a viscoelastic fluid, that is stable ligament formation and drop break off at the nozzle tip meniscus, Figure 6.15 b. Images are shown for the MicroFab fluids due to

better image quality but are representative of those using Dimatix image software. Within the dilute solution regime the forces required to break the chains are transmitted through viscous energy dissipation due to friction between solvent and polymer molecules. In this regime chain breakage can be induced either by overstretching when the strain rate increases well beyond the critical strain rate (ε_{crit}), that is the stretching rate is high enough to exceed the rate of relaxation or by turbulence[6, 8, 15], it being shown that in dilute solution only those molecules that are virtually fully stretched can undergo central scission[24].

PMMA 909 kDa, PDi = 1.9, PS 340 PDi = 1.8 and PS 900 kDa, PDi = 1.8 show molecular weight degradation which is printhead (strain rate) and concentration dependant, with reproducible broadening in molecular weight distribution and a shift to lower molecular weight. The results are consistent with almost random scission along the chains inferring that the forces required to break the chain are transmitted either by valence bonds, i.e. network chains and junctions or discrete entanglements rather than by hydrodynamic interaction. Greater broadening is observed at low polymer concentrations, Figures (6.12-6.14) where we approach the concentration where chain interaction in elongational flow (c+) is not possible[23].

6.4 Conclusion.

We report the first evidence of flow-induced polymer degradation during inkjet printing for both poly(methylmethacrylate) and polystyrene in good solvent. Polymers having weight average molecular weight (M_w) either less than 100 kDa or greater than approximately 1,000 kDa show no evidence of molecular weight degradation. The lower boundary condition is a consequence of the low Deborah number imposed by the printhead geometry of narrow nozzle diameter and short residence time within the nozzle constriction, De < 1. The upper boundary condition is due to visco-elastic damping arising from polymer chain extension under elongational flow, De > 25. For intermediate molecular weights the effect is greatest at high elongational strain rate at low solution concentration with higher polydispersity polymers being most sensitive to molecular weight degradation. For low polydispersity samples, PDi ≤ 1.3 chain breakage is essentially centro-symmetric induced either by overstretching when the strain rate increases well beyond the critical strain rate, that is the stretching rate is high enough to exceed the rate of relaxation or by

turbulence. For higher polydispersity samples, PDi chain breakage is consistent with almost random scission along the chain inferring that the forces required to break the chain are transmitted either by valence bonds, i.e. network chains and junctions or discrete entanglements rather than by hydrodynamic interaction. These observations are contrary to those previously reported for either cross-slot devices, which generate an opposing-jets geometry or devices which generate a transient elongational flows imposed by sudden contractions. This is a consequence of both the short contact time between the fluid and the high elongational shear rate generated in the inkjet nozzle and the viscous damping imposed by the polymer solution.

6.5 References:

1. P. Calvert, *chem.mater*, 2001, **13**, 3299.
2. B. J. de Gens, P. C. Duineveld and U. S. Schubert, *Adv.Mater*, 2004, **16**, 203.
3. M. R. Böhmer, R. Schroeders, J. A. M. Steenbakkers, S. H. P. M. de Winter, P. A. Duineveld, J. Lub, W. P. M. Nijssen, J. A. Pikkemaat and H. R. Stapert, *Colloids and Surfaces A: Physicochemical and Engineering Aspects*, 2006, **289**, 96-104.
4. J. F. Dijksman, P. C. Duinevels, M. J. J. Hack, A. Pierik, J. Rensen, J. E. Rubingh, I. Schram and M. M. Vernhout, *J.materials chem*, 2007, **17**, 511.
5. D. Xu, V. Sanchez-Romaguera, S. Barbosa, W. Travis, J. d. Wit, P. Swan and S. G. Yeates, *Journal of Materials Chemistry*, 2007, **17**, 4902-4907.
6. B. J. de Gans, L. Xue, U. S. Agarwal and U. S. Schubert, *Macromolecular Rapid Communications*, 2005, **26**, 310-314.
7. B. J. de Gans, E. Kazancioglu, W. Meyer and U. S. Schubert, *Macromolecular Rapid Communications*, 2004, **25**, 292-296.
8. J. J. Cooper-White, J. E. Fagan, V. Tirtaatmadja, D. R. Lester and D. V. Boger, *Journal of Non-Newtonian Fluid Mechanics*, 2002, **106**, 29-59.
9. Y. Christanti and L. M. Walker, *Journal of Rheology*, **2002**, **46**, 733-748.
10. P. G. De Gennes, *The Journal of Chemical Physics*, 1974, **60**, 5030-5042.
11. B. A. Buchholz, J. M. Zahn, M. Kenward, G. W. Slater and A. E. Barron, *Polymer*, 2004, **45**, 1223-1234.
12. J. A. Odell, A. Keller and Y. Rabin, *The Journal of Chemical Physics*, 1988, **88**, 4022-4028.
13. A. J. Müller, J. A. Odell and A. Keller, *Journal of Non-Newtonian Fluid Mechanics*, 1988, **30**, 99-118.
14. J. Frenkel, *Acta Physicochim URSS*, 1944, **19**, 51.
15. A. J. Müller, J. A. Odell and S. Carrington, *Polymer*, **1992**, **33**, 2598-2604.
16. J. A. Odell, A. Keller and A. J. Muller, *Colloid & Polymer Science*, **1992**, **270**, 307-324.
17. T. Q. Nguyen and H.-H. Kausch, *Chimia*, **2001**, **55**, 147.
18. T. Q. Nguyen, Q. Z. Liang and H.-H. Kausch, *Polymer*, **1997**, **38**, 3783-3793.
19. O. G. Harlen, J. M. Rallison and M. D. Chilcott, *Journal of Non-Newtonian Fluid Mechanics*, **1990**, **34**, 319-349.
20. R. B. Bird, R. C. Armstrong and O. Hassager, *Dynamics Of Polymeric Liquids*, Wiley, New York, **1987**.
21. Renier, *http://www.chbmeng.ohio-state.edu/classes/775/rsb/deborah.pdf*, Accessed 10/09/2010.
22. S. D. Hoath, I. M. Hutchings, G. D. Martin, T. R. Tuladhar, M. R. Mackley and D. Vadillo, *Journal of Imaging Science and Technology*, **2009**, **53**, 041208-041208.
23. T. Q. Nguyen and H.-H. Kausch, *Journal of Non-Newtonian Fluid Mechanics*, **1988**, **30**, 125-140.
24. T. Q. Nguyen and H.-H. Kausch, *Chimia*, **1986**, **40**, 129.
25. P. Nghe, P. Tabeling and A. Ajdari, *Journal of Non-Newtonian Fluid Mechanics*, **2010**, **165**, 313-322.

26. A. F. M. Barton, *Handbook of Solubility and Other Cohesion Parameters*, CRC press, **1985**.

27. J. Burke, *AIC Book and Paper Group Annual*, **1984**.

28. W. Macosko, *RHEOLOGY:Principles,Measurment and Applications*, VCH,, New York, **1994**.

29. V. Sanchez-Romaguera, M.-B. Madec and S. G. Yeates, *Reactive and Functional Polymers*, **2008**, **68**, 1052-1058.

30. J. D. Meyer, A. A. Bazilevsky and A. N. Rozkhov, in *Int.Conf.On Digital Printing Technoloogies*, spring field, Editon edn., **1997**, vol. 13, p. 675.

31. R. P. Mun, J. A. Byars and D. V. Boger, *Journal of Non-Newtonian Fluid Mechanics*, **1998**, **74**, 285-297.

32. C. Clasen, J. P. Plog, W. M. Kulicke, M. Owens, C. Macosko, L. E. Scriven, M. Verani and G. H. McKinley, *Journal of Rheology*, 2006, **50**, 849-881.

33. Y. Rabin, *Journal of Polymer Science: Polymer Letters Edition*, **1985**, **23**, 11-13.

34. Y. Rabin, in *AIP Conference Proceedings* New York, Editon edn., **1985**, vol. 137.

35. M. Doi and S. F. Rewareds, *The Theory Of Polymer Dynamics2*, Oxford University Press, **1986**.

36. M.-B. Madec, D. Crouch, G. R. Llorente, T. J. Whittle, M. Geoghegan and S. G. Yeates, *Journal of Materials Chemistry*, 2008, **18**, 3230-3236.

37. A. B. Metzner and A. P. Metzner, *Rheologica Acta*, **1970**, **9**, 174-181.

Chapter Seven

Flow-Induced Polymer Degradation during

Ink-Jet Printing of Polysaccharides

The preparation and characterisation of model solutions of several galactomannan polysaccharides in water are reported and preliminary results on the effect of inkjet printing on molecular degradation discussed.

7.1   Background to Galactomannans.

Seed galactomannans are heterogeneous polysaccharides consisting of more than 5% galactose. Galactomannan gums have been used in many different fields including, drilling, food, pharmaceuticals, paper, global trend for using more plant for ecological reasons,etc., since they can form is that they form viscous solutions or gels in aqueous media[1,2]. Galactomannans are polysaccharides consisting mainly of a mannose backbone with galactose side groups (more specifically, a 1,4-linked beta-D-mannopyranose backbone with branch points from their 6-positions linked to alpha-D-galactose, i.e. 1,6-linked alpha-D-galactopyranose)[3] as in Figure 7.1.
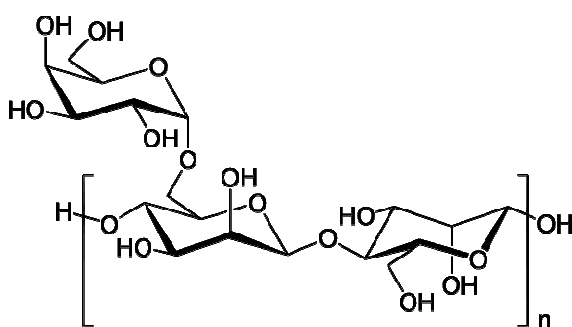
Figure 7.1 A segment of galactomannan showing mannose backbone (below) with a branching galactose unit (top)[3].

The mannose backbone takes up an essentially extended helical conformation stabilized through water promoted H-bonding of the galactose side chain with the mannose main chain. The

Galactomannans used in this study were obtained from Brazilian plants and their compositions are summarized in Table 7.1.

Table 7.1 Composition of Polysaccharides used in this study.

Code	Name	Ratio D-mannose: D-galactose: Arabinose: glucose w/w %			
		D-mannose	D-galactose	Glc	Ara
DM	Dimorphandra gardneriana polysaccharide Tul	64.2	34.7	1.1	0
JP	Guar gum	58.3	34.2	3.1	4.4

Mannose contains six carbon atoms and is a monomer of the aldohexose series of carbohydrates. In humans, mannose is not well metabolized and 90% of the mannose that is ingested and taken orally is excreted in the urine, unchanged, within one hour, with the rest being excreted within eight hours. Only very small traces have been found in blood plasma, not exceeding 1%. Another important characteristic is that it does not change blood glucose levels[4]. It has the structure shown below:
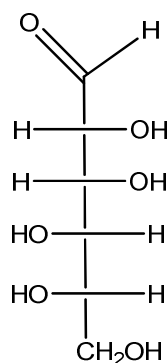
Figure 7.2 General structure of Mannose

Galactose is a monosaccharide that contains six carbon atoms with a carbonyl group at the end of the chain; the polymer of Galactose is called Galactan. It is water soluble but less so than Glucose. It has the structure shown below:
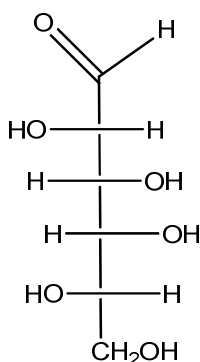
Figure 7.3 General structure of Galactose

Arabinose is a monosaccharide that contains five carbon atoms with an aldehyde functional group. It forms either L or D-arabinose, and it is also widely known as gum Arabic . Arabinose is a white crystal powder and is soluble in water. L-Arabinose is very common and is much used in many different fields such as biological research and more specifically in genetic and bioengineering research[3]. It has the structure shown below:
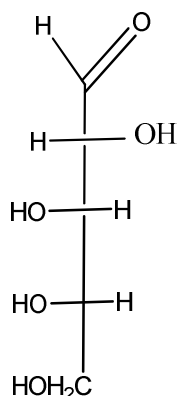
Figure 7.4 General structure of Arabinose

 Glucose is a monosaccharide that contains six carbon atoms, and is also known as grape sugar or dextrose. It is water soluble and partially soluble in alcohol. Glucose is a well-known sugar in white powder form. It has a structure of hexanal which is a chain of six carbons with an aldehyde group, the other five carbons forming an alcohol group as shown below. Glucose is naturally found in biological contexts including blood. Glucose can be synthesized in the liver and kidneys of animals and this process is known as gluconeogenesis[4].
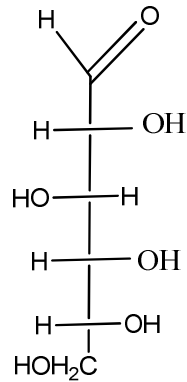
Figure 7.5 General structure of Glucose

Leguminous plants are the major source of seed gums with. two main groups of galactomannan polysaccharides being obtained either from the endosperms of the plant seeds or from microbial sources. A few species of galactomannans have been obtained from non-leguminous seeds such as the coffea Arabica, cocos nucifera, phoenix dactylifera and a few others. The endosperm of the plant has dual functions. It works as a food reserve for the germinating seeds and it also retains water conservation in order to prevent complete drying-out of the seeds which in return helps to avoid protein denaturation, specifically the denaturation of the enzymes which are essential in seed germination[2].

Dimorphandra gardneriana Tul (DM) is also known as "fava d'anta", and "faveiro". DM is a common tree that is native to South America, especially Brazil and Bolivia. The structure of DM is changeable depending on the ratios of galactose and maltose but in this work the ratio is 64.2 to 34.7 wt-% of maltose and galactose respectively[5].

7.2   Polysaccharides as Hydrocolloids.

There are many reports regarding the rheology of guar, carob and seed gums gums[3] also, comparing it with locust bean gum to study their effectiveness as thickning hydrocolloids[6]. And have shown that the polymer chain undergoes complete coil-stretch polymer transition in the dilute to semi-dilute regimes with polymer-polymer interactions were seen more in a concentrated solutions regime. Murrphy and his colleagues have found that for five different samples of guar galactomannan, that increase of viscosity is noticeable with increasing in concentration even below. The overlap concentration $c*$ which is equal $4/[\eta]$. So, below the overlap concentration an entaglement of polymer-polymer is happening at $c > c*$[7] .

Consequently polysaccharide hydrocolloids such as guar gum (GG) and xanthan gum (XG) have proved to be useful in the food industry due to their viscoelastic properties nature. The addition of small amounts of GG and XG to aqueous systems has shown to cause a drastic reduction of the frictional drag caused in turbulent flow[8]. Turbulent drag reduction requires a lower pressure gradient to maintain the same flow rate. This phenomenon can be applied to many different aspects in the engineering field; examples include firefighting, the manufacture of pipelines and boats, and in flood prevention[8]. However, the capability for drag reduction decreases as the polymers degrade due to mechanical shear under high intensity turbulence[9].

A number of investigations have been carried out on the origin of this degradation, as this will help in advancing the technology in many different fields[10]. GG is a water soluble galactomannan polysaccharide which is found in the seed of the guar plant and consists of linear chains of 1,4-linked b-D-mannopyranosyl units with a-D-galactopyrannosyl units, attached by 1,6-links in the ratio 2:1.

A study based on drag reduction efficiency was carried out using rotating disk apparatus. The polysaccharide GG was extracted from the guar bean, which is one of the most widely, used biopolymers in the food industry,also, used as a turbulent drag reducer that allow just a small amount of GG goes into the aqueous system . Empirical and fractional exponential decay

functions of GG were adopted in order to examine the time dependent drag reduction, the relationship between decrease in drag reduction and shearing time, and the ultrasonic thermal effect on polymer degradation.

Ultrasonication was used to obtain fractionated samples of the polysaccharide without any modifications. Aqueous GG solutions of 0.5 wt% concentration were stirred lightly for a week in deionized water. The water was exposed to ultrasound of 750 W at 28 kHz with an ultrasonicator. Subsequently virgin guar gum (GGV), guar gum ultrasonicated for 30 minutes (GG30), and guar gum ultrasonicated for 60 mintues (GG60) were obtained[10]. A decrease notice for drag reduction with sonicated times for GG, GGV, GG30 and GG60 since a study on their molecular weight applied on turbulent drag reduction. To conclude their work, the mechanical degradation of these different polysaccharide under turbulent flow was done through RDA also, a decrease in degradation rate while polymer concentration increases.

7.2.1   Flow behaviour of different polysaccharides

The galactomannan solutions, which have a wide range of polymer concentrations from 0-2 g/l to 50 g/l, were applied to flow behaviour obtained by two different viscometers. At lower concentrations no shear rate dependence was obtained experimentally, but the results show that at higher concentrations the solutions have shear thinning characteristics. The shear rate values demonstrate viscoelastic behaviour that decreases with increasing polymer concentration. In the other study, of the Newtonian plateau, the flow curves show dependence on shear rate that was determined by the galactomannan solutions. The values that were obtained were obtained by two different viscometers. Experimentally, no shear rate viscosity dependence was obtained for the lower concentrations of the solutions, but at high concentrations it was shown that the solution has shear thinning properties. It was observed that the transition from Newtonian to viscoelastic behaviour leads to lower values when the concentration increases.

7.2.2 Rheological properties of Galactomannans

In order to obtain the transition of all polysaccharides from dilute to semi-dilute concentration, different polymer concentrations were measured by a viscometer and the critical concentration was in the range of 2.5 +/- 0.5 / [η])[11] moreover, Morris found that some polysaccharides, such as glactomannan, behave at high concentration regimes as polymer-polymer interactions. Kapoor and colleagues have been working on the solution properties of a galactomannan which was extracted from the seed of cassia nodosa buch-hem, found in India as a tree, and also known by the name of "pink and white shower tree"[12] . They prepared different concentrations of galactomannan in water from 0.2 to 50 g/l and left the solution for 12 hours, the overall concentration being about 2g/l as calculated from the relationship between specific viscosity and shear rate. Experimentally, they realised that viscoelasticity behaviour started from 0.2 g/l polymer concentration, which is a similar value to that found for other randomly coiled polysaccharides, at 2-4 g/l[11].

Similar work has been done by Marguerite and her colleagues, who found that the critical concentration of galactomannan was about 1.8/8gl at which the shear rate decreased while polymer concentration increased (shear thinning). So, according to most of the sources in the literature, the transition from dilute to semi-dilute regime concentration was found to be at 2-4 g/l.

7.3 Other study carried out by Morris into the Rheological properties of Galactomannans

In the study that was carried out by Morris and his colleagues[7],the intrinsic viscosity of five samples was measured, as were their molecular weights from light scattering studies. They used the Mark-Houwink relationship as described in the equation $[\eta] = K^. M_r^\alpha$. This states that a polymer's intrinsic viscosity varies with its molecular weight. The parameters $K^.$ and α are related to the stiffness of the polymer. A flexible coil is usually assumed to be in the range of 0.5 – 0.8; if it adopts a very compact conformation in solution due either that to it being highly

branched or because of intramolecular segment-segment attractions then α is small and ranges from 0.1 - 0.3.

To measure $K^{\cdot}$ and α we can directly determine them by the logarithmic plot of [η] against M_r. The conditions of the operation are evidently important for the results; guar galactomannan acts as a random coil polymer and, by using one of the synthetic polymer studies and also applying it to a limited extent to the polysaccharide system, we can calculate the intrinsic chain flexibility. To determine the intrinsic chain flexibility the characteristic ratio (c ∞) is used. The simplest description of a linear polymer in a dilute solution is that the chain is a collection of stiff rods which are connected by completely flexible and universal joints. In practice the measurements are different due to the fact that the rotation in the inter-residue bonds is usually restricted to a small proportion of the conformational space. As shown in Figure 7.6, most of the combinations of the dihedral angles between adjacent residues are sterically or energetically disallowed, which would result in the chain being more directed than in the random flight model. Another factor is that the two segments which are a distance apart along the chain's backbone, and do not occupy the same amount of space, thus in return increase the overall end-to-end distance as shown in the figure below.
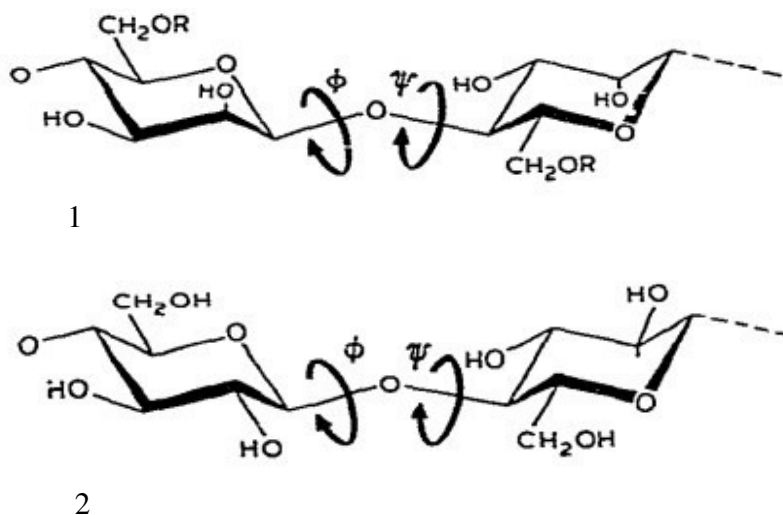
Figure 7.6 Guar Galactomannan 1 and cellulose 2 structures. Polymer configuration at C-2 can only be different for polymer backbones[7].

The characteristic ratio is important to measure, as it reflects local conformational freedom or intrinsic chain flexibility. In the same study that was carried out by Morris and his colleagues,

the characteristic ratio for carboxymethycellulose was calculated. Both polymers   the guar galactomannan and the cellulose are diequatorial, which is linked to the backbone structure, and the difference lies in the configuration at C-2 only. The axial orientation of the O-2 in the mannose chain leads to a lower characteristic ratio. This technique should not be used for polymers which are known to be very stiff intrinsically or where the α exponent is greater than 0.8[7] .

7.4 Determination of overlap concentration of polysaccharides used in this study.

The intrinsic viscosities for DM and JP in water were obtained using an Anton Parr viscometer at 25 °C as previously discussed, Figure 7.7, and overlap concentration calculated using $4/[\eta]$[7] and given in Tables 7.2 and solution properties in Table 7.3.

Table 7.2 Intrinsic viscosities of different polysaccharides at 25 °C in water.

Code	$[\eta]$ dl/g	c* (g/dl)
DM	11.1	0.39
JP	7.6	0.52

Table 7.3 Viscosities and surface tensions of different polysaccharides at 25 °C in water.

Polysaccharide	Reduced concentration c/c*	Viscosity η (cP)	Surface tension γ (mN/m)
DM	0.025	1.34	40.3
	0.125	2.58	
	0.25	5.36	42.6
JP	0.025	1.21	42.3
	0.125	2.34	
	0.25	5.06	44.6
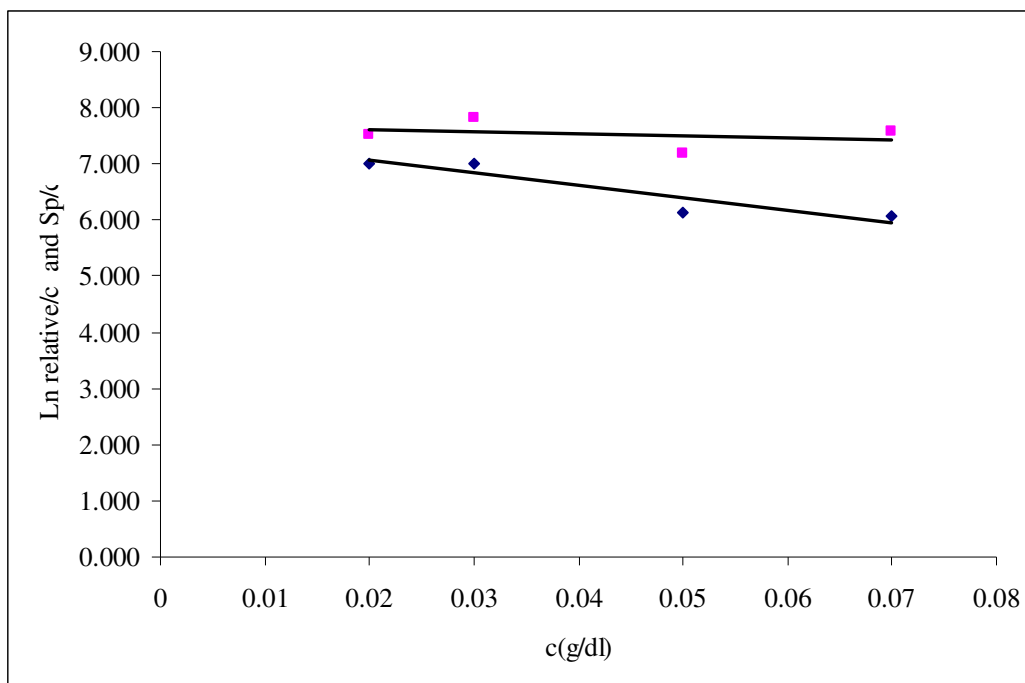
Figure 7.7 Intrinsic viscosity of JP in water using an Anton Parr viscometer at 25 °C.

7.5 Effect of inkjet printing on Molecular weight degradation of Galactomannan.

Solutions were all jetted using the Microfab single nozzle 50 μm nozzle printhead at 50 V drive voltage. Results for DM and JP are given below. A range of concentrations were evaluated c/c* = 0.025, 0.05, 0.125, 0.25, 0.35. 0.5 and for both the two polymers evaluated concentrations c/c* = 0.35 and 0.5 did not inkjet.

7.5.1 DM.

Table 7.4 GPC data for different concentration of DM before and after Microfab jetting at 50V.

c/c*	Mn Before (KDa)	Mw Before (KDa)	PDi Before	Mn After (KDa)	Mw After (KDa)	PDi After	Velocity (m/s)	Shear rate (s^{-1})
0.025	654	1120	1.8	551	1168	2.1	4.4	88000
0.125	654	1120	1.8	610	1048	1.7	2.6	52000
0.25	654	1120	1.8	7	38	4	3.5	70000
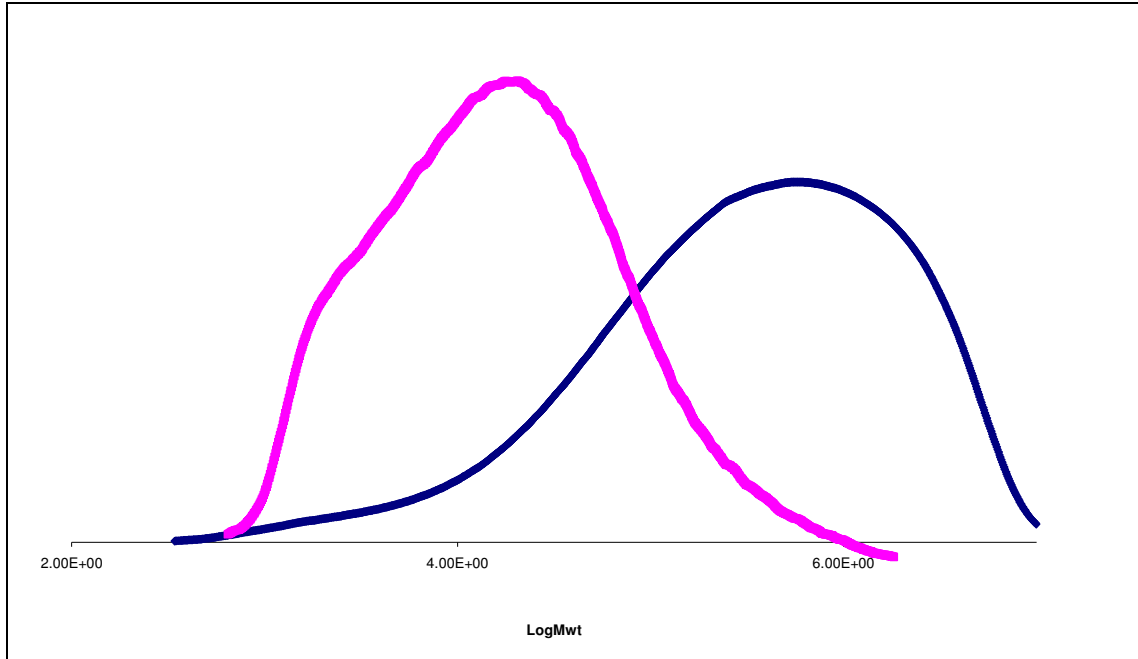
Figure 7.8 (WF/dLogMwt against log mol wt) before and after single pass jetting for DM polysaccharide at c/c* = 0.25 at 50 V using Microfab printhead at 25 ^{O}C. Before jetting (blue).

| 0 µs | 40 µs | 65µs |

Figure 7.9 Drop formation of DM during at c/c* = 0..125 in Microfab nozzle at 50 V.

7.5.2 JP.

Table 7.5 GPC data for different concentration of JP before and after Microfab Jetting at 50 V.

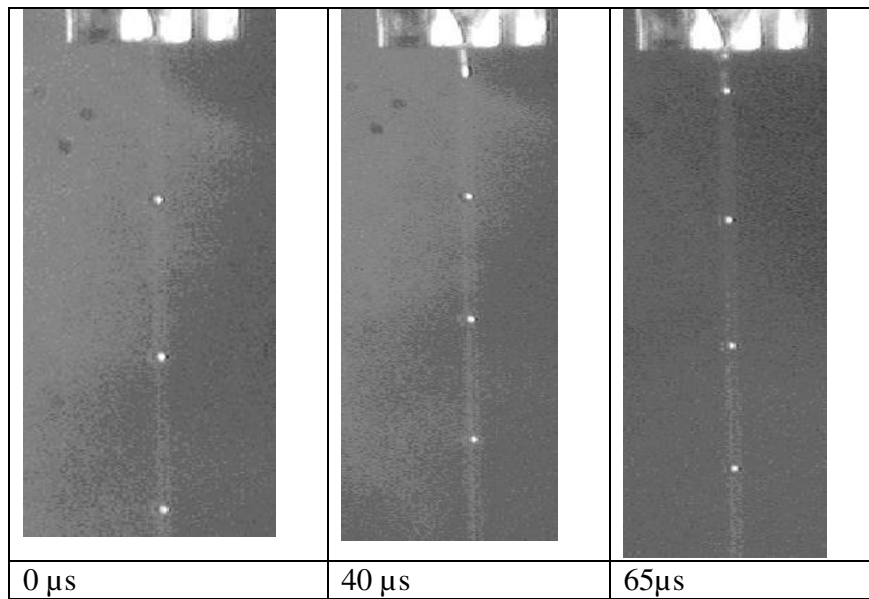| c/c*	Mn Before (KDa)	Mw Before (KDa)	PDi Before	Mn After (KDa)	Mw After (KDa)	PDi After	Velocity (m/s)	Shear rate (s^{-1})
0.025	2450	4580	1.9	3750	4860	1.4	2.2	44000
0.05	2450	4580	1.9	2761	3905	1.4	2.2	44000
0.125	2450	4580	1.9	72	500	6.9	6.4	128000
0.25	2450	4580	1.9	3	400	130	7.7	154000
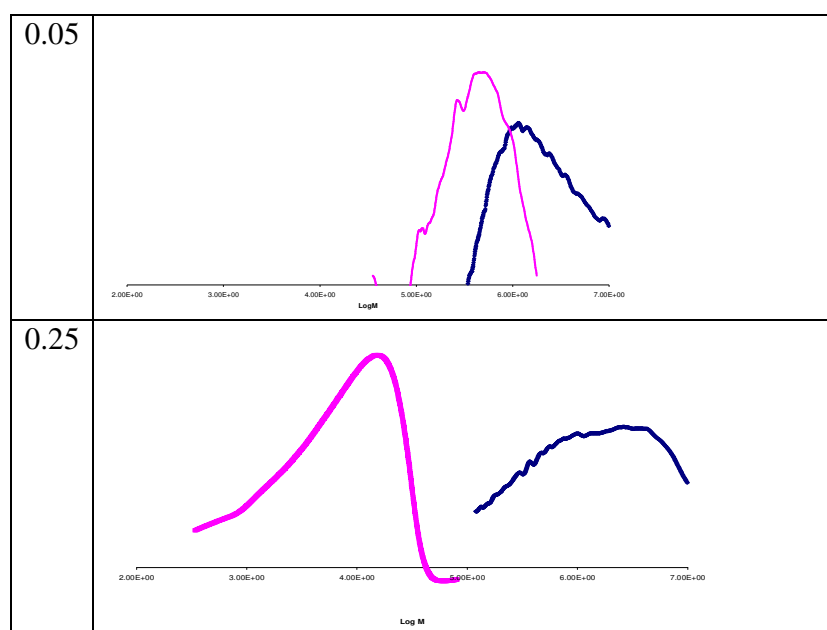
Figure 7.10 (WF/dLogMwt against log mol wt) before and after single pass jetting for JP polysaccharide low polydispersity at c/c* = 0.025 and 0.25 jetted at 50 V using Microfab Printhead at 25 $^{\circ}$C. Before jetting (blue). Single pass jetting (purple).

| 0.0.25 | 0.05 | 0.25 |
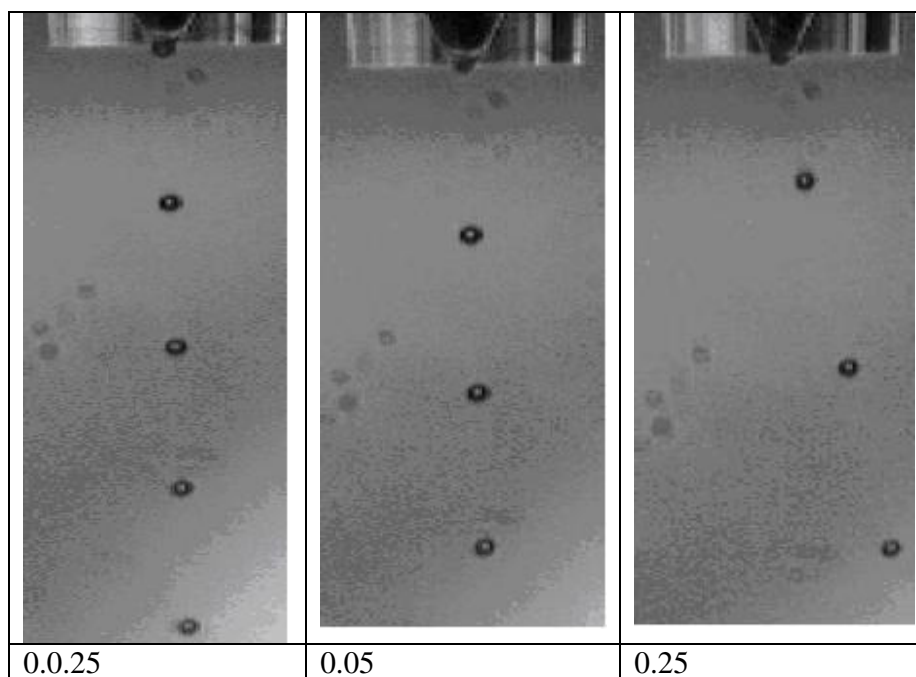
Figure 7.11 Drop formation of JP during the jet in Microfab nozzle at 50 V.

7.6   Discussion.

Overlap concentrations for the galactomannan polysaccharides were calculated using c* 4/[η][7] since the polymer chains are both branched and stiff due to intramolecular H-bonding (α = 0.1-0.3)[13] unlike in Chapter 6 where PMMA and PS are flexible –linear polymer chains with α = 0.6 - 0.8.

When ink jetted through a Microfab printhead at very dilute concentrations no reduction in molecular weight distribution for either galactomannan polysaccharides DM and JP in water is observed, c/c* < 0.1. Above this a decrease in the molecular weight distribution is observed for DM at c/c* = 0.25 and for JP at c/c* = 0.125 and 0.25, Figure 7.12.
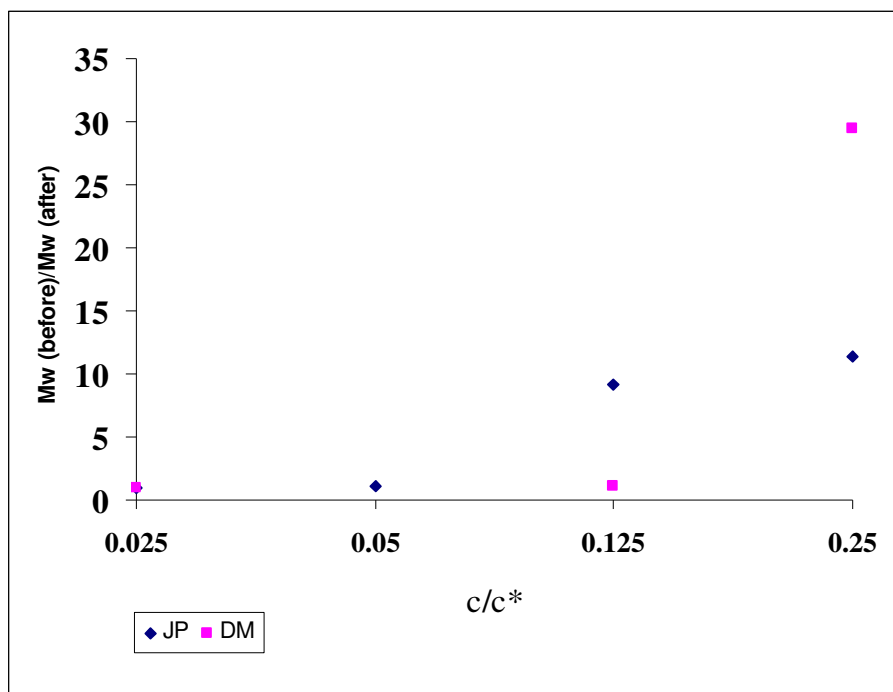
Figure 7.12 Plot of Mw (before jetting) Mw (after jetting) as a function of c/c* of DM and JP in water using a Microfab Printhead at 50 V.

In the case of linear mono-disperse PS and PMMA, albeit at higher shear rates, molecular weight degradation was seen to be centro-symmetric and for poly-disperse PS and PMMA random with a distribution of chain scission events leading to a significant broadening of molecular weight. In the case of the two galactomannan polysaccharides we have values of Mw and Mn which are high but PD's which are correspondingly narrow, PDi = 1.8 – 1.9. Given the difficulty in getting accurate molecular weight and distributions from GPC in water due to possible aggregation of the polysaccharide the values should be seen as indicative rather than absolute. When we see evidence of a decrease in molecular weight for DM at c/c* = 0.25 and for JP at c/c* = 0.125 and 0.25, the decrease is significant; Mw(before)/Mw after between 10-30, Figure 7.12, and Mn(before)/Mn after between 100 – 800. It is unlikely that this is a consequence in the difference in bond dissociation energies of C – C main chain in PS and PMMA, $\Delta H^o \approx 332$ kJmol^{-1} against C – O – C in galactomannan polysaccharides $\Delta H^o \approx 341$ kJmol^{-1} which are essentially the same[14]. This is high when compared with the bond energy of a typical O-H …. H hydrogen bond, which is of the order of 21 kJmol^{-1}. Therefore it is probable that the significant decrease in

148

molecular weight is a consequence of disaggregation through the breaking of H-bonds with a possible contribution due to main chain C – O – C bond rupture.

7.7 References.

1.   Hallagan, J. B.; La Du, B. N.; Pariza, M. W.; Putnam, J. M.; Borzelleca, J. F., *Food and Chemical Toxicology* **1997,** 35, (6), 625-632.

2.   Srivastava, M.; Kapoor, V., *Chemistry & Biodiversity* **2005,** 2, (3), 295-317.

3.   http://en.wikipedia.org/wiki/Guar_gum. (11/08/2010),

4.   Lim, S. T.; Choi, H. J.; Lee, S. Y.; So, J. S.; Chan, C. K., *Macromolecules* **2003,** 36, (14), 5348-5354.

5.   Cunha, P. L. R.; Vieira, Í. G. P.; Arriaga, Â. M. C.; de Paula, R. C. M.; Feitosa, J. P. A., *Food Hydrocolloids* **2009,** 23, (3), 880-885.

6.   Bourbon, A. I.; Pinheiro, A. C.; Ribeiro, C.; Miranda, C.; Maia, J. M.; Teixeira, J. A.; Vicente, A. A., *Food Hydrocolloids* **2010**
24, (2-3), 184-192.

7.   Geofferry, R.; Ross-Murphy, S. B.; Morris, E. R., *Carbohydrate Research* **1982,** 107, 17-32.

8.   Kim, N. J.; Lee, J. Y.; Yoon, S. M.; Kim, C. B.; Hur, B. K., *J. Ind. Eng. Chem* **2000,** 6, 412.

9.   Lim, S. T.; Park, S. J.; Chan, C. K.; Choi, H. J., *Physica A350* **2005**, 84.

10.   Hong, C. H.; Zhang, K.; Choi, H. J.; Yoon, S. M., *Journal of Industrial and Engineering Chemistry* **2010,** 16, (2), 178-180.

11.   Kapoor, V. P.; Sen, A. K.; Farooqi, M. I. H., *Indian J.Chem* **1989,** 28B, 928 -933.

12.   Kapoor, V. P.; Milas, M.; Taravel, F. R.; Rinaudo, M., *Carbohydrate Polymers* **1994,** 25, (2), 79-84.

13.   Chandrasekaran, R.; Radha, A.; Okuyama, K., *Carbohydrate Research* **1998,** 306, (1-2), 243-255.

14.   Sandurson R.T., *Chemical Bonds and Bond Energy* 2ed ed.; Academic Press.: in New York., **1976**; p 224.

Chapter Eight

Conclusions and Recommended Further Work

8.1 Conclusions

8.1.1 The effect of low molar mass H-bonding additives on the inkjet drop generation of polymer-containing fluids

The effect of hydrogen bonding interactions on the drop generation of both acid and hydroxyl-containing polymer solutions is reported showing that polymer chain relaxation can be influenced through the use of appropriate polymer co-solvent interactions for polymers having weight average molecular weight (M_w) < 100 kDa.

Low molecular weight MMA/MAA co-polymers, Mn = 7 – 10 kDa, Mw = 11 – 15 kDa in a good non-H-bonding solvent, γ-butyrolactone, in combination with miscible H-bonding co-solvents t-butanol and acetic acid.

The effect of the cosolvents are to reduce the overlap concentration of the polymers studied which is believed to be evidence for breaking of intra-molecular polymer H-bonds in favour of polymer-so-colvent H-bonding. On inkjet printing it was observed that the ligament at rupture is much longer in the presence of t-butanol and that the time to rupture has increased by approximately 33%. It had been expected the t-butanol would disrupt any transient network formation occurring upon elongation. If this had been the case, a decrease in ligament length may have been expected. That this is not seen maybe due either to stabilization of the extended state, which is unlikely, or the 'solvation state' of the polymer changing on jetting, with the polymer becoming more swollen and thus increasing the non-elongational viscosity. This may result from breaking intra-molecular MAA/MAA H-bonding on extension and replacing it fully with MAA/t-butanol H-bonding on relaxation. This is possible given the large molar excess of t-butanol to the available MAA. .

Medium molecular weight *cellulose acetate butyrate (CAB2) supplied by Eastman, Mn = 30.7 kDa, Mw = 76.6 kDa, 1 wt-% Hydroxyl content in a good non-H-bonding solvent, γ-butyrolactone, in combination with a miscible H-bonding co-solvent.*

Cellulose ester (CAB2) in γ-butyrolactone: Before jetting, the polymer coils are in the solution and behave as intra-chain associations. When an elongational shear is applied the polymer chain will extend and can form inter-chain H-bonds which rapidly create a gel as previously observed for FM9[4]. After the shear is removed the chains will relax back to the coiled state more slowly than the calculated Zimm relaxation rate due to the need to break the formed inter-molecular H-bonds.

Cellulose ester (CAB2) in γ-butyrolactone with either t-butanol or acetic acid at 1: mole ratio: In this case, an equal combination of CAB2 and CAB2/additives is considered, so the intra-chain of this combination is extended and the additive, for example t-butanol, will react, either H-bonding with CAB2 or directly with CAB2 itself. The inter-chain that would be produced for either t-butanol H-bonding with CAB2. CAB2 has a large viscosity due to performing a network of both inter-chain forms. The hydrogen bonding here is not strong enough for the remaining gel. The effect of adding the same molar amount of additive to CAB2 would allow us to predict that there is not a big change either in the ligament length at rupture or the time of rupture.

Cellulose ester (CAB2) in γ-butyrolactone with either t-butanol or acetic acid at a molar excess ≥ 2:1: In this regime, co-solvent was added such that it was in ≥ 2:1 excess over the hydroxyl groups on the polymer chain. As shown in both Figures 5.21 and 5.22, there was a decrease in the ligament length which can be explained as a case of the intra-chain of a combination of double the amount of t-butanol H-bonding or acetic acid H-bonding strongly reacting with CAB2 H-bonding while extended. After some time these intra-chains will reform as inter-chain associations with very large viscosity and form a network that will decay by the time of the chain returning when the elongational force is switched off. But as to what leads to a decrease in the ligament length, the answer would be that additional amounts of co-solvent would disrupt any network formed during the elongation.

8.1.2 Flow-Induced Polymer Degradation during Ink-Jet Printing of Poly(methylmethacrylate) and Polystyrene

Reported for the first time is evidence of flow-induced polymer degradation during inkjet printing for both poly(methylmethacrylate) and polystyrene in good solvent. Polymers having M_w either less than 100 kDa or greater than approximately 1,000 kDa show no evidence of molecular weight degradation. The lower boundary condition is a consequence of low Deborah number imposed by the printhead geometry and the upper boundary condition due to visco-elastic damping. For intermediate molecular weights the effect is greatest at high elongational strain rate and low solution concentration with higher polydispersity polymers being most sensitive to molecular weight degradation. For low polydispersity samples, PDi ≤ 1.3 chain breakage is essentially centro-symmetric induced either by overstretching when the strain rate increases well beyond a critical value, that is the stretching rate is high enough to exceed the rate of relaxation or by turbulence. For higher polydispersity samples, PDi chain breakage is consistent with almost random scission along the chain inferring that the forces required to break the chain are additionally transmitted either by valence bonds, i.e. network chains and junctions or discrete entanglements rather than solely by hydrodynamic interaction.

8.1.3 Flow-Induced Polymer Degradation during Ink-Jet Printing of Polysaccharides

Overlap concentrations for the galactomannan polysaccharides were calculated using c* 4/[η] since the polymer chains are both branched and stiff due to intramolecular H-bonding (α = 0.1-0.3) unlike in Chapter 6 where PMMA and PS are flexible –linear polymer chains with α = 0.6 - 0.8. When ink jetted through a Microfab printhead at very dilute concentrations no reduction in molecular weight distribution for either galactomannan polysaccharides DM and JP in water is observed, c/c* < 0.1. Above this a decrease in the molecular weight distribution is observed for DM at c/c* = 0.25 and for JP at c/c* = 0.125 and 0.25.

In the case of linear mono-disperse PS and PMMA, albeit at higher shear rates, molecular weight degradation was seen to be centro-symmetric and for poly-disperse PS and PMMA random with a distribution of chain scission events leading to a significant broadening of molecular weight. In

the case of the two galactomannan polysaccharides we have values of Mw and Mn which are high but PDi's which are correspondingly narrow, PDi = 1.8 – 1.9. Given the difficulty in getting accurate molecular weights and distributions from GPC in water due to possible aggregation of the polysaccharide the values should be seen as indicative rather than absolute. When we see evidence of a decrease in molecular weight for DM at c/c* = 0.25 and for JP at c/c* = 0.125 and 0.25, the decrease is significant; Mw(before) / Mw (after) between 10 -30, and Mn (before) / Mn (after) between 100 – 800. It is unlikely that this is a consequence in the difference in bond dissociation energies of C – C main chain in PS and PMMA, $\Delta H^o \approx 332$ kJmol^{-1} against C – O – C in galactomannan polysaccharides $\Delta H^o \approx 341$ kJmol^{-1} which are essentially the same [16]. This is high when compared with the bond energy of a typical O-H …. H hydrogen bond, which is of the order of 21 kJmol^{-1}. Therefore it is probable that the significant decrease in molecular weight is a consequence of disaggregation through the breaking of H-bonds with a possible contribution due to main chain C – O – C bond rupture.

8.2   Recommended Further Work.

1.   Effect of alternative H-bonding co-solvents, such as urea, on inkjet printing of designed hydroxyl and methacrylic acid containing methacrylate copolymers over a broad range of molecular weights.

2.   Effect of solvent on molecular weight degradation of PMMA and PS using less good solvents such as acetopheneone and solvent mixtures. Extend to study to consider polyethylene oxide and polyacrylamide and polyvinylalcohol in water in the presence and absence sodium chloride.

3.   Preliminary work indicates that H-bonds are broken preferentially and that main chain bond scission is probably occurring. Detailed structural analysis on recovered DM and JP after jetting by NMR and X-ray crystallography to determine whether degradation of the structure is reversible or irreversible.

4.   Evaluate the drag reduction and solution thickening properties of polysaccharides before and after jetting.

5.   Extend study to alternative polysaccharides, for example schizopyllan which takes up a random coil configuration in water/glycerol and water/DMSO.

6.   Although out of the scope of a chemistry group a systematic study on the nature of nozzle size and shape on polymer degradation.